THE COORDINATION CHEMISTRY AND MAGNETISM OF COMPOUNDS DERIVED FROM FORMYLPHENOLS AND DIAMINOMALEONITRILE

MURRAY KITCHENER PARK

The Coordination Chemistry and Magnetism of Compounds Derived from Formylphenols and Diaminomaleonitrile

by

Murray Kitchener Park, B.Sc.(Honours), B.Ed.

A thesis submitted to the

School of Graduate Studies

in partial fulfilment of the

requirements for the degree

Master of Science

Department of Chemistry

Memorial University of Newfoundland

St. John's Newfoundland

Abstract

This thesis describes the synthesis, spectroscopic characterization, electrochemistry and magnetism of mononuclear and polynuclear coordination compounds derived from formylphenols and diaminomaleonitrile (DAM), as well as extended Hückel molecular orbital calculations concerning the magnetic behaviour of binuclear macrocyclic copper(II) compounds.

Chapter 1 provides an overview of the literature to date concerning these compounds, with an emphasis on the current understanding of the magnetic properties of binuclear copper(II) systems from experimental (magnetostructural correlations) and computational (extended Hückel and *ab initio*) points of view. Chapter 2 describes the syntheses of mononuclear and polynuclear copper(II) compounds derived from formylphenols and DAM. A discussion of the x-ray diffraction structures of two copper(II) compounds along with infrared, UV-visible, electrochemical and variable temperature magnetism studies on the DAM-based systems is presented in chapter 3. While copper(II) readily templated the desired DAM-based product, this was not found in general for other metal ion salts and a series of IR guidelines was established to assess the structure and nuclearity of the products isolated. The UV-visible spectra of the copper(II) DAM systems are dominated by charge transfer bands that originate from the π framework of the ligand, in contrast to related binuclear copper(II) systems. Cyclic voltammetry revealed that the binuclear copper(II) systems all exhibit a single non-reversible one-electron reduction at uncharacteristically high electrode potentials,

except in the case of a diacetonyl adduct (formed upon reaction of a binuclear copper(II) macrocyclic compound with acetone) which undergoes two one-electron reductions to a binuclear copper(I) species via a mixed valence intermediate. The magnetism of the binuclear copper(II) systems is greatly affected by the electronic structure of the DAM residues, and this is discussed in detail. The presence of antiferromagnetic exchange in the acetonyl adduct ($2J = -25 cm^{-1}$) despite having the smallest average phenoxide angle reported to date (92.4°) provides experimental support for the results of the extended Hückel study on macrocyclic phenoxide bridged binuclear copper(II) systems.

Acknowledgements

First of all, I would like to thank Dr. Laurence Thompson for his guidance, intuition and support during the course of the research presented in this thesis. I would also like to gratefully acknowledge the support of each member of my supervisory committee: Dr. Thompson, Dr. C. Robert Lucas and Dr. Howard Clase who, during the final draft of this thesis, went above and beyond the usual role of supervisory committee members.

NSERC is acknowledged for financial assistance during this research, and the North Atlantic Treaty Organization is acknowledged for financial assistance to present much of this work at a workshop at Carcans-Maubuisson, France, September 1995. The Department of Chemistry and the School of Graduate Studies of Memorial University of Newfoundland are gratefully acknowledged for their fellowship support.

Special acknowledgement is extended to Dr. John Bridson and Mr. David Miller not only for the x-ray structure determinations, but also for their efforts in attempting to obtain structures for crystals of a chemical system that did not always want to cooperate. Thanks are also extended to Ms. Marion Baggs for mass spectrometry and to Dr. Chet Jablonski and Dr. Fransesc Lloret for their initial guidance during the MO calculations.

I would also like to thank my colleagues of the Thompson research group. Thanks to Dr. Santokh Tandon and Dr. Makoto Handa for their advice concerning the syntheses and spectra analyses, Mr. Mike Manuel and Mr. Chris Sheppard for their aid in obtaining

room temperature magnetic moments and fitting the variable temperature magnetic data, and Mr. Zhiqiang Xu for providing useful ligand starting materials. The camaraderie of this group will always be remembered.

Many thanks are extended to my fellow students and the staff of the Department of Chemistry at Memorial University for making my years there enjoyable. Special thanks are extended to Mr. Alan Swinamer for our discussions concerning chemistry and topics beyond chemistry.

Finally, I would like to thank my parents, Richard and Ethel, and my sister, Michelle, for providing twenty-five years of support, encouragement and friendship. Final thanks are extended to my wife, Yvette, for her unconditional love; this thesis is dedicated to you.

Table of Contents

Title i

Abstract ii

Acknowledgements iv

Table of Contents vi

List of Tables ix

List of Figures x

List of Abbreviations xv

Chapter 1 **Introduction** 1

1.1. Molecular Magnetism - Unifying Physical Science with Life Science 1

1.2. Principles of Magnetochemistry 2

1.3. The Determination of the Isotropic Interaction Parameter, *J*, for Homo-binuclear Compounds 5

1.4. Magnetostructural Correlations for Binuclear Copper(II) Compounds with Single-Atom Bridges 8

1.5. The Choice of a Model: Theoretical Approaches to Understanding Isotropic Spin Interaction 10

1.6. Molecular Orbital Theory and Magnetism: The Concept of Accidental Orthogonality 13

1.7. Coordination Compounds of Binucleating Macrocyclic Hexadentate Ligands 22

1.8. Diaminomaleonitrile - a Precursor to Symmetrical Robson-Type Macrocycles 25

1.9. The Objective of the Research Presented in this Thesis 29

Chapter 2 **Experimental** 32

2.1. Physical Measurements 32

2.2. Syntheses of Mononuclear and Polynuclear Copper(II) Compounds by Template Methods 33

2.3. General Comments Regarding the Solubility and Crystallization Attempts of the Polynuclear Copper(II) Coordination Compounds Presented 38

Chapter 3 **Discussion of Results** 40

3.1. Description of X-Ray Diffraction Structures 40

3.2. Mechanistic Considerations on the Formation of $[Cu_2M4](CH_3COCH_3)$ and $[CuL2(CH_3SOCH_3)]$ 52

3.3. Infrared Spectroscopy - Providing a Cornerstone for the Structural Analysis of Diaminomaleonitrile Derivatives 56

3.4. UV-Visible Spectra of the Copper(II) Coordination Compounds 74

3.5. Electrochemical Studies 80

3.6. Magnetochemistry 87

3.7. Extended Hückel Molecular Orbital Model Study 98

Chapter 4 **Conclusions** 104

References 106

Appendices 112

Appendix I: Input File and Parameters Used in the Extended Hückel Molecular Orbital Model Study 112

Appendix II: Crystallographic Data 114

Appendix III: Magnetic Data 116

List of Tables

Table

3.1.1. Interatomic Distances (Å) and Angles (deg.) Relevant to the Copper Coordination Spheres in $[Cu_2M4](CH_3COCH_3)$, **(5)**. 41

3.1.2. Interatomic Distances (Å) and Angles (deg.) Relevant to the Copper Coordination Sphere for $[CuL2(CH_3SOCH_3)]$, **(7)** 50

3.3.1. Infrared Data 59

3.3.2. C, H, N Microanalytical Data for the Product Obtained from Each of the Attempted Template Syntheses of $M1^{2-}$ Using Mn(II), Zn(II) and Pb(II) 66

3.3.3. Analytical Data for the Products Obtained from Attempts to Synthesize Binuclear Nickel(II) and Vanadyl(II) Compounds of $M1^{2-}$ and $M2^{2-}$ 70

3.3.4. Effective Ionic Radii of Metal Ions as Determined by X-ray Crystallography ... 71

3.4.1. Absorption Maxima and Extinction Coefficients for Copper(II) Compounds of Diaminomaleonitrile-Derived Ligands 75

3.5.1. $E_{1/2}$ Values for the Non-Reversible Waves Found in the Cyclic Voltammograms of **(1)**, **(2)**, **(4)**, **(8)** and **(9)** 82

3.6.1. Magnetic Data 88

List of Figures

Figure

1.1.1. Diaminomaleonitrile 2

1.2.1. Schematic representation of the temperature dependence of magnetic susceptibility for (a) simple paramagnetic, (b) ferromagnetic and (c) antiferromagnetic compounds. 3

1.2.2. Schematic representation of the variation of $\chi_m T$ versus T for (a) simple paramagnetic, (b) ferromagnetic and (c) antiferromagnetic compounds. 5

1.4.1. Binuclear copper(II) core with monoatomic bridges provided by the ligand group X. α denotes the angle at the bridge. 8

1.4.2. Alkoxide bridged binuclear copper(II) system studied by Merz and Haase [11]. .. 9

1.6.1. Relative energies of MOs γ_1 and γ_2 and their component magnetic orbitals ϕ_A and ϕ_B for an unsymmetrical Cu_ACu_B system. 16

1.6.2. The model compound used by Kahn and coworkers to calculate the dependence of J_{AF} on α [14a]. 17

1.6.3. Variation in extended Hückel triplet MO energies for planar hydroxide bridged binuclear copper(II) compounds [24]. 18

1.6.4. Illustration of α_o and α_c for a spin exchange system whereby $2J$ increases with a

decrease in bridge angle. 19

1.6.5. The model used by Kahn and coworkers [14] to calculate the dependence of J_{AF} on dihedral angle. 20

1.6.6. Variation in extended Hückel triplet MO energies with dihedral angle δ for hydroxide bridged binuclear copper(II) coordination compounds. 21

1.7.1. Binuclear Schiff base macrocyclic coordination compounds containing two phenoxide bridges. 22

1.7.2. Plot of the isotropic interaction parameter, $2J$, versus Cu-OPh-Cu angle, α. ... 23

1.8.1. Ligands derived from the Schiff base condensation of a) 1:1 DAM:salicyl-aldehyde and b) 1:2 DAM:salicylaldehyde. 25

1.8.2. Schematic of the symmetrical coordination compounds derived from a d^8 metal ion (Ni^{2+}, Pd^{2+}, Pt^{2+}) and two doubly-deprotonated DAM ligands [52]. 26

1.8.3. The Robson-type macrocycle obtained using the diamine diaminomaleonitrile (R = CH_3, t-Bu). 27

1.8.4. High-nuclearity coordination compound obtained upon coordinating paramag-netic ions (schematically denoted by half-arrows in circles) in σ-fashion to the cyano functions. 28

1.9.1. Macrocyclic ligands presented in this thesis. 30

1.9.2. Non-macrocyclic ligands presented in this thesis. 31

3.1.1. X-ray crystal structure of $[Cu_2M4](CH_3COCH_3)$, (**5**) viewed down onto the

Cu_2O_2 core. 42

3.1.2. X-ray crystal structure of (5) viewed along the O-O axis. 43

3.1.3. X-ray crystal structure of [CuL1], (6), as obtained from a sample prepared by MacLachlan. Reproduced from reference [60]. 46

3.1.4. Bond lengths for (a) a DAM fragment of (5) (where -R = $-CH_2COCH_3$) and (b) the DAM fragment of (6). 47

3.1.5. Schematics of the π electron framework of the DAM fragment of (5), derived from x-ray crystal structure considerations. 48

3.1.6. X-ray crystal structure of [CuL2(CH_3SOCH_3)], (7). 51

3.2.1. (a) Conjugate addition from a synthetic organic chemistry point of view, and (b) extended conjugate addition as envisaged for [Cu_2M4](CH_3COCH_3), (5). .. 53

3.3.1. Proposed structures for compounds (1) - (9). 60

3.3.2. IR spectrum of [Cu_2M1](ClO_4)$_2$(H_2O)$_3$(CH_3OH), (1). 63

3.3.3. IR spectrum of HL5, (3). 63

3.3.4. IR spectrum of [Cu_2M4](CH_3COCH_3), (5). 64

3.3.5. IR spectrum of [CuL2(CH_3SOCH_3)], (7). 64

3.3.6. IR spectrum of [Cu_2L3](ClO_4)(C_2H_5OH), (8). 65

3.3.7. IR spectrum of the product obtained from the attempted template synthesis of $M1^{2-}$ using Zn^{2+} as the templating ion. 67

3.3.8. IR spectrum of the product obtained from the attempted template synthesis of $M1^{2-}$ using Ni^{2+} as the templating ion. 68

3.3.9. IR spectrum of the product obtained from the attempted template synthesis of $M1^{2-}$ using VO^{2+} as the templating ion. 68

3.3.10. Attempted synthesis of Mn(II) / Cu(II) heterobinuclear Robson type macrocycle, from reference [64]. 72

3.3.11 (a) Expected and (b) obtained product from the reaction shown in Figure 3.3.10 [64]. 73

3.4.1. UV-visible spectrum of 2.2×10^{-5} mol·L^{-1} solution of **(1)** in DMF. 76

3.4.2. UV-visible spectrum of 3.1×10^{-5} mol·L^{-1} solution of **(5)** in DMF. 77

3.4.3. UV-visible spectrum of 2.6×10^{-5} mol·L^{-1} solution of **(7)** in DMSO. 77

3.4.4. UV-visible spectrum of 1.4×10^{-5} mol·L^{-1} solution of **(8)** in DMF. 79

3.5.1 Cyclic voltammograms for **(1)** over the ranges of (a) outer ± 1.50V, inner ± 0.40V, and (b) ± 0.40V at variable scan rate. 80

3.5.2. Cyclic voltammograms for **(8)** over the ranges of (a) outer ± 1.25V, inner +0.40V to -0.30V, and (b) ± 0.40V at variable scan rate. 83

3.5.3. Variable scan-rate cyclic voltammograms of **(5)** in dry DMSO over the -0.20V to -1.35V range. 84

3.5.4. Macrocyclic binuclear copper(II) compounds studied by Mandal and coworkers [44] to determine the variation in one-electron reduction potentials as a function of saturation at the azomethine linkage. 86

3.6.1. Variable temperature magnetic susceptibility data (▲) for $[Cu_2M1](ClO_4)_2(H_2O)_3(CH_3OH)$, **(1)** with least squares line (-). 89

3.6.2. Variable temperature magnetic susceptibility data (▲) for $[Cu_2M2](ClO_4)_2$, **(2)** with least squares line (-). 90

3.6.3. Variable temperature magnetic susceptibility data (▲) for $[Cu_2M3](ClO_4)_2(H_2O)_2$, **(4)** with least squares line (-). 91

3.6.4. Macrocyclic ligands with electronic or structural features similar to H_2M1 - H_2M3. 92

3.6.5. Variable temperature magnetic susceptibility data (▲) for $[Cu_2M4](CH_3COCH_3)$, **(5)** with least squares line (-). 94

3.6.6. Binuclear copper(II) coordination compound shown by Wieghardt and coworkers [68] to exhibit intramolecular antiferromagnetic exchange. 96

3.6.7. Proposed alternative antiferromagnetic exchange routes from the phenoxide bridge route which utilize the unsaturated azomethine linkages in binuclear Robson macrocylces. 97

3.7.1. A schematic of the copper(II) phenoxide bridged compounds (left) from which the model compound (right) was derived. R = CH_3, t-Bu. 99

3.7.2. Triplet molecular orbitals (contracted by the CACAO program by a factor of 1.5 for clarity) for the model system shown in Figure 3.7.1. (a) b_{3u}; (b) b_{2g}. 101

3.7.3. Variation in triplet MO energies (ε_{b3u}, ε_{b2g}) as a function of Cu-OPh-Cu bridge angle,α, of the model system shown in Figure 3.7.1. 102

List of Abbreviations

DAM	Diaminomaleonitrile
DFMP	2,6-diformyl-4-methylphenol
DFTBP	2,6-diformyl-4-t-butylphenol
$E_{½}$	One-electron reduction potential
E_i	Energy of the level *i* in the absence of a magnetic field
Fc	Ferrocene
$\tilde{\mathbf{H}}g$	*g*-factor or Landé splitting factor
Hss	Orbital energy for a "s" atomic orbital (Appendix I)
	Heisenberg-Dirac-Van Vleck Hamiltonian
j	Exchange integral
J	Isotropic exchange parameter
k	Boltzmann constant
K_{con}	Conproportionation constant
L	Non-macrocyclic Ligand
M	Macrocyclic Ligand
MO	Molecular orbital
n	Number of moles

N	Avagadro's number
$N\alpha$	Temperature independent paramagnetism
Q	Faraday constant
R	Molar gas constant
R	Residual factor
R1,R2	Spacer groups within Robson-type macrocyclic ligands (Figure 1.7.1)
S	Spin angular momentum quantum number
$\hat{\mathbf{S}}S'$	Spin state energy level
$\boldsymbol{S}$	Overlap integral
$_A$	Local spin operator of paramagnetic centre A
SCE	Saturated calomel electrode
T	Temperature, measured in Kelvin
T_C	Curie temperature
T_N	Néel temperature
α	Angle at the monoatomic bridge between paramagnetic centres
α_o	Angle of accidental orthogonality
α_C	Crossover angle from antiferromagnetism to ferromagnetism (and vice versa)
β	Electronic Bohr magneton
χ_m	Molar magnetic susceptibility
δ	Dihedral angle at monoatomic bridges between paramagnetic centres
Δ	Energy difference between molecular orbitals

ΔE_p	Peak-to-peak separation between waves of an one-electron redox step
ε_γ	Energy of the molecular orbital γ
ϕ_A	Magnetic orbital of paramagnetic centre A
γ_i	Molecular orbital *i* arising from MO treatment of magnetic orbitals
μ_B	Bohr magneton (unit)
ρ	Fraction of paramagnetic impurity
σ	Estimated standard deviation in crystal structure bond length
θ	Weiss correction
τ	Energy difference between magnetic orbitals
Ψ	Heitler-London (two-electron) wavefunction
ζ	Atomic orbital exponent

Chapter 1. Introduction

1.1. Molecular Magnetism - Unifying Physical Science with Life Science

Molecular magnetism holds a unique position in the world of science: it successfully unites the realms of physics, chemistry and biology. In 1932, the physicist J.H. Van Vleck [1] introduced the fundamental equations describing magnetic susceptibility, which, twenty years later, B. Bleaney and K.D. Bowers [2] were able to apply to the then "anomalous" magnetic susceptibility of copper(II) acetate monohydrate reported by B. Guha [3]. Not only were Bleaney and Bowers able to define correctly the electronic ground state of the compound from their new interpretation of Guha's magnetic measurements, but they consequently predicted the compound's correct dimeric molecular structure. This structure was finally confirmed in 1973 by neutron diffraction [4] and x-ray diffraction [5] structural studies.

This ability to correlate magnetic susceptibility with electronic and molecular structure - especially during an era when x-ray crystal structures were uncommon - made magnetochemistry an important tool for biologists, biochemists and chemists studying enzyme chemistry. Inorganic coordination compounds were synthesized as models of the active sites of enzymes, such that the magnetochemistry of the model systems could be compared to that of the bioactive molecules. Such model studies provided a means for the early characterization of the active sites of hemocyanin, hemerythrin, ribonucleotide reductase and cytochrome c oxidase, to name only a few examples [6,7].

With the advent of routine x-ray crystal structure determination as well as high powered computers, the opportunity to make further advancements into the understanding of molecular magnetism is apparent now more than ever. Using these tools, this thesis will describe the synthesis and characterization of copper(II) and nickel(II) coordination compounds of ligands derived from the condensation of formylphenols and diaminomaleonitrile (DAM, shown in Figure 1.1.1), and will present both a magneto-structural and molecular orbital understanding of the magnetochemistry observed for phenoxide bridged binuclear copper(II) complexes.

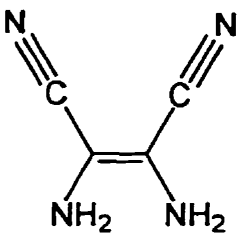

Figure 1.1.1. Diaminomaleonitrile.

1.2. Principles of Magnetochemistry

All chemical compounds exhibit some form of magnetic behaviour when placed in an applied external magnetic field. From the point of view of magnetic properties, a chemical compound may be first classed as being either *diamagnetic* or *paramagnetic*. Diamagnetic compounds have all electrons paired and as a consequence, are weakly ***repelled*** by the field gradients of an applied external magnetic field. Conversely,

paramagnetic compounds contain centres with unpaired electrons and are *attracted* into an applied external magnetic field.

Paramagnetic compounds may be further differentiated as being either simple paramagnetic, ferromagnetic or antiferromagnetic compounds. Figure 1.2.1 illustrates idealized molar susceptibility, χ_m, versus absolute temperature plots for these various types of paramagnetic materials. For simple paramagnetic compounds, the spins of the

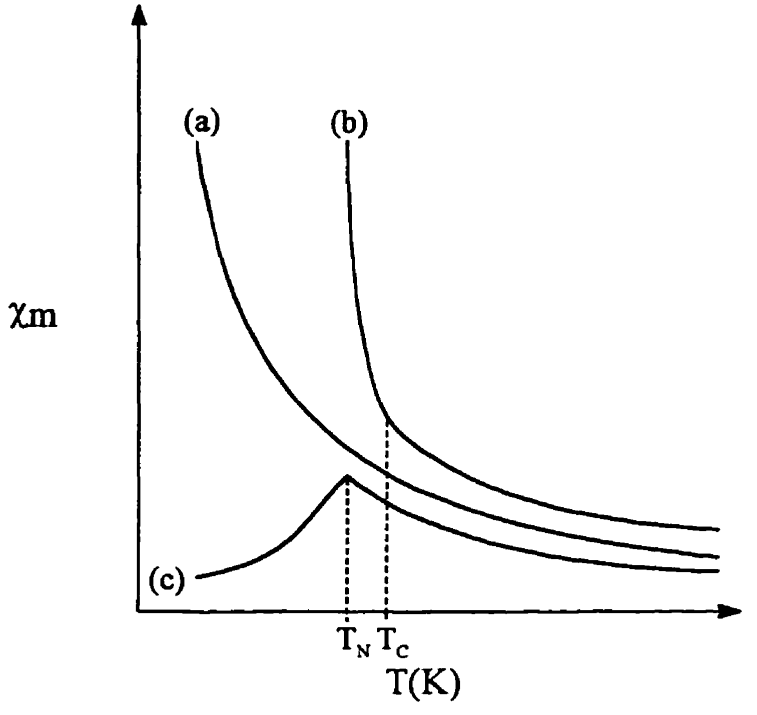

Figure 1.2.1. Schematic representation of the temperature dependence of magnetic susceptibility for (a) simple paramagnetic, (b) ferromagnetic and (c) antiferromagnetic compounds.

paramagnetic centres do not interact. Placing such a substance in a magnetic field will cause the spins to align with the field, an alignment which thermal energy (kT) attempts to

oppose. At high temperatures (T), thermal energy is sufficient to randomize the spins of the sample in the magnetic field. Yet, upon continual cooling, spin alignment may overcome the randomization of spins and the susceptibility thus increases. This behaviour is described by the Curie Law:

$$\chi_m = \frac{Ng^2\beta^2}{3kT}(S(S+1)) \qquad \ldots (1.2.1)$$

For ferromagnetic compounds, the behaviour of the sample in a magnetic field is analogous to that of a simple paramagnetic compound at temperatures above the Curie temperature, T_C. At the Curie temperature, the tendency of paramagnetic spins to align *parallel* becomes dominant, overcoming thermal randomization. Continued cooling below T_C thereby yields an increase in χ_m *greater* than that expected for a simple paramagnet. Conversely, for antiferromagnetic compounds, the randomization of spins (again by thermal energy) that occurs above the Néel temperature, T_N, becomes controlled by the *antiparallel* alignment of spins upon cooling below T_N. Accordingly, a *maximum* in the χ_m versus T curve for an antiferromagnetic compound is observed at T_N, and the susceptibility decreases upon further cooling.

Figure 1.2.1 shows a somewhat idealized perspective of magnetic behaviour; in practice, it is quite common to observe no obvious discontinuity at T_C for the χ_m versus T curve of a ferromagnetic compound. For this reason, a plot of $\chi_m T$ versus T, illustrated by Figure 1.2.2, may be utilized. Such a plot yields a clear distinction between all types of paramagnetic behaviour.

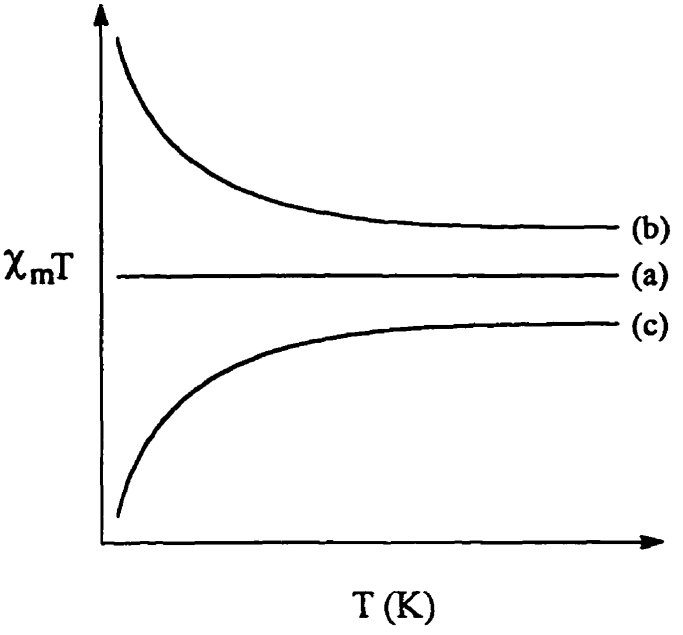

Figure 1.2.2. Schematic representation of the variation of $\chi_m T$ versus T for (a) simple paramagnetic, (b) ferromagnetic and (c) antiferromagnetic compounds.

1.3. The Determination of the Isotropic Interaction Parameter, *J*, for Homo-binuclear Compounds

For a binuclear coordination compound containing paramagnetic centres A and B, the coupling between the local spin operators $\hat{S}_A$ and $\hat{S}_B$ is given by the isotropic Heisenberg-Dirac-Van Vleck (HDVV) Hamiltonian

$$\hat{H} = -2J(\hat{S}_A \cdot \hat{S}_B) \qquad \ldots (1.3.1)$$

For a $S = ½, ½$ system, such as A = B = Cu^{2+}, equation (1.3.1) yields a $S' = 0$ singlet state

and a $S' = 1$ triplet state. When the ground state is the singlet state, then the coupling is *antiferromagnetic* and J is *negative*. When the triplet state is the ground state, the coupling is then *ferromagnetic* and J is *positive*. It follows that the energy gap between the singlet and triplet levels is

$$E(S' = 1) - E(S' = 0) = 2J \qquad \ldots (1.3.2)$$

If $2J$ is of the order of the magnitude of thermal energies, the population of each level will be given by a Boltzmann distribution. According to Van Vleck [1], the molar magnetic susceptibility is given by the population-weighted average of the susceptibility of the energy levels:

$$\chi_m = \frac{N\Sigma_i \left(\left(E_{i(1)}^2 / kT \right) - 2E_{i(2)} \right) \exp\left(-E_{i(0)} / kT\right)}{\Sigma_i \exp\left(-E_{i(0)} / kT\right)} \qquad \ldots (1.3.3)$$

where $E_{i(0)}$ is the energy of the level i in the absence of a magnetic field. $E_{i(1)}$ and $E_{i(2)}$ are the coefficients of the first and second order Zeeman effects, respectively. Upon placing a sample in a magnetic field, the first order Zeeman effect splits each level symmetrically into $2S' + 1$ component levels, ranging in energy from $-g\beta S'$ to $+g\beta S'$. This yields

$$\frac{E_{i(1)}^2}{kT} = \frac{g^2\beta^2}{kT}\left[(S')^2 + (S'+1)^2 + \ldots 0 \ldots (-S')^2\right] = \frac{g^2\beta^2}{kT}\left(\frac{S'(S'+1)(2S'+1)}{3}\right) \qquad \ldots (1.3.4)$$

Since each component of a degenerate set of levels must be counted separately, the denominator of equation (1.3.3) must include the factor $(2S' + 1)$. Furthermore, it can be shown [1,9] that the result of the second order Zeeman effect is to make a temperature independent contribution to χ_m. With these two points in mind, the equation (1.3.3) reduces to

$$\chi_m = \frac{Ng^2\beta^2}{3kT}\left(\frac{\Sigma_i S'(S'+1)(2S'+1)\exp(-E_{i(0)}/kT)}{\Sigma_i (2S'+1)\exp(-E_{i(0)}/kT)}\right) + N\alpha \quad \ldots (1.3.5)$$

where $N\alpha$ is a term which accounts for temperature independent paramagnetism. The above form of the Van Vleck equation can be used to generate the fundamental expression describing the temperature dependence of molar susceptibility for any homobinuclear paramagnetic system of total angular momentum S'. Substitution of $S' = 0,1$ and $E_{i(0)} = 2J$ into equation (1.3.5) yields, for a binuclear copper(II) system

$$\chi_m = \frac{Ng^2\beta^2}{3kT}\left[\frac{1}{1 + (1/3)\exp(-2J/kT)}\right] + N\alpha \quad \ldots (1.3.6)$$

At this point, it should be noted that 1) such compounds normally contain a small amount of (simple) paramagnetic impurity and 2) non-localized *intermolecular* spin interactions are commonly observed. For these reasons, equation (1.3.6) is modified to

$$\chi_m = \frac{Ng^2\beta^2}{3k(T-\theta)}\left[\frac{1}{1 + (1/3)\exp(-2J/kT)}\right](1-\rho) + \left(\frac{Ng^2\beta^2}{4kT}\right)\rho + N\alpha \ldots (1.3.7)$$

where ρ is the fraction of paramagnetic impurity and θ is the Weiss-like correction which accounts for intermolecular interactions. Equation (1.3.7) is the modified Bleaney-Bowers equation, and it is used to fit the variable temperature magnetic susceptibility data for all new binuclear copper(II) compounds presented in this thesis.

1.4. Magnetostructural Correlations for Binuclear Copper(II) Compounds with Single-Atom Bridges

Since this thesis will first review an experimentally-based magnetostructural understanding [8] of the isotropic exchange exhibited by phenoxide bridged binuclear copper(II) macrocycles and then present a theoretical understanding of the same based upon extended Hückel calculations, it is of importance to first discuss the experimental and theoretical advances with related bridge systems upon which the phenoxide bridge study is based. Compounds with the Cu_2X_2 core shown in Figure 1.4.1 will be considered.

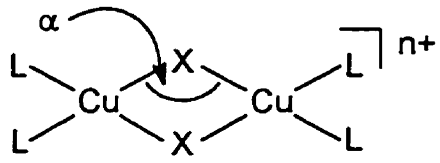

Figure 1.4.1. Binuclear copper(II) core with monoatomic bridges provided by the ligand group X. α denotes the angle at the bridge.

X may be a polyatomic ligand group, yet only one (diamagnetic) atom of the group bridges both copper(II) centres.

Hatfield and coworkers [10] were the first to correlate experimentally the angle at the bridge, α, with the magnitude and sign of the exchange parameter, *2J*, for hydroxide

bridged compounds corresponding to $X^- = OH^-$ and $n = 2$ in Figure 1.4.1. All twelve representative compounds are planar, and the peripheral ligands are neutral chelating amino ligands. The bridge angle α was found to vary from 95.5° to 104.1°, with $2J$ ranging from $+172cm^{-1}$ to $-509cm^{-1}$, respectively. From these data, Hatfield and coworkers were able to determine a very good linear correlation:

$$2J(cm^{-1}) = -74\alpha(\text{degrees}) + 7270 \qquad \ldots (1.4.1)$$

which predicts $2J = 0$ for $\alpha_c = 97.5°$. According to equation (1.4.1), antiferromagnetic behaviour is expected for compounds with Cu-OH-Cu angles *greater than* 97.5°, while compounds with Cu-OH-Cu angles *less than* 97.5° should be ferromagnetic. The angle at which this crossover from ferromagnetic to antiferromagnetic behaviour occurs is denoted the crossover angle, α_c.

Merz and Haase [11] reported an analogous magnetostructural correlation for alkoxide bridged binuclear complexes of the form shown in Figure 1.4.2. By varying R as methyl, ethyl, n-propyl and n-butyl, seven representative compounds were obtained for $X^- = NCO^-$, Br^- and Cl^-. The Cu-O(R')-Cu angles ranged from $\alpha = 95.7°$ to 105.0°, with a parallel variation in $2J$ from $-8.7cm^{-1}$ to $-800cm^{-1}$. This allowed Merz and Haase to

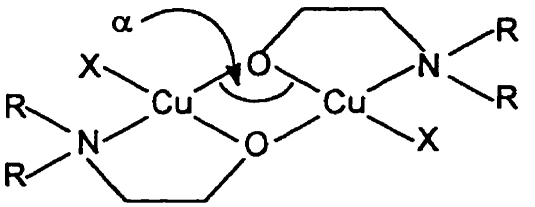

Figure 1.4.2. Alkoxide bridged binuclear copper(II) system studied by Merz and Haase [11].

deduce the linear relationship:

$$2J(cm^{-1}) = -82\alpha(\text{degrees}) + 7857 \quad \ldots (1.4.2)$$

and a crossover angle of $\alpha_c = 95.7°$. Merz and Haase reasoned that it is the difference in the electronic structure of hydroxide and alkoxide oxygen that causes the difference in crossover angles for the two systems [11]. This interesting point will be re-examined upon reviewing the magnetostructural correlation for phenoxide bridged complexes in section 1.7 of this thesis.

1.5. The Choice of a Model: Theoretical Approaches to Understanding Isotropic Spin Interaction

In recent years, many attempts have been made to understand as well as to quantify the isotropic exchange parameter, $2J$, using various levels of theory and computational methods. These studies differ in the degree of theoretical and computational *complexity*, of course, and upon examining the results from the various methods it soon becomes clear that increasing complexity does not necessarily equate to better results when attempting to describe the process of spin interaction.

Early theoretical and computational studies by Hoffmann and coworkers [12] and Kahn and coworkers [13,14] developed relatively simple theoretical descriptions of spin interaction that could be easily applied to molecular orbital (MO) schemes obtained from simple extended Hückel calculations. When applied to their formulations, the MO results for hydroxide bridged binuclear copper(II) model complexes were in agreement with the

magnetic behaviour (antiferromagnetic or ferromagnetic) that was observed experimentally by Hatfield [10]. After this success, Kahn continued to use this level of theory and extended Hückel calculations to qualitatively describe spin interactions in dithioxamide, oxalate, bis-$\mu_{1,1}$-azide, bis-$\mu_{1,3}$-azide, μ-phenoxide-$\mu_{1,1}$-azide and μ-phenoxide-$\mu_{1,1}$-cyanate bridged binuclear copper(II) coordination compounds [15,16].

Although many authors attempted to go beyond the qualitative approaches at the extended Hückel level developed by Hoffmann and Kahn, it proved impossible to predict $2J$ accurately by this method. In 1981, de Loth and coworkers [17] hoped to quantitatively calculate $2J$ for the classic case of copper(II) acetate monohydrate by developing an *ab initio* perturbational approach that accounted for configuration interactions (CI). Although they obtained the correct magnitude and sign of the isotropic interaction parameter, the limitations of their perturbational approach were realized in the discrepancy between the calculated ($2J$ = -120.2cm^{-1}) and experimental ($2J$ = -286cm^{-1} [18]) values. Some years later, Astheimer and Haase [19] attempted to use the same *ab initio* perturbational CI method to obtain a quantitative model for the coupling that Haase had experimentally observed [11] for alkoxide bridged binuclear copper(II) complexes. Although Astheimer and Haase [19] were able to calculate the same qualitative dependence of $2J$ on α, in order to obtain quantitative agreement between the calculated and experimental values , the calculated values had to be scaled by a factor of -800cm^{-1} !

Kida and coworkers [20] attempted a different *ab initio* unrestricted Hartree-Fock (UHF) formulation to describe the bridge angle dependence on the isotropic interaction

parameter for analogous methoxide bridged complexes. This method again gave results that were, trend-wise, in qualitative agreement with the observed type of paramagnetic behaviour, yet the authors were forced to admit that "agreement between [calculated and experimental] numerical values is poor" [20].

With the apparent quantitative deficiencies of computationally expensive *ab initio* calculations, the merits of the early theoretical frameworks of Hoffmann and coworkers and Kahn and coworkers gained much support [21,22], even from those presenting *ab initio* calculations [17]. With the above considerations in mind, the model study for phenoxide bridged copper(II) complexes presented in this thesis follows that proposed by Kahn [13,14], utilizing the extended Hückel program of Mealli and Proserpio [23].

Before continuing further with discussions of results obtained from extended Hückel calculations, a point of caution must be noted. Hoffmann [12] warns that the interpretation of extended Hückel results should remain at the qualitative level. Kahn is in agreement with this philosophy [24], and he has become a strong advocate of computational studies which utilize post Hartree-Fock wavefunctions including configuration interactions, as well as becoming an advocate of density functional studies [24,25].

1.6. Molecular Orbital Theory and Magnetism: The Concept of Accidental Orthogonality.

In order to provide a better understanding of the extended Hückel study of phenoxide bridged binuclear copper(II) systems to be presented later, it is of pedagogical value to introduce Kahn's theoretical model and the definition of accidental orthogonality. It is noteworthy that the theoretical models of Hoffmann and Kahn are not identical in algorithm, yet they reach the same final working equations which allow the dependence of $2J$ on structural parameters to be studied in the same way.

The main difference between the formulations of Hoffmann and Kahn originates in the type of *magnetic orbitals* that each uses. For binuclear compounds containing paramagnetic centres A and B, the magnetic orbital ϕ_A may be defined as a semilocalized orbital which is singly occupied by the unpaired electron arising from A [24]; it follows that ϕ_B is defined in an analogous manner. Hoffmann's formulation constructs strictly *orthogonalized* magnetic orbitals; alternatively, Kahn's formulation maintains that the magnetic orbitals are inherently *non-orthogonal* such that overlap between them is an essential feature of the interaction phenomenon [13a]. Kahn and coworkers have accordingly termed the non-orthogonal magnetic orbitals as being *natural* magnetic orbitals [26] .

These two different points of view lead to different interpretations of the *origin* of antiferromagnetic exchange. The (Hoffmann) orthogonal magnetic orbital model dictates that stabilization of the singlet state can only arise from an interaction between the ground

configuration and the metal-metal charge transfer configuration; hence, no antiferromagnetic exchange originates *directly* from the ground configuration. For the (Kahn) natural magnetic orbital model, both ferromagnetic and antiferromagnetic contributions arise from the ground configuration, and the interaction between ground and metal-metal charge transfer configurations is assumed to be negligible. A much more detailed comparison of the two models may be found in references [13a] and [24]. The following pages briefly describe the Kahn model and its successes with hydroxide bridged copper(II) compounds.

For a binuclear copper(II) system (denoted as Cu_ACu_B) with magnetic orbitals ϕ_A and ϕ_B, the ground state configuration $\phi_A\phi_B$ gives rise to a spin singlet and a spin triplet state, separated by an energy gap $2J$. Given the assumption that the interaction between the paramagnetic ions is weak, as a first approximation the MOs of the low-lying singlet and triplet states may be given by Heitler-London [27] wavefunctions of the form

$$\Psi_{S,T} = [\, 2\,(1 \pm S^2)\,]^{-\frac{1}{2}}\,[\,\phi_A(1)\phi_B(2) \pm \phi_A(2)\phi_B(1)] \qquad \ldots (1.6.1)$$

where the positive sign yields the singlet wavefunction and the negative sign yields the triplet wavefunction. In the normalization coefficient, S denotes the overlap integral between the magnetic orbitals:

$$S = \langle \phi_A \mid \phi_B \rangle \qquad \ldots (1.6.2)$$

The second assumption made is that the metal-metal charge transfer configurations $\phi_A\phi_A$ and $\phi_B\phi_B$ (spin singlet excited states) are too high in energy to couple with the ground configuration. This assumption is based on the fact that for Cu(II)-Cu(II) systems, the

Cu(III)-Cu(I) configuration has never been unambiguously detected by electronic spectroscopy [24]. Accordingly, this second order stabilization of the low lying singlet state may be neglected and the singlet-triplet energy gap $2J$ may be expressed simply as J_T, the sum of a positive ferromagnetic component, J_F, and a negative antiferromagnetic component, J_{AF}:

$$2J \equiv J_T = J_F + J_{AF} \qquad \ldots(1.6.3)$$

Expressions for J_F and J_{AF} may be now obtained after solving the eigenvalue equation for the wavefunctions of equation (1.6.1) using the electrostatic (non-phenomenological) Hamiltonian, the latter given by

$$\hat{H} = \mathbf{h}(1) + \mathbf{h}(2) + 1/r_{12} \qquad \ldots(1.6.4)$$

where $\mathbf{h}(i)$ is the one-electron Hamiltonian for electron i and r_{12} is the interelectronic distance. Extracting J_F and J_{AF} from the resulting eigenvalues yields [13]

$$J_{AF} = -2S(\Delta^2 - \tau^2)^{1/2} \qquad \ldots(1.6.5)$$

$$J_F = 2 \langle \phi_A(1)\phi_B(2) \,|\, (1/r_{12}) \,|\, \phi_A(2)\phi_B(1) \rangle = 2j \qquad \ldots(1.6.6)$$

where j is the two-electron exchange integral. Δ, as shown in Figure 1.6.1 (following page), is the energy difference between the singly occupied *molecular* orbitals γ_1 and γ_2 for the triplet state of Cu_ACu_B, derived from magnetic orbitals ϕ_A and ϕ_B. τ is the energy difference between the magnetic orbitals, and in the event that Cu_ACu_B is symmetrical, ϕ_A and ϕ_B have the same energy resulting in $\tau = 0$. Thus, for a symmetrical Cu_ACu_B system, equation (1.6.6) simplifies to

$$J_{AF} = -2S\Delta \qquad \ldots(1.6.7)$$

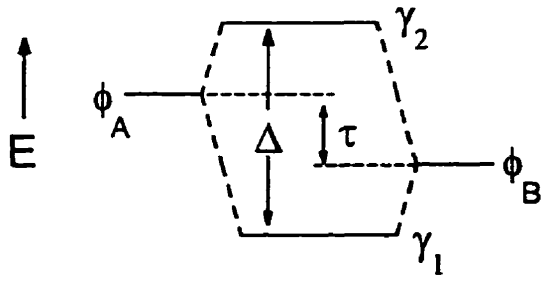

Figure 1.6.1. Relative energies of MOs γ_1 and γ_2 and their component magnetic orbitals ϕ_A and ϕ_B for an unsymmetrical Cu_ACu_B system.

Kahn and coworkers have shown [28] that at first order, S is proportional to Δ, and that Δ appears as the preponderant factor for J_{AF}. Hence, it is concluded that

$$J_{AF} \propto -\Delta^2 \qquad \ldots (1.6.8)$$

This expression for J_{AF}, along with equation (1.6.6) for J_F are the same expressions that Hoffmann derived for the qualitative dependence of $2J$ on molecular orbital energies. Since the MOs of a system are highly dependent on structural parameters such as the bridge angle in hydroxide, alkoxide or phenoxide bridged binuclear coordination compounds, this theory provides a means for predicting the expected magnetic behaviour for a given set of structural parameters. It may be evident from the above equations that MO studies which involve the stepwise variation of a structural parameter (such as bridge angle) for a given compound do not actually compute J_F, J_{AF} nor the crossover angle, α_c, at which $|J_F| = |J_{AF}|$ and overall $2J = 0$. Instead, the angle of *accidental orthogonality*, α_o, is the angle which is determined. The angle of accidental orthogonality is the angle at

which the energies of the MOs γ_1 and γ_2 are equal and $\Delta = 0$. It follows that at α_o, $J_{AF} = 0$ and the situation is completely analogous to the case when the magnetic orbitals are truly orthogonal.

The concept of accidental orthogonality may be illustrated by the classic extended Hückel study by Kahn and coworkers [14] for hydroxide bridged binuclear copper(II) compounds. This theoretical study hoped to yield the angle of accidental orthogonality for the system studied magnetostructurally by Hatfield and coworkers [10] (depicted in Figure 1.4.2) and therefore used the model coordination compound shown in Figure 1.6.2 below:

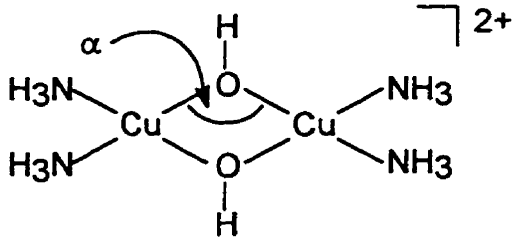

Figure 1.6.2. The model compound used by Kahn and coworkers to calculate the dependence of J_{AF} on α [14a].

Hatfield had shown for the set of planar hydroxide compounds studied in his magnetostructural correlation that the Cu-O and Cu-N bond lengths were relatively constant (1.92(2)Å and 1.98(2)Å, respectively). Accordingly, Kahn maintained constant Cu-O and Cu-N bond lengths, along with a constant N-Cu-N angle in his planar model compound. This revealed that the observed variations in the bridge angle could be viewed as a function of Cu···Cu separation. The extended Hückel results for the variation of α in the range of 85° - 110° are shown in Figure 1.6.3.

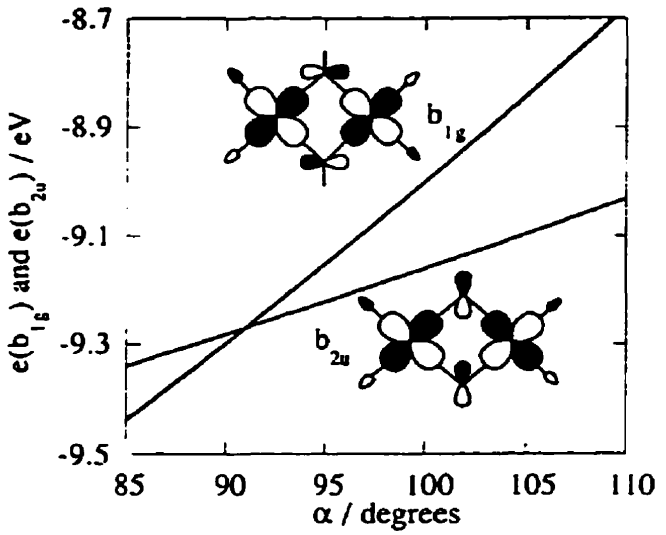

Figure 1.6.3. Variation in extended Hückel triplet MO energies for planar hydroxide bridged binuclear copper(II) compounds [24].

Two features of Figure 1.6.3 are noteworthy: 1) the trend in MO energy difference with decreasing bridge angle and 2) the angle of accidental orthogonality, α_o. Firstly, the plot shows a *decrease* in the energy difference Δ between the antisymmetric b_{1g} triplet MO and the symmetric b_{2u} MO with a *decrease* in Cu-OH-Cu angle α. Since $J_{AF} \propto \Delta^2$ (equation (1.6.8.)), this translates as a *decrease in the magnitude* of J_{AF} (making the always negative J_{AF} term more positive) with a *decrease* in bridge angle. *These MO calculations predict that 2J overall will increase with decreasing bridge angle* - exactly the behaviour that was described experimentally by Hatfield [10].

At α~91°, one finds that the triplet state MO energies are equal, and thus the MOs have become accidentally degenerate by simply varying only the bridge angle. This angle, α_o = 91°, is the angle of accidental orthogonality for the system. Recalling that Hatfield

had experimentally found the crossover angle for the same system to be $\alpha_C = 97.5°$, the distinction between α_C and α_o may be clearly understood. First of all, it must be realized that α_C and α_o have *no mathematical relationship to each other*. Remembering that J_F is always positive and J_{AF} is always negative or zero, for the magnetic behaviour of this system (an increase in $2J$ with an decrease in bridge angle) α_o will always be less than α_C for the following reasons:

1) At α_o, $J_{AF} = 0$; equation (1.6.8) yields:

$$2J = J_F$$

2) At α_C, $|J_F| = |J_{AF}|$; equation (1.6.8) yields:

$$2J = 0$$

This relationship is illustrated in Figure 1.6.4 and will be of interest when discussing the results of extended Hückel calculations for the analogous phenoxide study presented in this thesis.

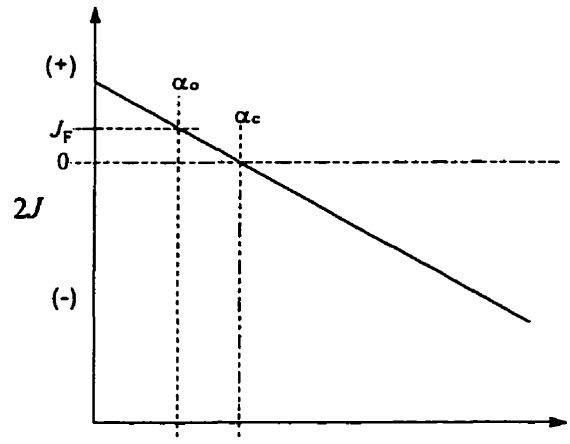

Figure 1.6.4. Illustration of α_o and α_C for a spin exchange system whereby $2J$ increases with a decrease in bridge angle.

While the hydroxide bridged compounds of Hatfield's magnetostructural correlation are all planar, this is not always the case for such bridged compounds [14,29]. For this reason, Kahn also studied [14] the dependence of $2J$ on dihedral angle, δ, for the hydroxide bridged system. The dihedral angle for the system was defined as the angle created by bending the molecule about the O-O axis, as depicted by Figure 1.6.5.

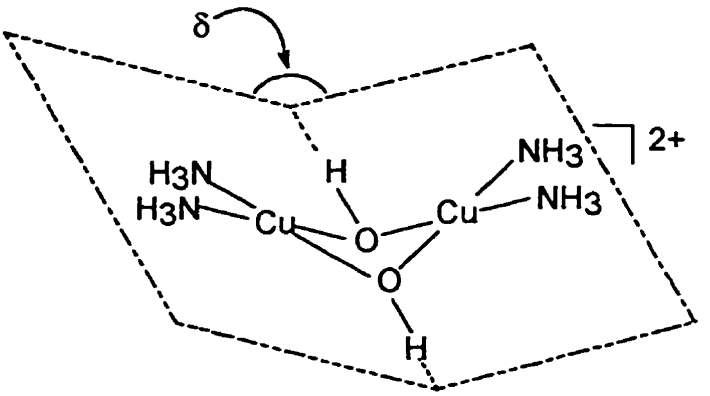

Figure 1.6.5. The model used by Kahn and coworkers [14] to calculate the dependence of J_{AF} on dihedral angle.

Assuming constant Cu-O and Cu-N bond distances along with constant N-Cu-N angles, Kahn varied δ and again monitored the energy difference Δ between the triplet MOs. The results of the study are shown in Figure 1.6.6 (following page). It is seen that by bending the molecule from planar (δ = 180°) to increasingly larger dihedral distortions (δ < 180°), the energy gap Δ becomes drastically smaller. This means that for the hydroxide bridge, J_{AF} becomes more positive (smaller in magnitude) as δ decreases from a planar to a dihedrally distorted structure and that overall, $2J$ will substantially increase for even small

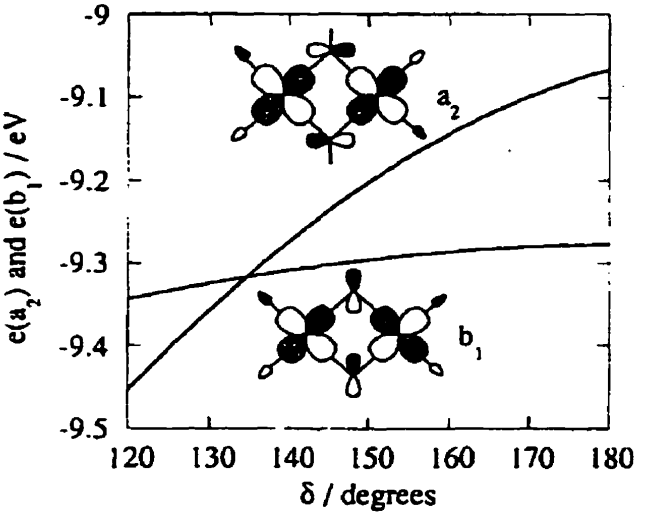

Figure 1.6.6. Variation in extended Hückel triplet MO energies with dihedral angle δ for hydroxide bridged binuclear copper(II) coordination compounds.

deviations from planarity. This dependence of $2J$ on dihedral angle is reflected in experimental data for non-planar hydroxide bridged copper(II) compounds, which were found to have higher than expected values of $2J$ when their bridge angles α are substituted into Hatfield's equation (1.4.1) for analogous planar compounds [14b].

1.7. Coordination Compounds of Binucleating Macrocyclic Hexadentate Ligands

In 1970 N.H. Pilkington and R. Robson [30] were the first to report the synthesis of the macrocyclic binucleating ligand framework shown in Figure 1.7.1. By simply combining 2,6-diformyl-4-methylphenol (DFMP), 1,3-diaminopropane and various M^{2+} cations of the first transition series under template conditions, Robson obtained

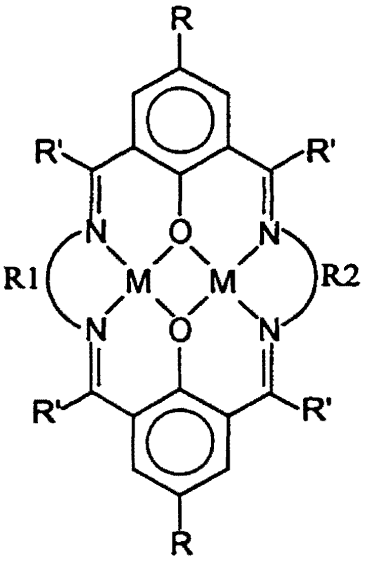

Figure 1.7.1 Binuclear Schiff base macrocyclic coordination compounds containing two phenoxide bridges. R1, R2 denote spacer groups.

symmetrical coordination compounds (R1 = R2 = $(CH_2)_3$) for M^{2+} = Cu^{2+}, Ni^{2+}, Co^{2+}, Fe^{2+}, Mn^{2+} and Zn^{2+}. Less than two years later, H. Ōkawa and S. Kida [31] used a linear synthetic strategy, building unsymmetrical (R1 ≠ R2) binuclear coordination compounds in a step-wise fashion for Cu^{2+} and Ni^{2+}. Since these pioneering reports, many authors have utilized these synthetic strategies to synthesize a variety of symmetrical and unsymmetrical binuclear phenoxide bridged coordination compounds containing a very wide variety of metal ions, chelating groups and substituents (R, R') [32-43].

A magnetostructural correlation has recently been proposed for phenoxide bridged binuclear copper(II) macrocycles [8], somewhat analogous to that of Hatfield [10] for the

hydroxide bridge system. The symmetrical (R1 = R2) copper(II) coordination compounds considered [37,38,40,44,45] all have simple aliphatic C_2 - C_4 chains as spacer groups. The binuclear core is either planar or virtually planar in all cases, and the ground state magnetic orbital of each copper(II) centre has $d_{x^2-y^2}$ symmetry. Furthermore, the binuclear core is in all cases devoid of any unusual structural or electronic perturbations that could be perceived to influence exchange in any significant manner. After taking these factors into account, the dependence of $2J$ on average phenoxide bridge angle (α) was considered. A variation in $2J$ from -689 to -902 cm^{-1} was found for a parallel variation in α from 98.2° to 104.7° [8]. Figure 1.7.2 shows a plot of the data, which yields a reasonable linear

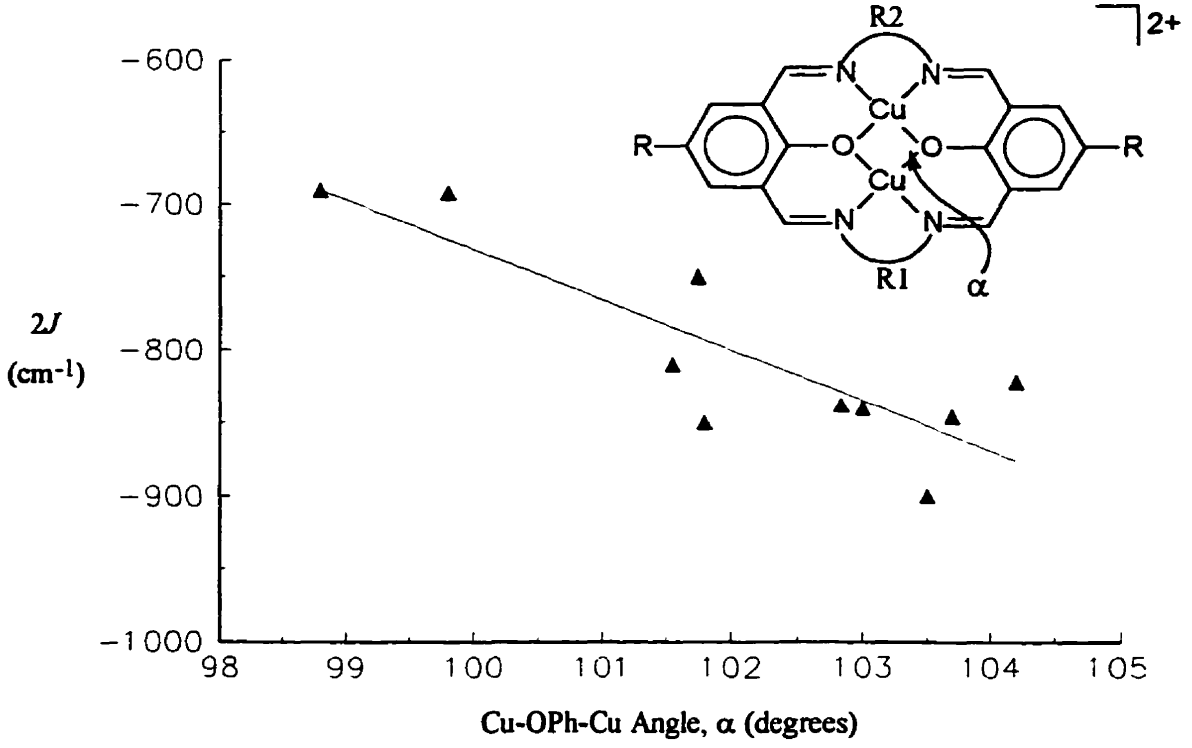

Figure 1.7.2. Plot of the isotropic interaction parameter, $2J$, versus Cu-OPh-Cu angle, α.

correlation of

$$2J\,(cm^{-1}) = -31.95\alpha(\text{degrees}) + 2462 \qquad \ldots (1.7.1)$$

The surprising result of this phenoxide bridge magnetostructural correlation is the extremely small predicted crossover angle of $\alpha_c = 77°$! This result is well below that of the alkoxide bridge correlation ($\alpha_c = 95.7°$, [11]) or the hydroxide bridge correlation ($\alpha_c = 97.5°$, [10]) presented earlier. Considering the closed nature of the binucleating macrocycles, it is highly unlikely that such low bridge angles can be achieved experimentally: at such low angles the Cu_2O_2 core would be very compressed, with very small Cu···Cu separations. This latter point accordingly brings about the following hypothesis:

> *It seems likely that all phenoxide bridged binuclear copper(II) macrocycles will experimentally exhibit overall antiferromagnetic behaviour even with very small bridge angles α.*

Such a bold statement can only achieve credibility with supporting experimental evidence. This thesis will describe a series of diaminomaleonitrile-derived macrocyclic coordination compounds, and one derivative that still exhibits antiferromagnetic coupling at $\alpha = 92.4°$. In addition, an extended Hückel MO study for the variation of J_{AF} with α for a related phenoxide bridged binuclear copper(II) model system will be presented.

1.8. Diaminomaleonitrile - a Precursor to Symmetrical Robson-Type Macrocycles

It was suggested in 1928 [46] that the tetramer obtained via base polymerization of hydrogen cyanide had the structure of diaminomaleonitrile (DAM, Figure 1.1.1). This structure was not confirmed until 1961 when Penfold and Lipscomb [47] obtained a single crystal X-ray diffraction structure of the molecule. In the years that followed, there were surprisingly few reports of the use of DAM in coordination chemistry, possibly due to its unusual reactivity.

Despite its symmetric structure, DAM has generally been found to react *unsymmetrically* in the formation of both ligands as well as metal coordination compounds. For example, condensation of DAM with salicylaldehyde yields the 1:1 Schiff base condensation product 1-amino-2-salicylideneamino-(Z)-1,2-dicyanoethene (HsalDAM, Figure 1.8.1a) *irrespective* of the amount of aldehyde used [48]. In the absence of a templating metal ion, the only means of generating the 1:2 DAM:salicylaldehyde product (H_2disalDAM, Figure 1.8.1b) is by the addition of sulphuric

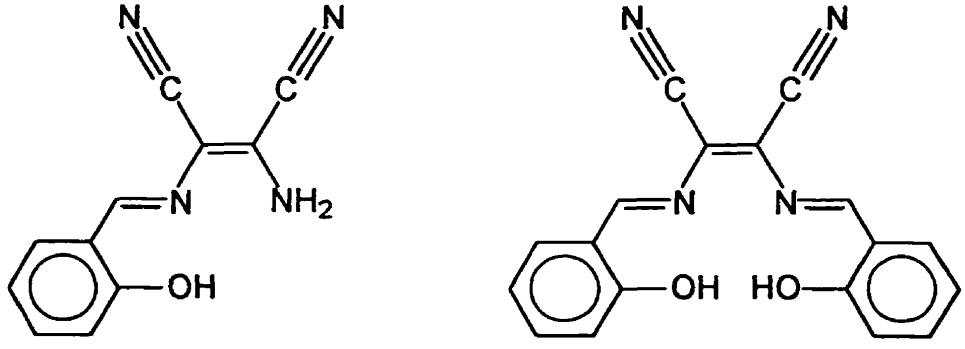

a) HsalDAM b)H_2disalDAM

Figure 1.8.1. Ligands derived from the Schiff base condensation of a) 1:1 DAM:salicylaldehyde and b) 1:2 DAM:salicylaldehyde.

acid or phosphorus pentoxide [49,50]. Regarding its metal complexes, DAM was first reported to react unsymmetrically as a monodentate amine with Na_2PdCl_4 in acidic media [51]. It was later reported that d^8 M^{2+} ions in basic media yielded *symmetrical* DAM coordination compounds, affording neutral $[M(C_4H_2N_4)_2]$ molecules (Figure 1.8.2). Both DAM molecules lose two hydrogens (one at each amino nitrogen) upon coordination, resulting in a delocalized π-electron system according to the x-ray structure determination [52].

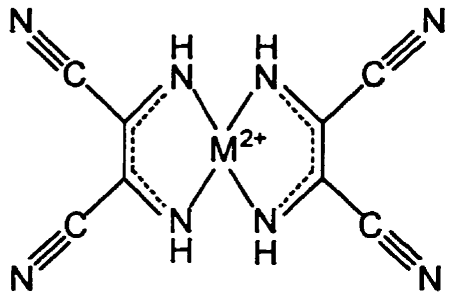

Figure 1.8.2. Schematic of the symmetrical coordination compounds derived from a d^8 metal ion (Ni^{2+}, Pd^{2+}, Pt^{2+}) and two doubly-deprotonated DAM ligands [52].

In 1976 Iwamoto and Suzuki demonstrated that copper(II) is able to template the condensation of salicylaldehyde and DAM to form the coordination compound [Cu(disalDAM)] (refer to Figure 1.8.1b) although no structure was reported [49]. More recent studies of the coordination compounds formed from the templated Schiff-base condensation of DAM with polymeric formylphenols have yielded materials with interesting catalytic [53] and non-linear optical properties [54].

Diaminomaleonitrile is a very attractive precursor for the formation of symmetrical Robson-type coordination compounds. The binuclear M^{n+} coordination compounds that should result after templating the [2+2] condensation of a 2,6-diformyl-4-(R)phenol (R = CH_3, t-Bu) and DAM are shown in Figure 1.8.3. These very interesting compounds may be studied from a number of points of view.

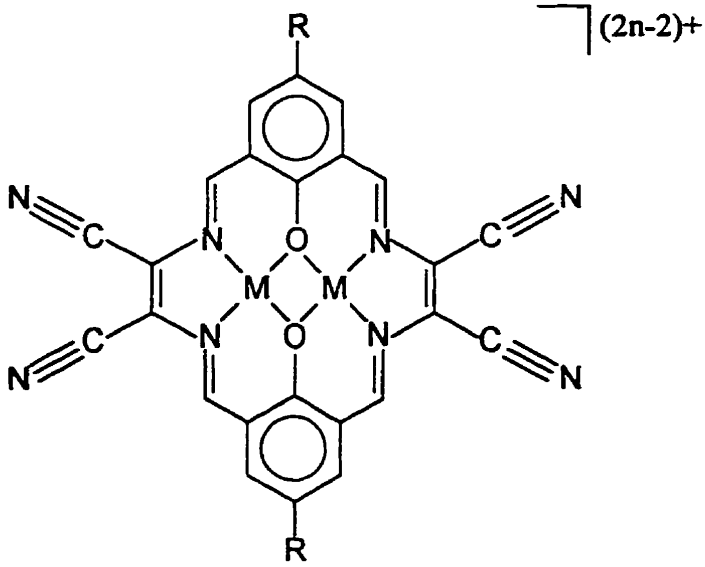

Figure 1.8.3. The proposed Robson-type macrocyclic coordination compounds from the diamine diaminomaleonitrile (R = CH_3, t-Bu).

First of all, the effect of the electron-withdrawing cyano functions on the isotropic exchange parameter, $2J$, may be ascertained from temperature dependent magnetic susceptibility data. The cyano functions are linked to the Cu_2O_2 core by a π-electron framework and thus it is expected that the copper(II) centres would have enhanced electropositive character. Such electropositive character would most likely be reflected in

the electrochemical properties of these compounds as well.

Secondly, the cyano functions may provide enormous synthetic potential. Organic elaboration of the cyano functions has been carried out [55], resulting in new extended phthalocyanine and hemiporphyrazine-like ligands. Preliminary results indicate that extensive elaboration of these peripheral cyano functions to yield polydentate ligands is quite likely [55].

Finally, it may be possible to utilize the potential σ-donor capabilities of the cyano functions to yield high-nuclearity compounds (Figure 1.8.4). Should paramagnetic ions be coordinated at each cyano function, the resulting compound may have very interesting magnetic properties - especially given the extensively conjugated electronic structure of the macrocyclic ligand.

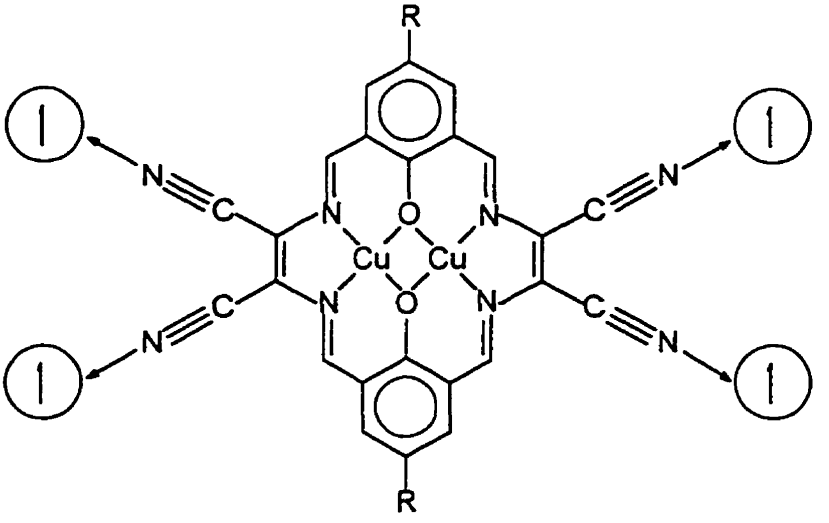

Figure 1.8.4. High-nuclearity coordination compound obtained upon coordinating paramagnetic ions (schematically denoted by half-arrows in circles) in σ-fashion to the cyano functions.

1.9. The Objective of the Research Presented in this Thesis

This thesis reports the synthesis and characterization of macrocyclic (Figure 1.9.1) and non-macrocyclic (Figure 1.9.2) ligands derived from formylphenols and diamino-maleonitrile under template conditions using copper(II) and nickel(II) salts. It should be noted that "M" denotes a macrocyclic ligand while "L" denotes a non-macrocyclic ligand. The magnetochemistry and cyclic voltammetry of the copper(II) coordination compounds will be presented, and an extended Hückel computational study, as described in the introduction, will be presented to provide further understanding of the observed magnetic properties of binucleating dicopper(II) coordination compounds of Schiff base derived ligands containing bridging phenoxide groups.

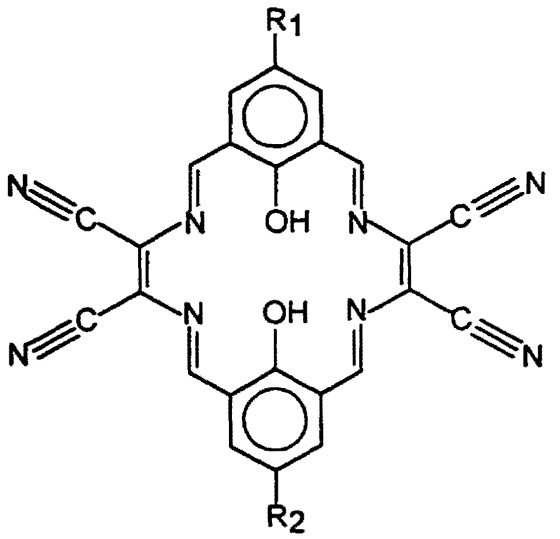

$R_1, R_2 = CH_3, CH_3$ (H_2M1)

R_1, R_2 = t-Bu, t-Bu (H_2M2)

$R_1, R_2 = CH_3$, t-Bu (H_2M3)

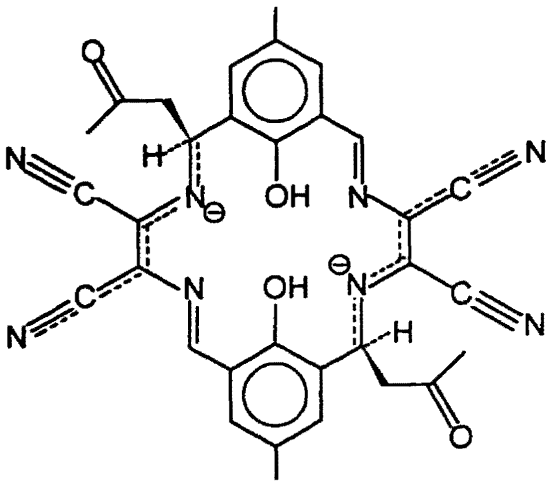

H_2M4^{2-}

Figure 1.9.1. Macrocyclic ligands presented in this thesis.

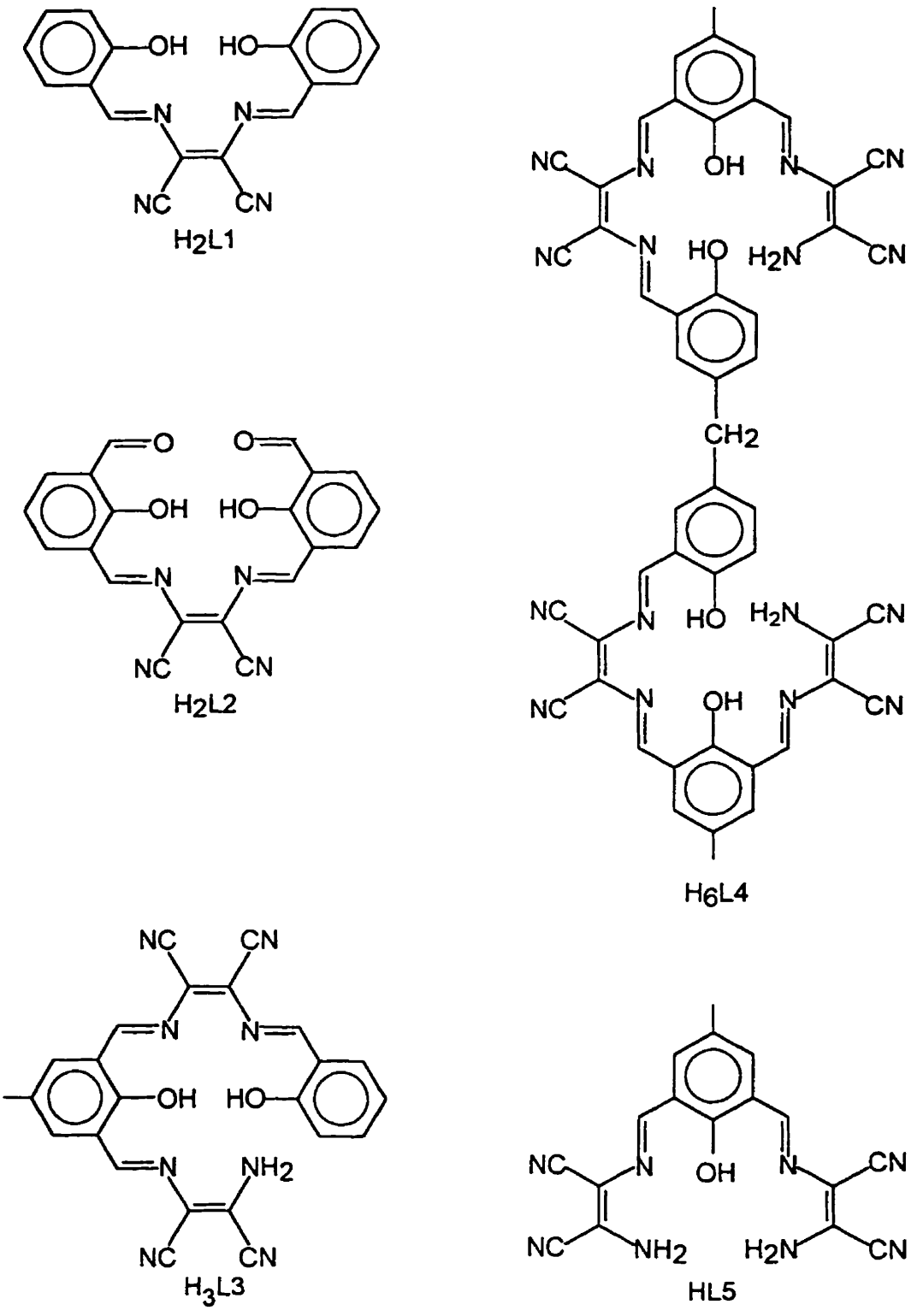

Figure 1.9.2. Non-macrocyclic ligands and ligand precursors presented in this thesis.

2. Experimental

2.1. Physical Measurements

Infrared spectra were recorded as Nujol mulls on KBr disks using a Mattson Polaris FT-IR instrument calibrated at $4cm^{-1}$ resolution. Solution UV-visible spectra were recorded using matched quartz cells with a Cary 5E spectrometer. X-ray diffraction data was obtained using a Rigaku AFC6S diffractometer with graphite monochromated Mo Kα radiation and a 2kW sealed tube generator.

Metal analyses were determined by flame AA spectroscopy using a Varian Techtron AA-5 instrument, while C,H,N analyses were performed by Canadian Microanalytical Service, Delta, BC, Canada. Mass spectra were obtained using a VG Micromass 7070HS spectrometer.

Electrochemical data were recorded at room temperature in dimethylsulfoxide (dried over molecular sieves) under O_2-free conditions on a BAS CV27 voltammograph with a BAS X-Y recorder. The electrochemical cell consisted of a Pt wire auxiliary electrode, a SCE reference electrode and a glassy-carbon-disk working electrode. Concentrations of 0.1 $mol{\cdot}L^{-1}$ supporting electrolyte (tetraethylammonium perchlorate (TEAP)) and 10^{-3} - 10^{-4} $mol{\cdot}L^{-1}$ coordination compound were used in the cell. Potentials were recorded versus SCE.

Room temperature magnetic susceptibilities were recorded by the Faraday method using a Cahn 7600 Faraday Magnetic Balance. Variable temperature magnetic data

collection (4-305K) was performed on an Oxford Instruments superconducting Faraday Susceptometer equipped with a Sartorius 4432 microbalance, employing a main solenoid field of 1.5T and a gradient field of $10T \cdot m^{-1}$. $Hg[Co(NCS)_4]$ was used as a calibration standard for both instruments.

2.2. Syntheses of Mononuclear and Polynuclear Copper(II) Compounds by Template Methods.

Commercially available reagents were used as received without further purification. 2,6-diformyl-4-methylphenol (DFMP) and 2,6-diformyl-4-t-butylphenol (DFTBP) were synthesized according to standard literature procedures (references [33] and [56], respectively). Methylene-4,4'-bis(salicylaldehyde) was provided by Z. Xu and was synthesized according to a literature procedure [57].

Safety Cautions:

Perchlorate salts are strong oxidants and furthermore, perchlorate coordination compounds are potentially explosive. To test the explosive potential of these compounds, controlled mechanical impact of small samples was regularly performed. Though the small quantities used in this study presented no hazards, caution should be exercised at all times when dealing with such materials.

Subjecting bare skin to either DFMP or DFTBP causes a yellow discolouration of the skin which persists for several days. For this reason, it is suggested that plastic gloves should be used when handling these materials.

$[Cu_2M1](ClO_4)_2(H_2O)_3(CH_3OH)$, **(1)**

DFMP (0.164g, 1.00mmol) and copper(II) perchlorate hexahydrate (0.371, 1.00mmol) were dissolved together in methanol (75mL), resulting in a pale green solution. After refluxing the solution for five minutes, a solution of DAM (0.108g, 1.00mmol) in methanol (20mL) was added dropwise. Within a few seconds the reaction mixture appeared as a thick red-brown suspension, which was allowed to reflux for 48 hours. The mixture was then allowed to cool to room temperature and the resulting maroon solid was filtered off, washed with 3x5mL portions of cold methanol, and dried under vacuum. Yield: 0.33g, 81%. Anal. Calc'd for $[Cu_2(C_{26}H_{14}N_8O_2)](ClO_4)_2(H_2O)_3(CH_3OH)$, **(1)**: C, 36.74; H, 2.75; N, 12.70; Cu, 14.41. Found C, 36.51; H, 2.48; N, 12.94; Cu, 14.66.

$[Cu_2M2](ClO_4)_2$, **(2)**

Using DFTBP, **(2)** was prepared in a manner completely analogous to **(1)**. Yield: 45%. Anal. Calc'd for $[Cu_2(C_{32}H_{26}N_8O_2)](ClO_4)_2$ **(2)**: C, 43.64; H, 2.98; N, 12.72; Cu, 14.43. Found C, 43.24; H, 3.05; N, 12.64; Cu, 14.45.

HL5: 2,6-bis(N-(2'-amino-(Z)-1',2'-dicyanoetheneimino))-4-methylphenol, **(3)**

HL5 (Figure 1.9.2) was synthesized according to a procedure outlined by Dickson and Robson [58] for an analogous compound. DFMP (1.68g,10.2mmol) was dissolved in 1:1 methanol:ethanol (85mL). The clear yellow solution was brought to reflux and a solution of DAM (5.38g, 49.8mmol) in hot methanol (35mL) was added. After three minutes of

refluxing and stirring, a very thick beige-orange suspension was obtained. Vigorous stirring and reflux were maintained for another 30 minutes, at which time the suspension had become yellow in colour and very thick. The suspension was allowed to cool to room temperature and the yellow solid was filtered, washed with 2x10mL portions of cold methanol and dried under vacuum. Yield: 2.09g, 87%. Anal. Calc'd for $C_{17}H_{11}N_8O$ **(3)**: C, 59.30; H, 3.51; N, 32.54. Found: C, 59.14; H, 3.61; N, 30.95. Mass spectral data: 344 (89.68%, M^+), 252 (66.67%, M^+ - $C_4H_2N_3$ chain), 237 (100%, (M^+ - $C_4H_2N_3$)-NH), 224 (53.97%, M^+- $C_5H_3N_4$ chain). **(3)** was utilized in the templated syntheses of $M3^{2-}$, $L3^{3-}$, and $L4^{6-}$ without further purification.

$[Cu_2M3](ClO_4)_2(H_2O)_2$, **(4)**

This compound was synthesized according to a procedure outlined by Nag and coworkers [35, 59] for a similar system. HL5 ((**3**); 0.348g, 1.01mmol) was suspended in methanol (50mL) with copper(II) perchlorate hexahydrate (0.755g, 2.04mmol), yielding a brown suspension. The brown mixture was heated to almost reflux when DFTBP (0.208g, 1.01mmol) in methanol (20mL) was added. After five minutes of heating and stirring, the reaction mixture assumed a red-brown colour. The mixture was heated at reflux for 48 hours, then was allowed to cool to room temperature. The resulting garnet coloured solid was filtered and washed with 2x10mL portions of cold methanol and dried on the vacuum line. Yield: 0.58g, 68%. Anal. Calc'd for $[Cu_2(C_{29}H_{20}N_8O_2)](ClO_4)_2(H_2O)_2$ **(4)**: C, 39.83; H, 2.77; N, 12.81; Cu, 14.53. Found: C, 39.80; H, 2.76; N:13.04; Cu, 14.88.

[Cu_2M4](CH_3COCH_3), **(5)**

(1) (0.230g, 0.260mmol) was suspended in acetone (15mL) in a well sealed 25mL vial. The vial was then mechanically shaken for five minutes. The resulting red suspension was filtered through a slow filter paper (Whatman #5) into a clean 25mL vial. The vial and the resulting clear ochre red solution were then placed in a jar containing approximately 50mL of hexane. The jar was sealed tightly and placed in the dark, undisturbed, for three days. After this time, dark orange-brown crystals formed which were suitable for x-ray diffraction. Yield: 0.036g, (18%). Anal. Calc'd for [$Cu_2C_{32}H_{24}N_8O_4$](CH_3COCH_3) **(5)**: C, 54.61; H, 3.93; N, 14.56. Found C, 54.38; H, 4.06; N, 14.24.

[CuL1], **(6)**

[CuL1] was originally synthesized by Iwamoto and Suzuki [49], yet they encountered trouble in obtaining pure samples and no x-ray crystal structure was reported. Our laboratory has recently reported the x-ray crystal structure of **(6)** from a pure sample prepared by MacLachlan [60].

[CuL2(CH_3SOCH_3)], **(7)**

Recrystallization of a sample of **(1)** in undried dimethylsulfoxide yielded deep red crystals of **(7)** which were suitable for x-ray diffraction. Anal. Calc'd for [Cu($C_{22}H_{14}N_4O_4$) (C_2H_6SO)] **(7)**: C, 53.38; H, 3.73; N, 10.37. Found C, 53.61; H, 3.70; N, 10.69.

$[Cu_2L3](ClO_4)(C_2H_5OH)$, **(8)**

HL5 ((**3**); 0.612g, 1.78mmol) was added to a 1:1 ethanol:methanol (75mL) solution of copper(II) perchlorate hexahydrate (1.45g, 3.91mmol) yielding a khaki coloured suspension. This suspension was stirred and heated to almost reflux when salicylaldehyde (0.221g, 1.81mmol) in methanol (15mL) was added, yielding a brown coloured suspension after ten minutes of stirring. Reflux was reached and sustained with stirring for 48 hours. After this time the brown suspension was allowed to cool in an ice bath, then was filtered under suction. The dark brown solid obtained was washed with 3x5mL portions of cold methanol and dried under vacuum for 24 hours. Yield: 1.07g (89%). Anal. Calc'd for $[Cu_2(C_{24}H_{13}N_8O_2)](ClO_4)(C_2H_5OH)$ (**8**): C, 43.49; H, 2.67; N, 15.61; Cu, 17.70. Found C, 44.01; H, 2.48; N, 15.44; Cu, 17.76.

$[Cu_4L4](ClO_4)_2(C_2H_5OH)_2$, **(9)**

Copper(II) perchlorate (1.02g, 2.75mmol) was stirred with HL5 ((**3**); 0.449g, 1.30mmol) in 1:1 ethanol:methanol (50mL), resulting in a khaki coloured suspension. The suspension was heated to near reflux with stirring. Methylene-4,4'-bis(salicylaldehyde) in methanol (20mL) was added, yielding a brick red suspension upon complete addition. At ten minutes past complete addition, the colour of the suspension had evolved to a very dark brown hue which persisted without change after 48 hours of stirring. Suction filtration of the ice cold reaction mixture yielded a very dark brown solid which was washed with 3x5mL portions of cold methanol and dried under vacuum. Yield: 0.775g (88%). Anal.

Calc'd for $[Cu_4(C_{49}H_{26}N_{16}O_4)](ClO_4)_2(C_2H_5OH)_2$ **(9)**: C, 43.96; H, 2.65; N, 15.48; Cu, 17.55. Found C, 44.51; H, 2.60; N, 15.71; Cu, 17.26.

2.3. General Comments Regarding the Solubility and Crystallization Attempts of the Polynuclear Copper(II) Coordination Compounds Presented.

The polynuclear copper(II) compounds **(1)**, **(2)**, **(4)**, **(8)** and **(9)** obtained directly from template syntheses exhibit similar solubility properties. All are insoluble in water, and the solubility of these compounds in lower alcohols and tetrahydrofuran is poor. Nitromethane and nitrobenzene proved to be somewhat better solvents for these compounds in comparison to alcohols, yet *N*, *N*-dimethylformamide, dimethylsulfoxide and acetonitrile were the only common solvents in which these compounds have any significant degree of solubility. It is this limited solubility in all other solvents except the latter three strong donor solvents which made crystal growth very difficult for this system. Attempts to recrystallize the macrocyclic complexes **(1)** and **(2)** from methanolic solutions yielded maroon needles with insufficient volume for an x-ray diffraction experiment. Furthermore, when **(1)** and **(2)** are dissolved in methanol in the presence of pyridine, the copper(II) ion is removed from the coordination compound by the strong Lewis base solvent. All attempts to concentrate or diffuse a more volatile solvent into nitromethane or nitrobenzene solutions of **(1)** and **(2)** yielded clean powders of the binuclear macrocyclic coordination compounds. *N*, *N*-dimethylformamide and dimethylsulfoxide facilitated relatively concentrated solutions of **(1)**, **(2)**, **(4)**, **(8)** and **(9)**, yet were reluctant

to release either crystals or powders of these compounds back into the solid phase. The most promising results for attempts at crystallizing these compounds were found using acetonitrile as a solvent. After individually obtaining clear dark maroon solutions of **(1)**, **(2)**, **(4)**, **(8)** or **(9)** in acetonitrile, slightly more than the equivalent amount of NH_4PF_6 that was required to exchange with the perchlorate anion was dissolved in the solution. The vial containing the maroon solution was then placed in a tightly covered jar containing sufficient diethylether to cover the bottom of the jar, and the jar was sealed tightly. Upon ether diffusion into the maroon solution over a 1-2 day period, red crystals with dimensions of approximately 0.5mm x 0.4 mm x 0.3mm were obtained. Unfortunately, these crystals appeared to lose lattice solvent immediately upon isolation from the solvent and upon cutting a cross-section of an isolated crystal, it was revealed that the crystal integrity was lost.

3. Discussion of Results

3.1. Description of X-Ray Diffraction Structures

$[Cu_2M4](CH_3COCH_3)$, **(5)**

The molecular structure of $[Cu_2M4](CH_3COCH_3)$ is displayed from two perspectives in Figures 3.1.1 and 3.1.2, with bond distances and angles relevant to the copper coordination spheres listed in Table 3.1.1. The coordination compound results from the addition of two negatively charged acetonyl ($CH_3COCH_2^{\ominus}$) groups to the azomethine carbons of two opposite Schiff base imine groups in **(1)**, resulting in M4 having a overall charge of 4- (the mechanism of the acetonyl addition will be discussed later in Section 3.2). Figure 3.1.1 yields a deceptive view of the molecule, as the macrocyclic framework appears at a first glance to be planar from this perspective; in fact, the macrocycle is highly distorted from planarity, as shown clearly by the perspective of Figure 3.1.2. The molecule has a saucer-like shape, with both acetonyl groups (bonded to C(8) and C(18)) projected off the convex face of the saucer-like conformation. The high degree to which the macrocyclic ligand framework is bent is ascertained from the 151.1° angle between the N_2O_2 mean coordination planes about the O(1)-O(2) axis, and angle sums of 335.7° and 337.7° at O(1) and O(2), respectively. The six membered chelate rings Cu(1)-N(4)-C(18)-C(16)-C(17)-O(2) and Cu(2)-N(2)-C(8)-C(6)-C(7)-O(1) have boat structures, facilitated by the flexibility of the *tetrahedral* C(8) and C(18) carbons.

The binuclear Cu_2O_2 core has the smallest dimensions of any known phenoxide

Table 3.1.1. Interatomic Distances (Å) and Angles (deg.) Relevant to the Copper Coordination Spheres in $[Cu_2M4](CH_3COCH_3)$, **(5)**.

Cu(1) Cu(2)	2.788(2)	Cu(1) Cu(2) O(1)	43.1(1)
Cu(1) O(2)	1.942(5)	Cu(1) Cu(2) O(2)	44.1(2)
Cu(1) N(4)	1.886(6)	Cu(1) Cu(2) O(2)	136.1(2)
Cu(2) O(2)	1.908(5)	Cu(1) Cu(2) N(3)	133.7(2)
Cu(2) N(3)	1.917(7)	O(1) Cu(2) N(2)	94.5(3)
Cu(1) O(1)	1.905(5)	O(1) Cu(2) N(3)	170.0(3)
Cu(1) N(1)	1.913(7)	O(2) Cu(2) N(2)	175.8(3)
Cu(2) O(1)	1.970(5)	O(2) Cu(2) N(3)	95.9(3)
Cu(2) N(2)	1.878(6)	N(2) Cu(2) N(3)	85.7(3)
O(1) Cu(1) O(2)	85.5(2)	Cu(1) O(1) Cu(2)	92.0(2)
O(1) Cu(1) N(1)	95.5(3)	Cu(1) O(1) C(7)	124.0(5)
O(1) Cu(1) N(4)	174.1(3)	Cu(2) O(1) C(7)	119.7(5)
O(2) Cu(1) N(1)	167.1(3)	Cu(1) O(2) Cu(2)	92.8(2)
O(2) Cu(1) N(4)	93.5(3)	Cu(1) O(2) C(17)	120.9(5)
N(1) Cu(1) N(4)	86.8(3)	Cu(2) O(2) C(17)	124.0(5)

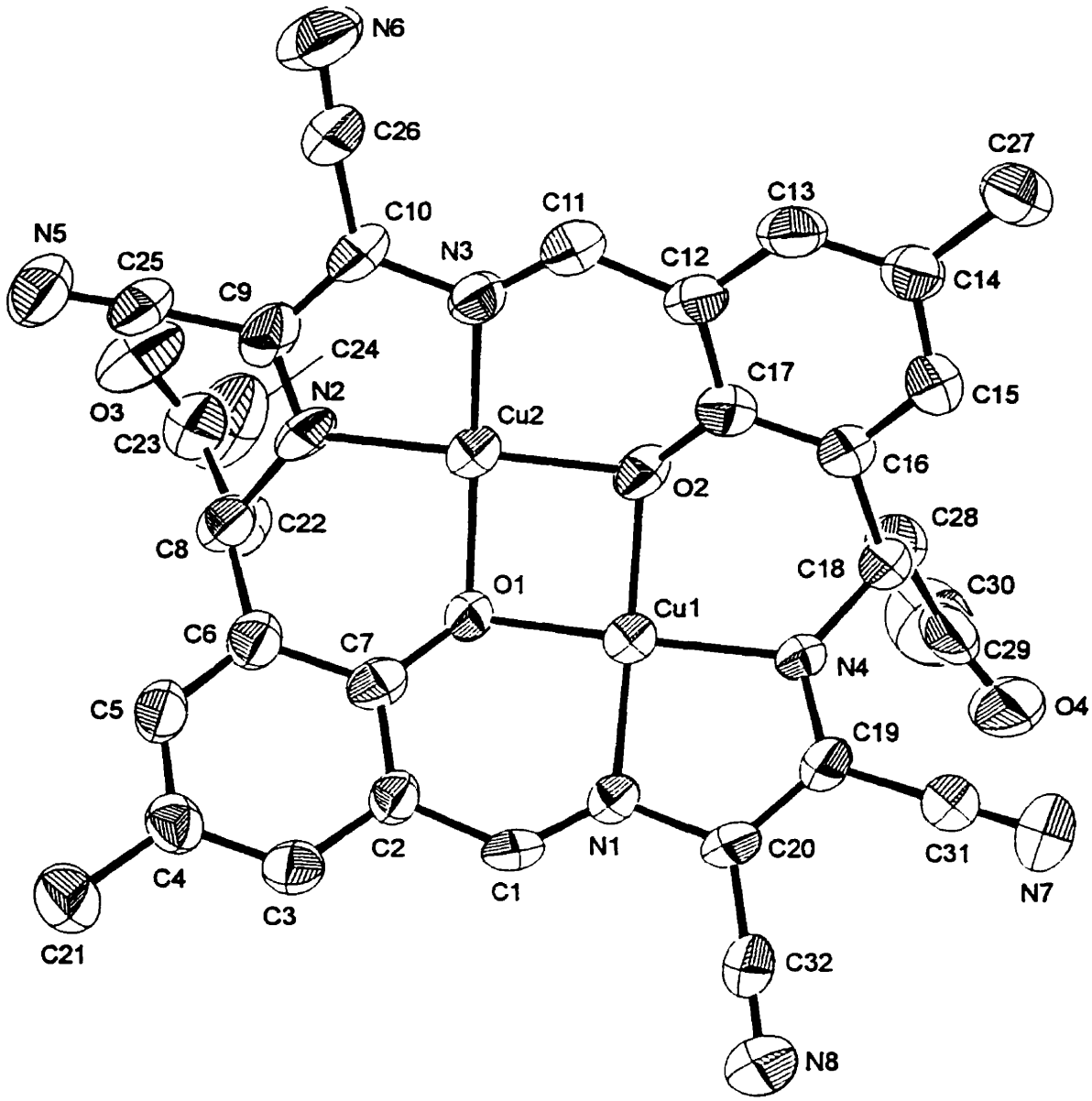

Figure 3.1.1. X-ray crystal structure of $[Cu_2M4](CH_3COCH_3)$, **(5)** (lattice acetone and hydrogens have been removed for clarity) viewed down onto the Cu_2O_2 core.

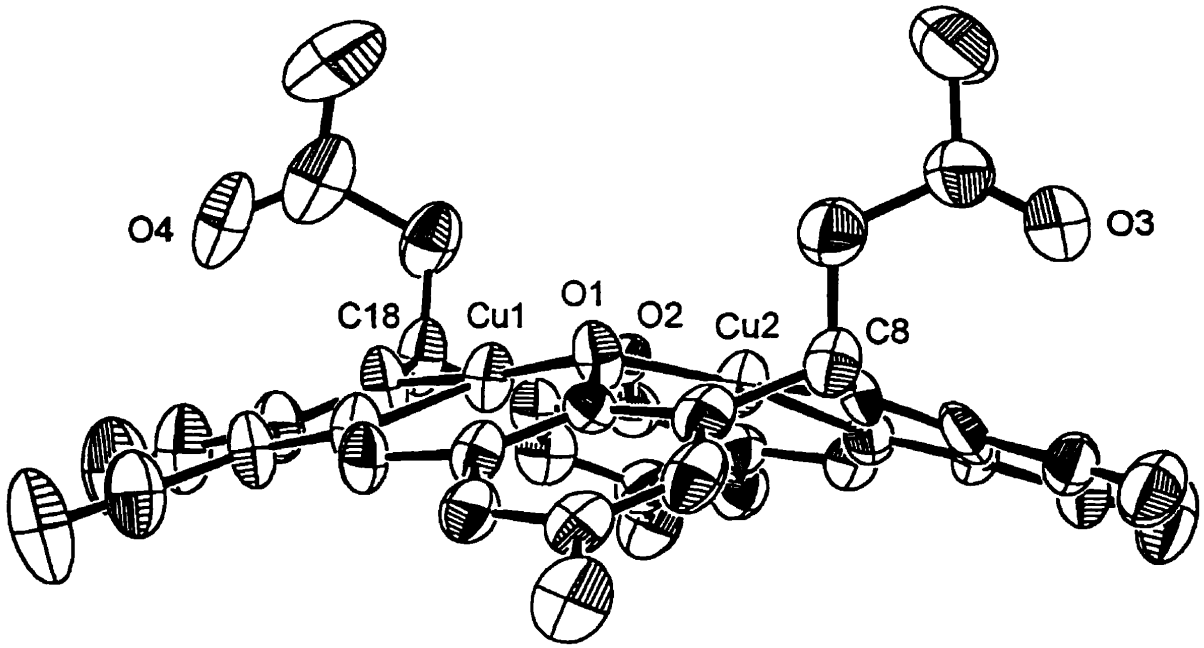

Figure 3.1.2. X-ray crystal structure of **(5)** viewed along the O-O axis.

bridged binuclear copper(II) macrocyclic compound. The Cu···Cu separation is 2.788(2) Å, while the Cu-OPh-Cu bridge angles are 92.0(2)° and 92.8(2)°. To date, no other examples of analogous macrocyclic coordination compounds containing a simple two-carbon olefinic spacer group have been reported. However, Brychcy and coworkers [61] have reported a series of (symmetrical) Robson-type binuclear copper(II) macrocyclic compounds with *o*-phenylenediamine derived spacer groups. In contrast to the structure of **(5)**, Brychcy reports the crystal structures of four essentially flat binuclear copper(II) macrocyclic compounds with C_6H_4 and C_6F_4 spacers between Schiff base imine groups. These coordination compounds have much larger Cu_2O_2 cores, with Cu···Cu separations ranging from 2.886-2.940 Å and Cu-OPh-Cu bridge angles in the range of 97.9-100.9° [61]. Robson-type macrocycles with two-carbon aliphatic spacer groups are also very rare. The x-ray crystal structure has been reported for the binuclear copper(II) compound that results from the template condensation of 2,6-diacetyl-4-methylphenol with ethylenediamine [8], and this structure has Cu_2O_2 core dimensions comparable to the structures reported by Brychcy [61]. This macrocyclic compound is essentially flat; the sum of the angles at the oxygen bridge is 357.0°, indicating only minor distortions from planarity. For the binuclear core, a Cu···Cu separation of 2.997(3) Å and a Cu-OPh-Cu bridge angle of 98.8(4)° are observed [8]. From these comparisons to the closest structural analogs, it is seen that **(5)** has a Cu_2O_2 core with both an extremely small Cu···Cu separation and a very low average phenoxide bridge angle.

It is suspected that **(1)**, the parent compound of **(5)**, has a planar structure due to

the extensive π conjugation throughout the ligand framework. This is reasonable since the highly planar crystal structures reported by Brychcy [61] and MacLachlan, Park and Thompson [60] all have extensive π conjugation similar to **(1)**. Alternatively, the structure of **(5)** exhibits extreme distortions from planarity, with tetrahedral (former azomethine) carbons at C(8) and C(18). It follows that the ligand structure of **(5)** cannot be expected to have the same extent of π conjugation as that of its parent **(1)** or even the non-macrocyclic compound [CuL1], **(6)**. Accordingly, the modified ligand π framework of the acetonyl adduct **(5)** is expected to be reflected in the bond lengths of the macrocyclic ligand. For comparison purposes, the crystal structure of [CuL1], **(6)**, follows in Figure 3.1.3. The imine groups and the DAM fragment in this compound have retained a normal tautomeric π structure, as indicated by the bond lengths and angles within the C(7)-N(1)-C(8)-C(9)-N(2)-C(10) chain. The Schiff base linkages of C(7)-N(1) and C(10)-N(2) have expected lengths for such double bonds (1.309(5) Å and 1.294(5) Å, respectively) and the C(8)-C(9) bond of the DAM fragment has retained the expected olefinic bond length (1.338(6) Å). For the cyano functions of **(6)** the C(8)-C(17), C(9)-C(18) linkages may be considered as pure single bonds (1.447(5) Å and 1.440(6) Å, respectively) while the C(17)-N(3) and C(18)-N(4) linkages may be considered as pure triple bonds (1.133(5) Å and 1.139(5) Å, respectively). Comparison of these data to the corresponding DAM fragments in the structure of **(5)** (Figure 3.1.4) reveals differences which indicate that a *shift of the π electron structure* has occurred upon formation of the acetonyl adduct. Referring now to the structure of **(5)** (Figure 3.1.1), C(8)-N(2) and

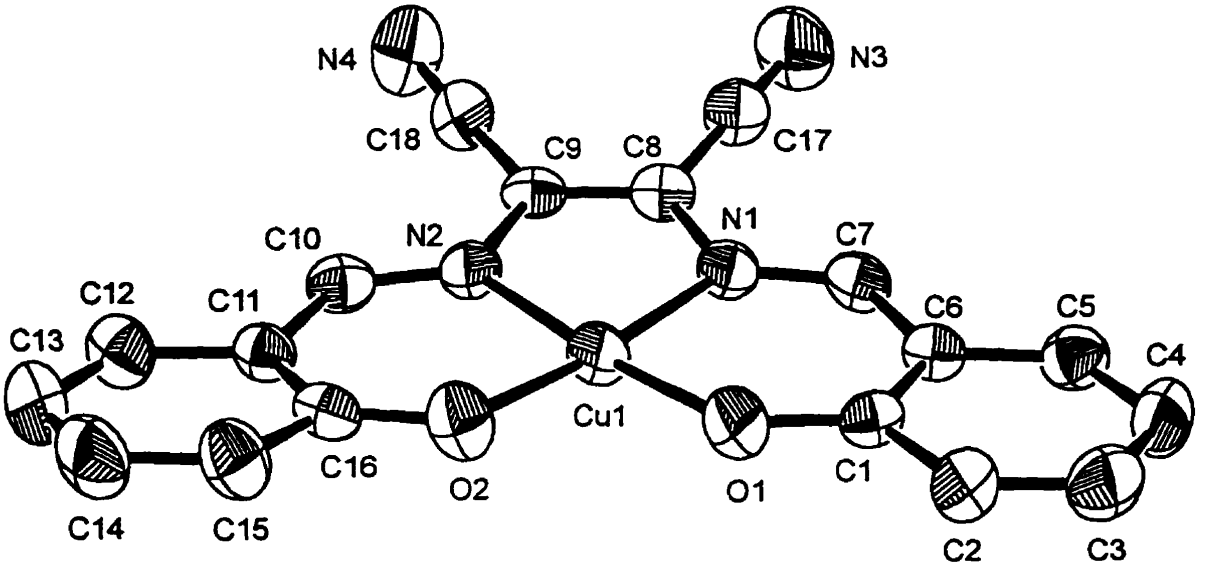

Figure 3.1.3. X-ray crystal structure of [CuL1], **(6)**, as obtained from a sample prepared by MacLachlan. Reproduced from reference [60].

C(18)-N(4), both originally Schiff base imine linkages in the parent **(1)**, now are single bonds with lengths of 1.49(1) Å and 1.53(1) Å, respectively. Significant double bond character is now observed for N(2)-C(9) (1.29(1) Å) and N(4)-C(19) (1.33(1) Å), while in keeping with this shift, C(9)-C(10), C(19)-C(20), C(10)-C(26) and C(20)-C(32)

(1.42(1) Å, 1.38(1) Å, 1.41(1) Å and 1.43(1) Å, respectively) all have bond lengths which are intermediate between those expected for pure single or double bond character. Upon extending the π electron shift to the cyano functions C(26)-N(6) and C(32)-N(8) (both 1.14(1) Å), the bond lengths found are slightly lengthened when compared to those of **(6)**, indicating a slight reduction in the triple bond character. While a difference of less than 3σ (estimated standard deviation) is not normally regarded as significant in terms of bond length differences, the fact that the differences noted occur over several bonds (and in some cases are larger than 3σ) suggests that the observed effects are real.

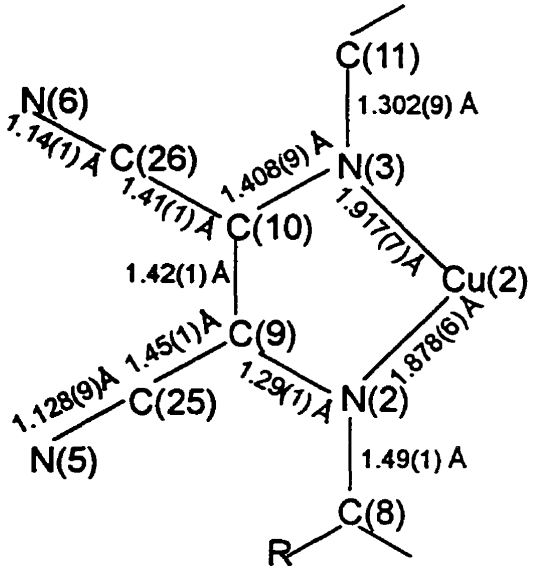

(a) $[Cu_2M4](CH_3COCH_3)$, **(5)**

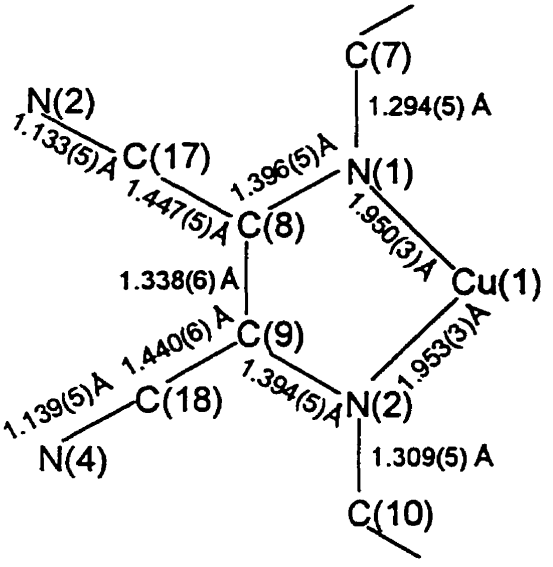

(b) [CuL1], **(6)**

Figure 3.1.4. Bond lengths for (a) a DAM fragment of **(5)** (where -R = $-CH_2COCH_3$) and (b) the DAM fragment of **(6)**.

Recalling that **(5)** is a *neutral* phenoxide bridged copper(II) macrocyclic compound of $M4^{4-}$, the above discussion and Figure 3.1.4 may be of use in determining where the non-phenolic negative charge is expected to reside in the ligand framework. First, consider Figure 3.1.5, which is a schematic representation of canonical forms which result from the above discussion of the π electron shift observed in the DAM fragment upon formation of **(5)**. If each acetonyl group brings a single negative charge with it,

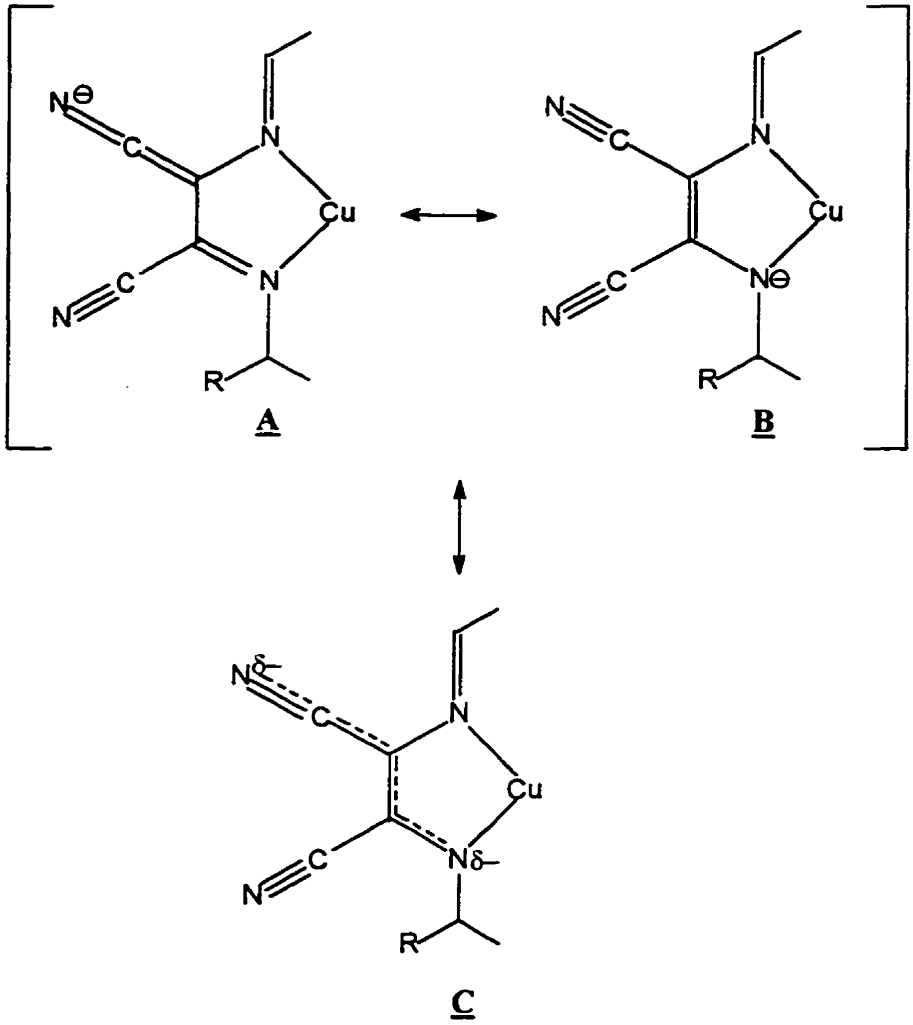

Figure 3.1.5. Schematics of the π electron framework of the DAM fragment of **(5)**, derived from x-ray crystal structure considerations.

simple octet rule and charge considerations for canonical forms **A** and **B** show that the negative charge resides on either the nitrogen of the cyano function (as in **A**) or on the nitrogen coordinated to the copper(II) centre (as in **B**). With the x-ray structure bond lengths in mind, the most valid description of the DAM fragment that emerges is that shown by **C**, whereby for a single acetonyl addition to C(8), for example, the negative charge is delocalized over the N(2)-C(9)-C(10)-C(26)-N(6) chain with charge concentrations at N(2) and N(6). The same argument applies to the N(4)-C(19)-C(20)-C(32)-N(8) chain. Such a distribution of the negative charge in the DAM fragment would not only explain the lengthened bonds in the cyano functions C(26)-N(6) and C(32)-N(8), but also the relatively short copper-nitrogen distances for Cu(1)-N(4) and Cu(2)-N(2) (1.886(6) Å and 1.878(6) Å, respectively) observed in the crystal structure of **(5)**.

[CuL2(CH_3SOCH_3)], **(7)**

The structure of **(7)** is illustrated in Figure 3.1.6, and bond distances and angles relative to the copper coordination sphere are listed in Table 3.1.2. The copper atom is square-pyramidal with an axially bound dimethylsulfoxide (Cu(1)-O(5) = 2.457(4) Å), and is displaced slightly toward O(5), a distance of 0.080 Å above the N_2O_2 mean plane. The dimensions of both the DAM fragment and the CuN_2O_2 coordination sphere resemble those found for [CuL1], **(6)**, the only exceptions being slightly longer copper-oxygen bond distances (for **(6)**, Cu(1)-O(1) = 1.892(3) Å, Cu(1)-O(2) = 1.887(3) Å; for **(7)**,

Cu(1)-O(1) = 1.903(3) Å, Cu(1)-O(2) = 1.912(3) Å). These slightly longer Cu-O distances for **(7)** in comparison to **(6)** are attributed to the difference in the geometry of the copper atoms: in **(7)** the square-pyramidal copper is slightly raised out of the N_2O_2 plane, whereas in **(6)** the copper has square planar geometry and lies in the N_2O_2 plane. As in **(6)**, a normal tautomeric π structure is found for **(7)** through the C(7)-N(1)-C(8)--C(9)-N(2)-C(10) chain which contains the Schiff base condensed DAM fragment.

Table 3.1.2. Interatomic Distances (Å) and Angles (deg.) Relevant to the Copper Coordination Sphere for [CuL2(CH_3SOCH_3)], **(7)**.

Cu(1) O(1)	1.909(3)	N(2) C(10)	1.305(6)
Cu(1) N(1)	1.959(4)	N(3) C(21)	1.126(6)
Cu(1) O(2)	1.912(3)	N(4) C(22)	1.119(6)
Cu(1) N(2)	1.954(4)	O(1) Cu(1) O(2)	90.6(1)
Cu(1) O(5)	2.457(4)	O(1) Cu(1) N(1)	92.7(2)
C(8) C(9)	1.359(6)	O(1) Cu(1) N(2)	175.0(2)
C(9) C(22)	1.448(7)	O(2) Cu(1) N(1)	172.8(2)
C(8) C(21)	1.436(7)	O(2) Cu(1) N(2)	93.1(2)
N(1) C(7)	1.302(6)	N(1) Cu(1) N(2)	83.3(2)
N(1) C(8)	1.385(6)	N(1) C(8) C(9)	116.2(4)
N(2) C(9)	1.393(6)	N(2) C(9) C(8)	116.9(4)

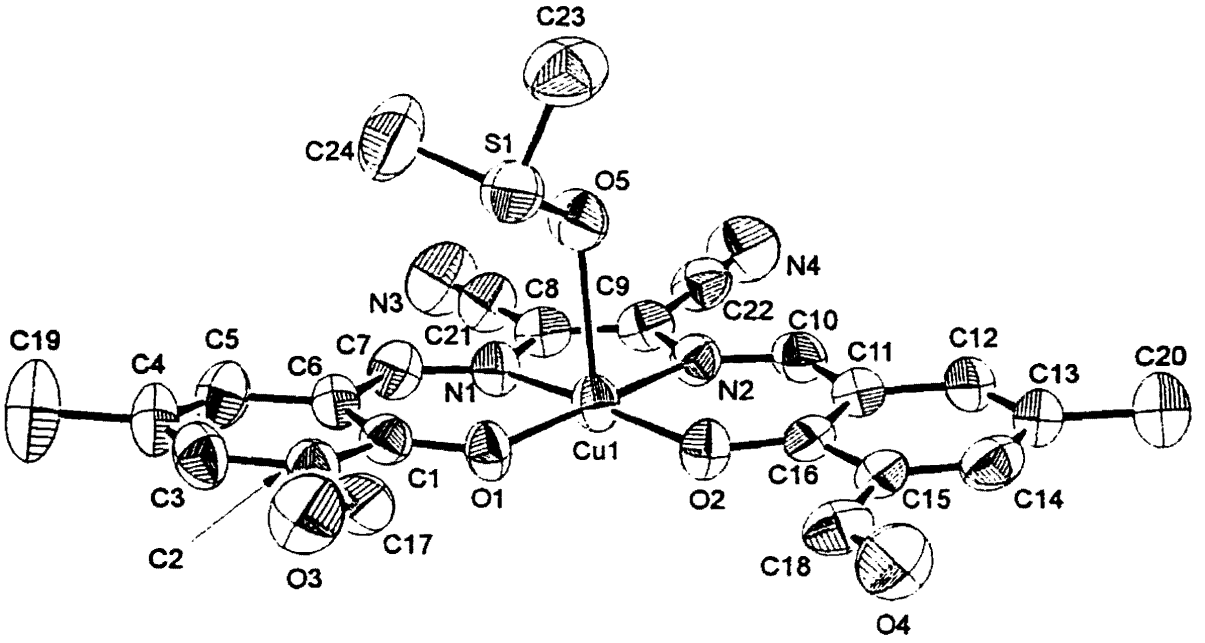

Figure 3.1.6. X-ray crystal structure of [CuL2(CH_3SOCH_3)], **(7)**.

3.2. Mechanistic Considerations on the Formation of $[Cu_2M4](CH_3COCH_3)$ and $[CuL2(CH_3SOCH_3)]$

Some brief comments are warranted on the mechanism of formation for the acetonyl adduct (5) as well as for the mononuclear compound (7), both derived from the binuclear macrocyclic compound (1). The preceding structural analysis concluded that delocalization of the π electron structure in the DAM fragments of (5) was first preceded by shifts in the tautomeric π electron structure of the DAM fragment of (1). Given the conjugation of the electron-withdrawing cyano groups through to the azomethine carbons of (1), the mechanism may be envisaged as Michael-like conjugate addition, commonly observed in synthetic organic chemistry. Figure 3.2.1 compares the mechanism of conjugate addition, from a synthetic organic viewpoint, to the proposed mechanism of conjugate addition displayed by the reaction of acetone with (1). In both cases, the nucleophile $R^{\ominus}$ attacks an sp^2 carbon, which has enhanced electrophilic character due to conjugation through to an electron-withdrawing (cyano) group. This produces a resonance stabilized intermediate which, in the case of organic syntheses, is usually treated with acidic workup to yield the final product shown at the far right of Figure 3.2.1(a). In the case of conjugate addition of the acetonyl nucleophile to (1), the resonance stabilized intermediate actually becomes the product (5), because coordination of the copper(II) ion to the adjacent nitrogen of the reacting π framework may actually stabilize the negative charge introduced by the anionic nucleophile. This mechanism is completely consistent with the electronic structure of (5), as described in Section 3.1.

(a) *Conjugate addition (Michael Addition)*

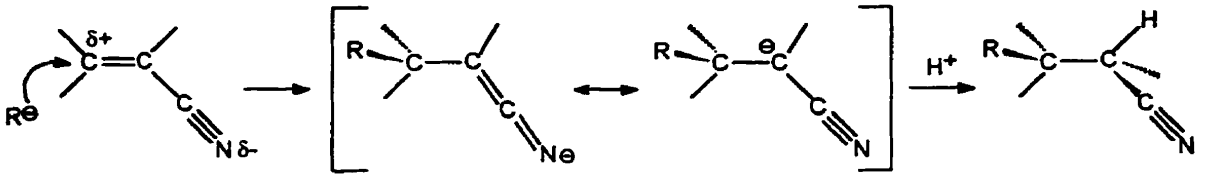

(b) *Acetonyl addition to* $[Cu_2 M1]^{2+}$

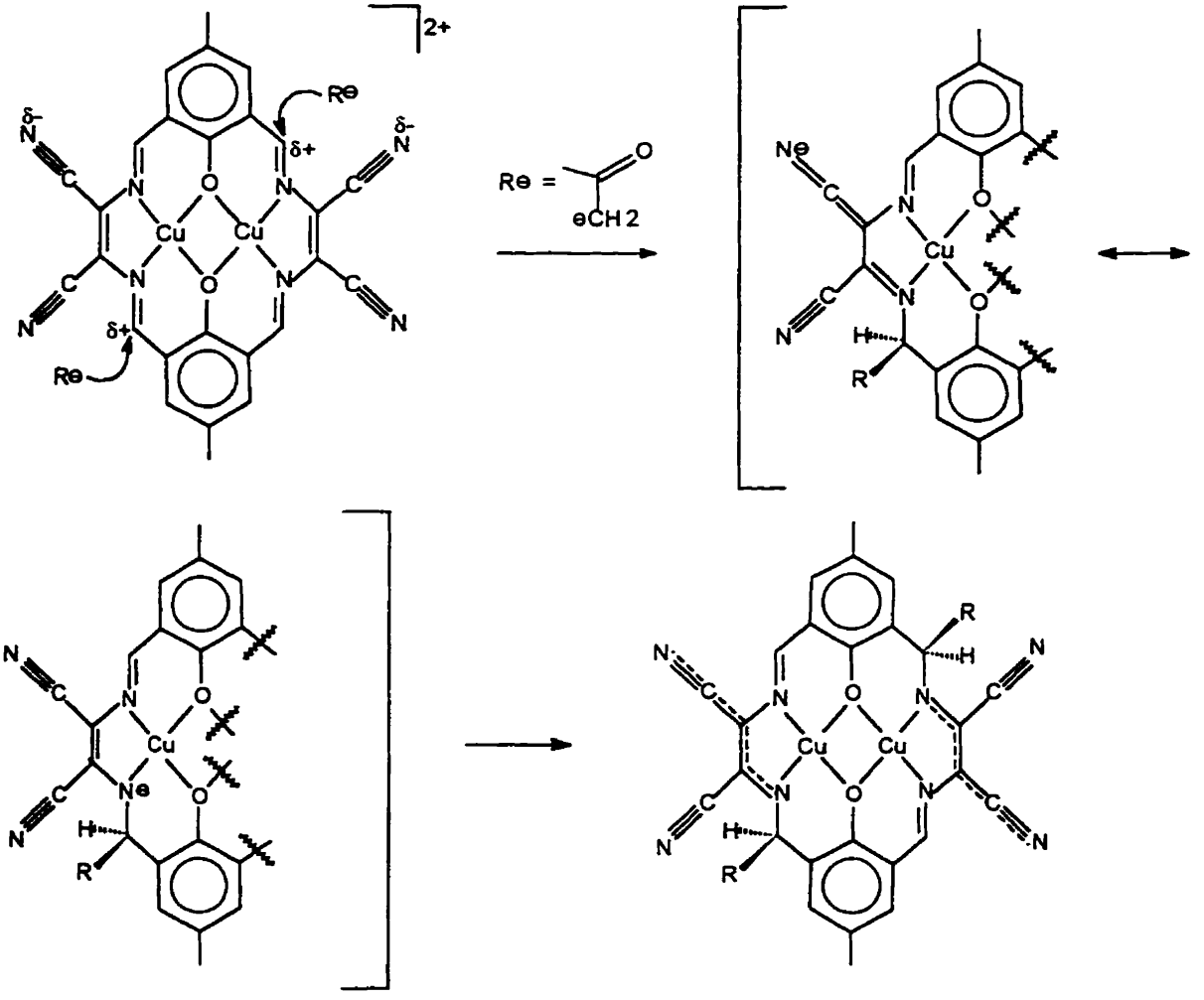

Figure 3.2.1. (a) Conjugate addition from a synthetic organic chemistry point of view, and (b) extended conjugate addition as envisaged for $[Cu_2M4](CH_3COCH_3)$, **(5)**.

While a conjugate addition mechanism explains how **(1)** reacts with acetone to form **(5)**, the questions of how the acetonyl nucleophiles are generated and why both acetonyl groups add exclusively to the same face of **(1)** remain to be addressed. In the absence of base, it is proposed that the acetonyl nucleophile may be generated by pre-coordination of acetone to the copper(II) centres of **(1)**, inducing a further increase in the inherent acidity of the methyl hydrogens of acetone. Dissociation of one of these hydrogens from a methyl group and concomitant enhanced α-carbanion character then leads to nucleophilic attack at an adjacent azomethine carbon centre, with the $Cu\text{-}O_{acetonyl}$ coordination providing anchimeric assistance. As the first acetonyl adds, the previously planar molecule will twist according to new-found flexibility at the former azomethine carbon, yielding, according to molecular models, a roofed structure about the binuclear core of the macrocycle. For the second acetonyl addition to occur, pre-coordination of the acetone presumably occurs again, yet the roof-shaped coordination sphere dictates that coordination to the convex face is highly preferred. The inductive generation of the acetonyl nucleophile then occurs for a second time, and this nucleophile then reacts according to the above sequence. The second conjugate addition occurs exclusively at the azomethine carbon diagonally opposite to the carbon of the previous addition not only because this former carbon is furthest away from the sterically bulky, pendant initial acetonyl residue, but also because maximal relief of geometric strain may be attained by reaction at the carbon "diagonally opposite" to the site of initial reaction, followed by flexing to the saucer-shaped macrocyclic structure. The reaction terminates after the

addition of two acetonyl groups for a number of reasons: Firstly, the driving force to relieve geometric strain has been realized upon addition of two acetonyl groups. Secondly, and possibly the most important point, the tautomeric π electron structures of both azomethine DAM fragments originally found in **(1)** have been destroyed after two acetonyl additions. Accordingly, further conjugate addition to the resulting delocalized π electron framework about the DAM fragments is highly unlikely. Moreover, anything beyond two acetonyl additions would entail an increase in negative charge beyond the point whereby the charge may be stabilized by the copper(II) centres.

Note that the generation of the acetonyl nucleophiles from an acetone solution of **(1)** to produce **(5)** implies the concomitant formation of perchloric acid. Accordingly, such solutions were handled with care.

The hydrolysis of **(1)** in undried dimethylsulfoxide to yield **(7)** is not surprising, especially in light of the enhanced electrophilicity of the azomethine carbons of **(1)**. Again, any inherent geometric strain about the binuclear copper(II) core of **(1)** would provide an additional driving force for this hydrolysis. Hydrolytic attack by water at two adjacent imine groups essentially reverses the Schiff base reactions that formed them, yielding the neutral mononuclear dialdehyde compound **(7)**. It was later discovered by Handa [62] that the same derivative of diaminomaleonitrile may be prepared in very good yield upon condensing 2,6-diformyl-4-methylphenol and DAM (2:1) in the presence of a copper(II) salt.

3.3. Infrared Spectroscopy - Providing a Cornerstone for the Structural Analysis of Diaminomaleonitrile Derivatives

While polynuclear compounds for $M1^{2-}$ - $M3^{2-}$, $L3^{3-}$ and $L4^{6-}$ were produced readily by template syntheses employing copper(II) salts, many more template syntheses employing other metal ions were carried out, which turned out to be unsuccessful. Throughout the course of this work, infrared spectroscopy proved to be an invaluable tool in the assessment of the products obtained from all attempted syntheses which incorporated diaminomaleonitrile and formylphenols. While examination of the $-NH_2$, -C=O, and -C=N- regions of an infrared spectrum provided valuable structural information, it was the -C≡N region which yielded a fast, reliable fingerprint directly related to the structure of the product. A combination of the above IR data, along with knowledge of the infrared bands for a given anion, facilitated the development of a set of criteria that were used to confidently determine the structure of a product simply from an analysis of its IR spectrum. Table 3.3.1 lists IR data for compounds **(1)** to **(9)**, while the spectra of Figures 3.3.2 to 3.3.5 also aid in illustrating the merits of IR spectroscopy upon elucidating the structures of the coordination compounds synthesized during this project (Figure 3.3.1). The criteria established for the analysis of the IR spectra of DAM-based compounds are listed as **I-V** below.

I. For the symmetric binuclear copper(II) macrocyclic coordination compounds of $M1^{2-}$ to $M3^{2-}$, a single weak -C≡N band is found at ~2236cm^{-1} along with an anion band.

II. The molecule HL5, **(3)**, has an IR spectrum which may be easily fingerprinted due to distinct -NH_2 bands, as well as two very intense -C≡N bands. The lower energy -C≡N band (2210cm^{-1}) is only slightly more intense than the other band (2232cm^{-1}).

III. The IR spectrum of [Cu_2M4](CH_3COCH_3), **(5)**, has a unique, very intense low energy -C≡N band at 2176cm^{-1}, with a weak satellite band at 2232cm^{-1}. The shift to lower energy for the cyano band of **(5)** compared to **(1)** provides further evidence for reduction in the triple bond character of two of the cyano groups in **(5)**, as proposed during the discussion of the x-ray crystal structure of this compound. No anion band is present in the spectrum, yet acetonyl and lattice acetone -C=O bands are present.

IV. The IR spectra of the mononuclear copper(II) compounds of $L1^{2-}$ and $L2^{2-}$ reflects the simple, highly symmetrical nature of these compounds. A single, very weak -C≡N band is observed at 2222cm^{-1} in each case, with a -C=O band being found for the free formyl groups of **(7)**. No anion bands, of course, are observed for the mononuclear copper(II) coordination compounds of these dianionic ligands.

V. Compounds **(8)** and **(9)** may be considered as close structural relatives, and this similarity is reflected in their IR spectra. The -C≡N infrared handle may again be used to distinguish these two similar compounds from the other ligand structural varieties, as two distinct cyano bands are found in this case: a medium intensity low energy band (~2198cm^{-1}) dominates a medium-weak high energy band (~2233cm^{-1}). As expected, an anion band is found and formyl groups are absent. Elemental analysis for **(8)** and **(9)** reveals the presence of one anion (ClO_4^-) per binuclear centre indicating proton loss from an NH_2 group. This is clearly revealed in the infrared spectra of **(8)** and **(9)** by the appearance of a single strong -NH band at ~3348cm^{-1}. This proton loss is justified in light of the π conjugation pathway linking the nitrogen to the electron-withdrawing cyano function, as well as the possibility of the coordinated copper(II) inducing and facilitating stabilization of the negative charge at that nitrogen.

Table 3.3.1 Infrared Data.[†]

Chemical Formula (or Acronym) and Number Designation	IR Bands (cm^{-1})				
	$-NH_2$ / -NH	-C=O	-C=N	-C≡N	Anion
$[Cu_2M1](ClO_4)_2 \cdot (H_2O)_3(CH_3OH)$ **(1)**	-	-	1604ms; 1574vs; 1547s	2234w	1096vs; (ClO_4^-)
$[Cu_2M2](ClO_4)_2$ **(2)**	-	-	1596s; 1570vs	2238w	1096vs; (ClO_4^-)
H_3L5 (BADCEMP) **(3)**	3452, 3415, 3186, m; 3299s;3350vs;1600vs	-	1604m; 1565m	2238s; 2210s	-
$[Cu_2M1](ClO_4)_2(H_2O)_2$ **(4)**	-	-	1601s; 1574vs; 1543s	2236w	1096vs; (ClO_4^-)
$[Cu_2M4](CH_3COCH_3)$ **(5)**	-	1694ms; 1712vw	1589m; 1552m	2232w; 2176s	-
[CuL1] **(6)**	-	-	1610m; 1585m; 1513m	2221vw	-
$[CuL2(CH_3SOCH_3)]$ **(7)**	-	1678s	1616mw; 1581mw; 1518m	2222vw	-
$[Cu_2L3](ClO_4)(C_2H_5OH)$ **(8)**	3349s	-	1610s; 1578vs; 1546s	2233mw; 2198m	1099s; (ClO_4^-)
$[Cu_4L4](ClO_4)_2(C_2H_5OH)_2$ **(9)**	3348s	-	1620m; 1583s; 1546ms	2232mw; 2199m	1099m; (ClO_4^-)

[†]Note for the intensities: v = *very*, w = *weak*, m = *medium*, s = *strong*

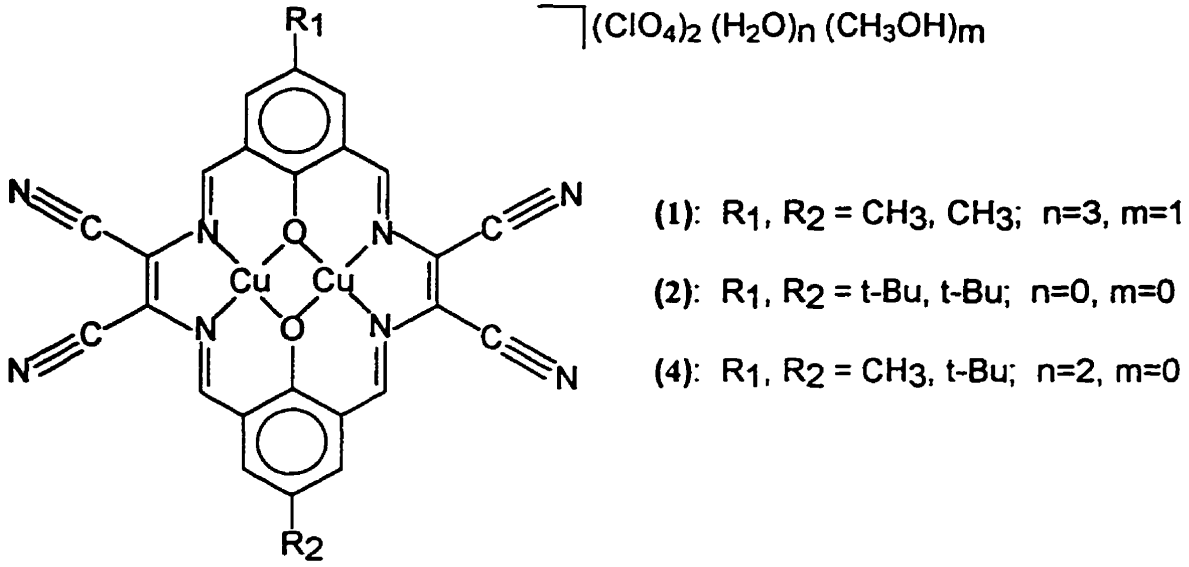

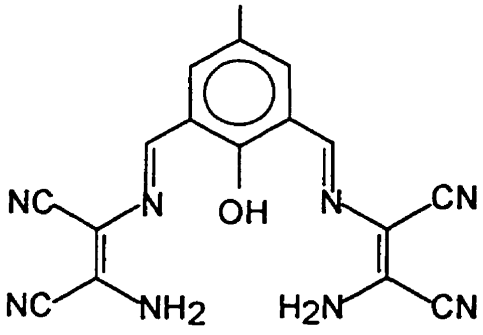

(3) HL5

Figure 3.3.1. Proposed structures for macrocyclic compounds **(1)**, **(2)**, and **(4)**, along with **(3)** (a precursor to **(4)**, **(8)** and **(9)**); the proposed structures of the remaining products follow.

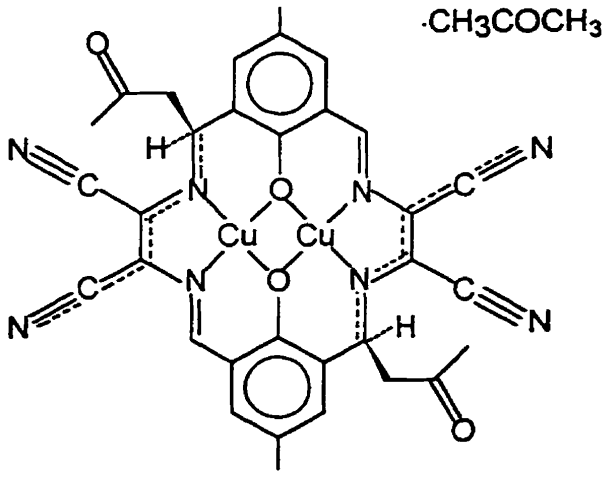

(5) $[Cu_2M_4](CH_3COCH_3)$

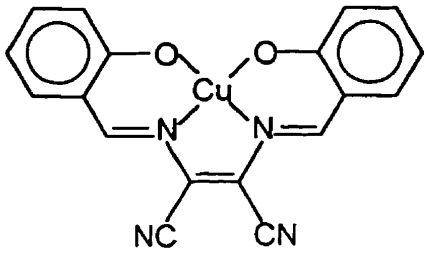

(6) [CuL1]

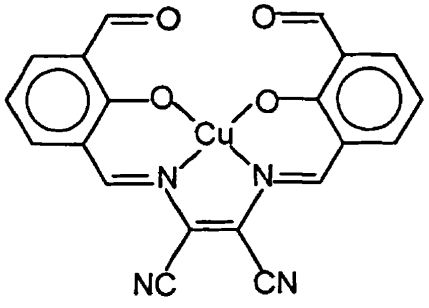

(7) $[CuL2(CH_3SOCH_3)]$

(Coordinated DMSO omitted for clarity)

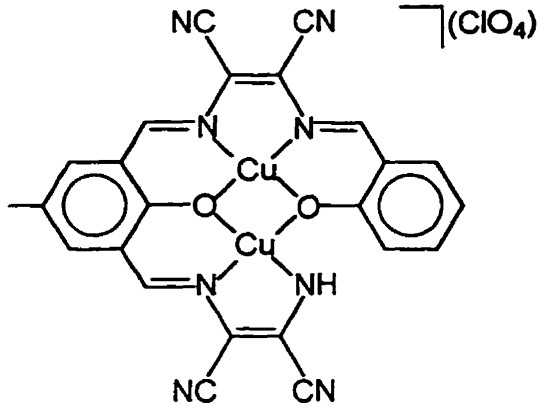

(8) $[Cu_2L3](ClO_4)(C_2H_5OH)$

(Lattice ethanol omitted for clarity)

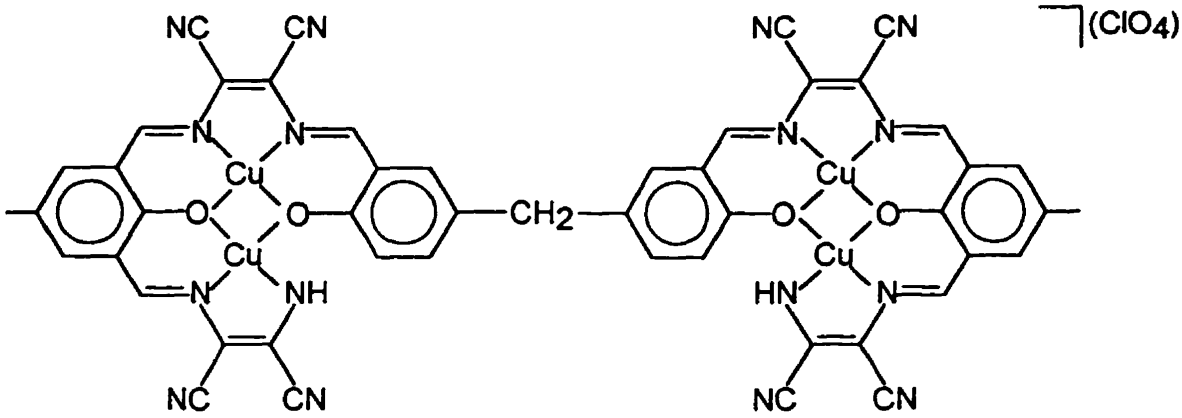

(9) $[Cu_4L4](ClO_4)_2(C_2H_5OH)_2$

(Lattice ethanol omitted for clarity)

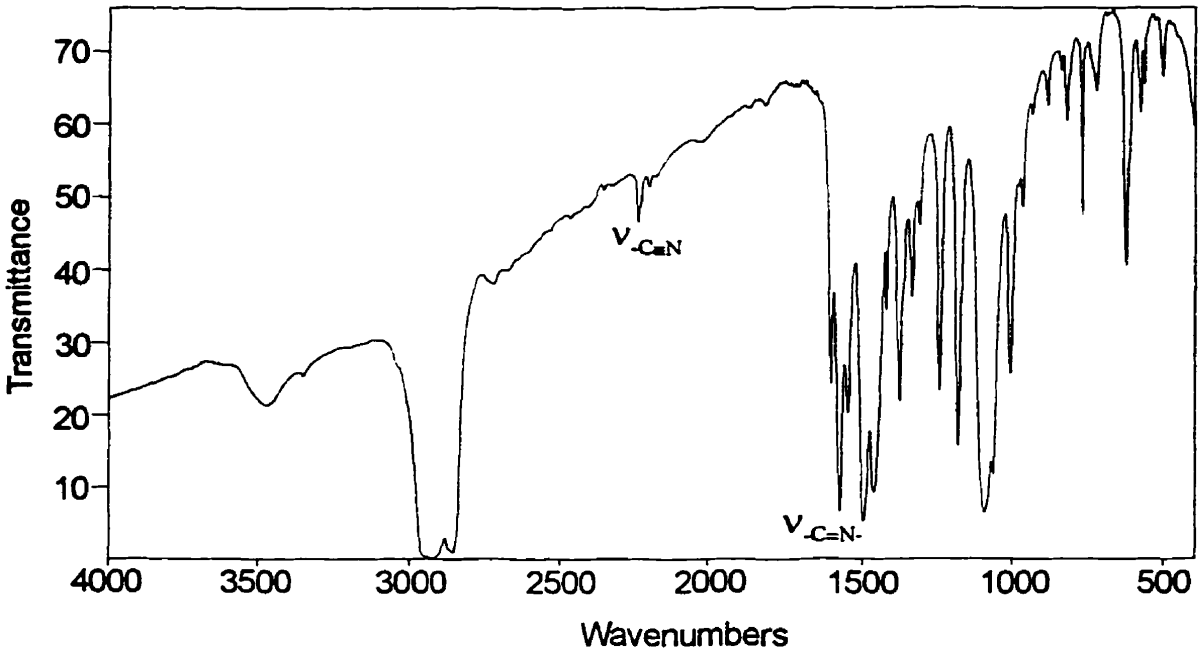

Figure 3.3.2. IR spectrum of $[Cu_2M1](ClO_4)_2(H_2O)_3(CH_3OH)$, **(1)**.

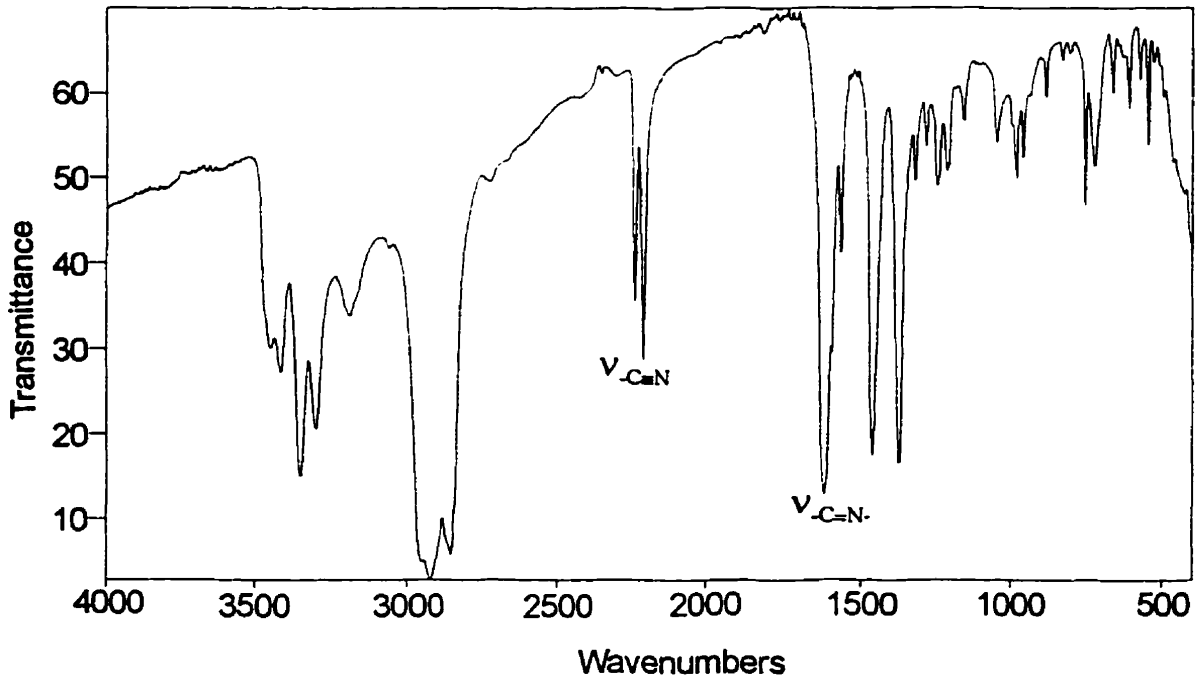

Figure 3.3.3. IR spectrum of HL5, **(3)**.

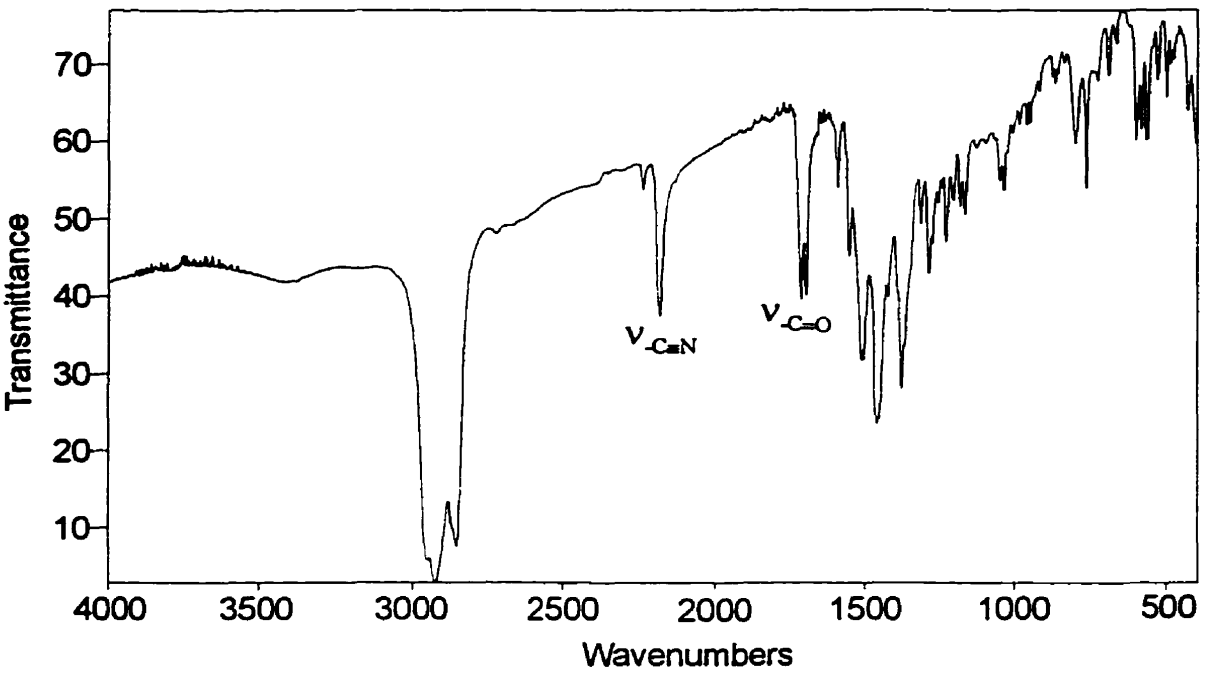

Figure 3.3.4. IR spectrum of $[Cu_2M4](CH_3COCH_3)$, **(5)**.

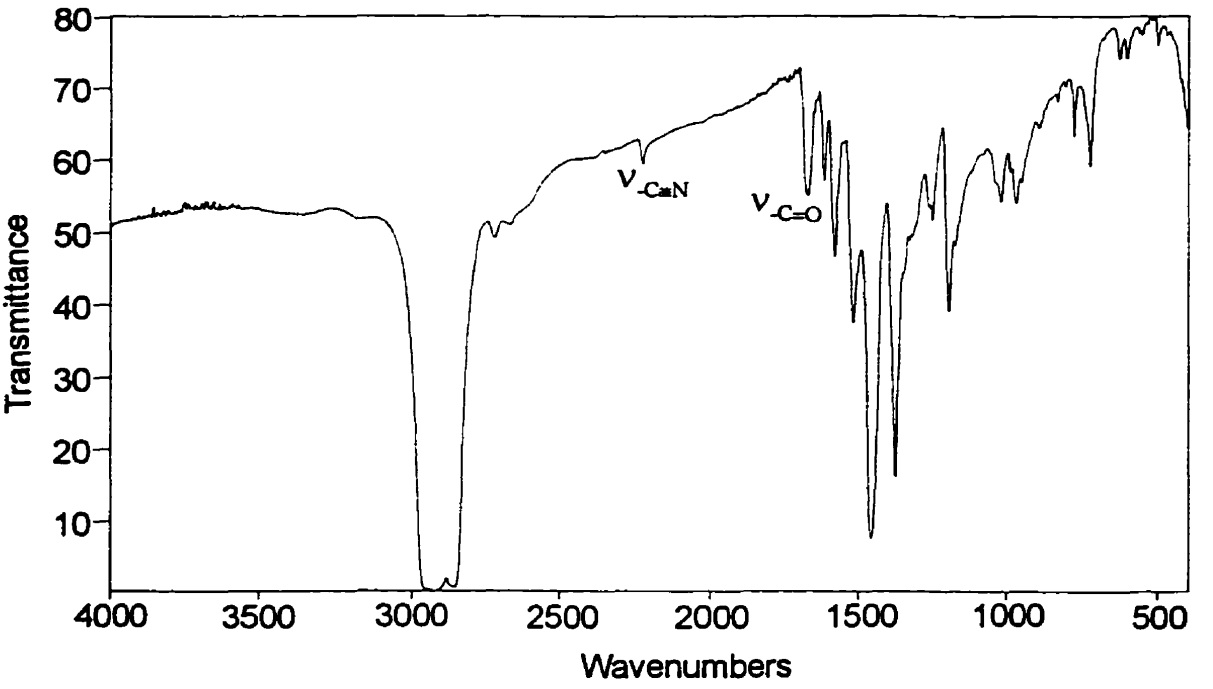

Figure 3.3.5. IR spectrum of $[CuL2(CH_3SOCH_3)]$, **(7)**.

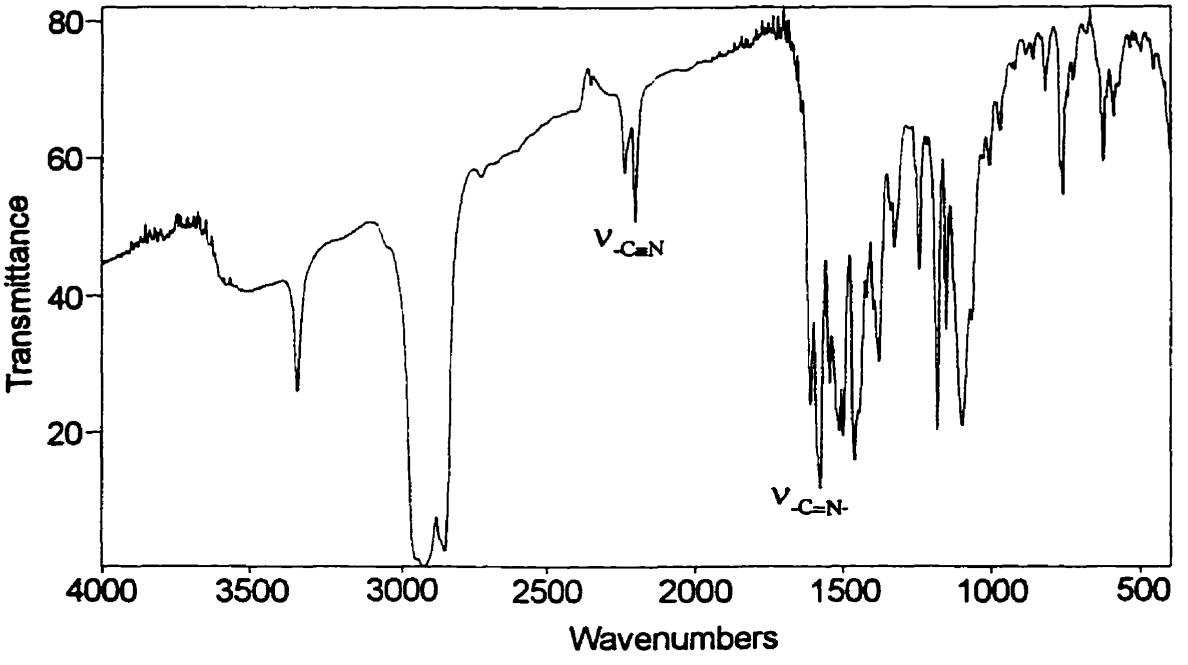

Figure 3.3.6. FT-IR spectrum of $[Cu_2L3](ClO_4)(C_2H_5OH)$, **(8)**.

The development of these guidelines during this project permitted structural analysis of products as soon as a dry sample was available for an IR spectrum. In the absence of an x-ray crystal structure, the most likely structure and nuclearity of a DAM-based compound could be assessed using infrared spectroscopy. The following discussion utilizes these guidelines along with analytical data to describe the results of unsuccessful, yet very noteworthy, template syntheses that were not described in the experimental section of this thesis.

As stated earlier, many metal ions other than copper(II) were employed in attempts to synthesize binuclear coordination compounds of $M1^{2-}$ - $M3^{2-}$ by the template strategy, yet only copper(II) was successful at this task. Attempted template syntheses using stoichiometric amounts of magnesium(II), manganese(II), zinc(II) or lead(II) with DFMP

and DAM failed to produce binuclear coordination compounds of $M1^{2-}$, yet every one of these attempts yielded the same product: HL5, **(3)**. This product was indicated in every case by the identity of the product's IR spectrum to the unique and characteristic IR of HL5 (Figure 3.3.3). Furthermore, microanalyses were obtained for some of these products, and these analytical data are presented in Table 3.3.2. The calculated C, H, N percentages for HL5 are C, 59.30; H, 3.51; N, 32.54.

Table 3.3.2. C, H, N Microanalytical Data for the Product Obtained from Each of the Attempted Template Syntheses of $M1^{2-}$ Using Mn(II), Zn(II) and Pb(II).

Attempted Template Synthesis	Microanalytical Data Found		
	C %	H %	N %
Mn(II) + DFMP + DAM	58.91	3.84	30.54
Zn(II) + DFMP + DAM	58.44	3.71	30.71
Pb(II) + DFMP + DAM	57.90	3.69	29.39

Though the C, H, N data in Table 3.3.2 in some cases show some discrepancy from the calculated values for HL5, the IR of the products are essentially identical to that of HL5. For comparison purposes, a representative IR for the product obtained from the zinc(II) attempted template reaction is shown in Figure 3.3.7. Flame atomic absorption analysis for the zinc content in this product found 0.0% Zn, in accordance with the assignment of HL5 as the product.

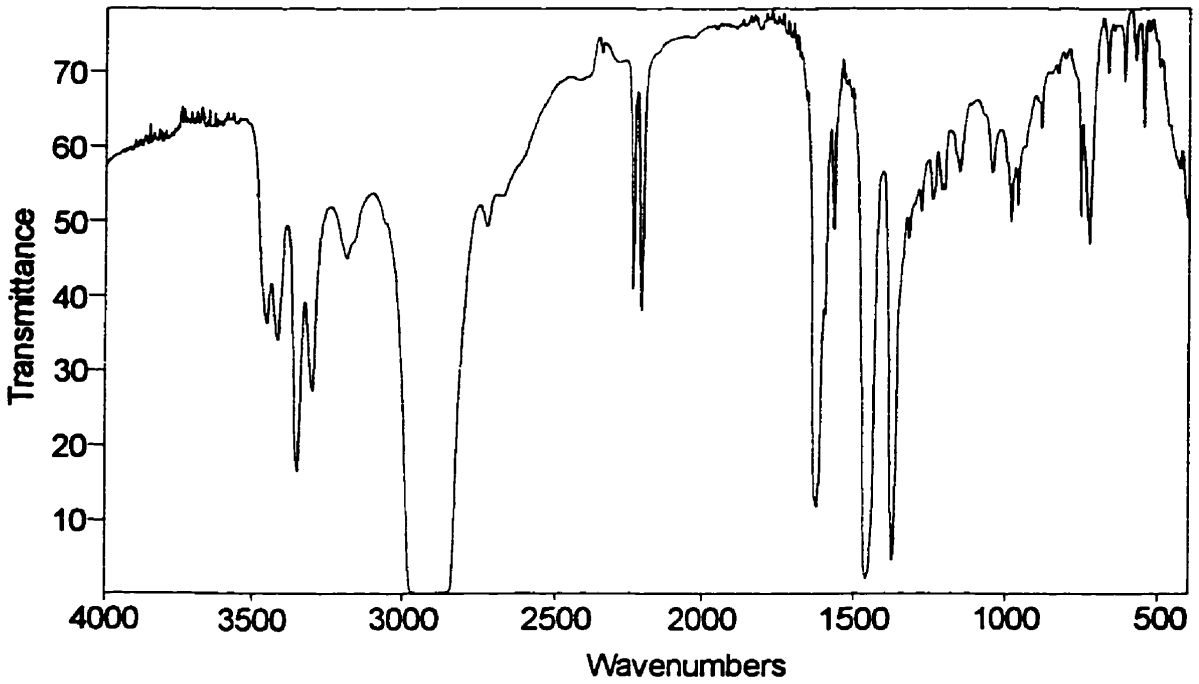

Figure 3.3.7. IR spectrum of the product obtained from the attempted template synthesis of $M1^{2-}$ using Zn^{2+} as the templating ion.

Another set of very interesting results was found for attempted template syntheses of $M1^{2-}$ and $M2^{2-}$ using nickel(II) and vanadium(IV) salts. It was quickly realized from the IR spectra guidelines (I-V) that the IR spectra of the products for the $Ni(ClO_4)_2 \cdot 6H_2O$ and $VO(SO_4) \cdot 2H_2O$ attempted template syntheses (see Figures 3.3.8 and 3.3.9 for $M1^{2-}$) were *not* in accordance with that of the desired symmetrical binuclear coordination compound (Figure 3.3.2). Analogous spectra were obtained for attempted syntheses of binuclear nickel(II) and vanadyl(II) compounds of $M2^{2-}$.

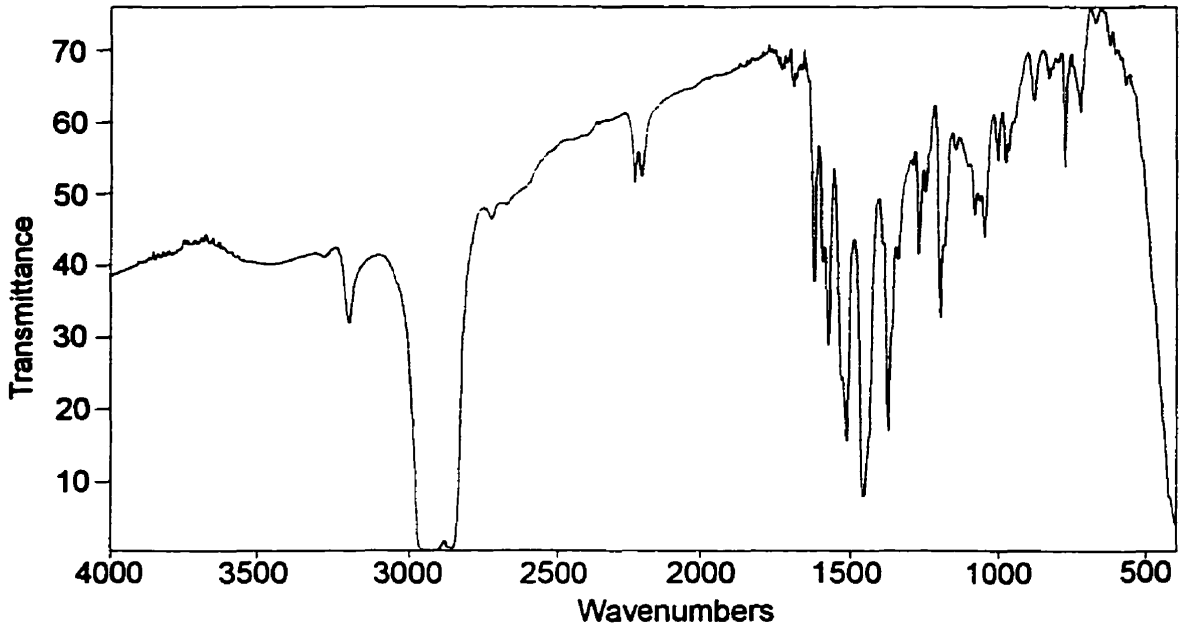

Figure 3.3.8. IR spectrum of the product obtained from the attempted template synthesis of $M1^{2-}$ using Ni^{2+} as the templating ion.

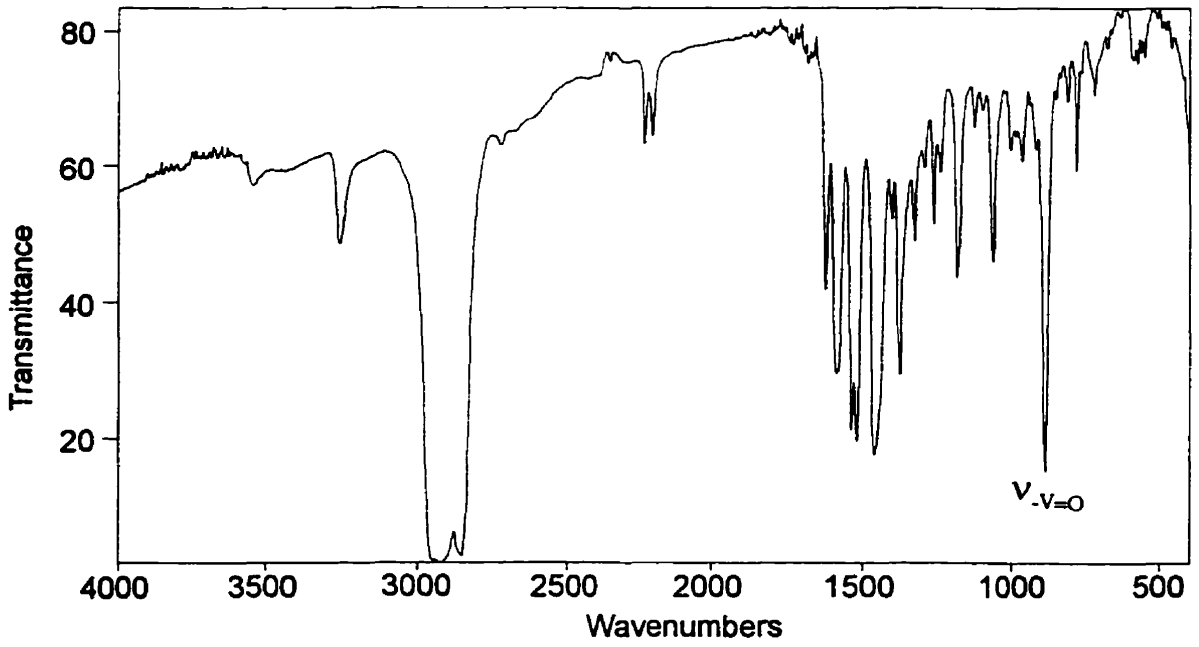

Figure 3.3.9. IR spectrum of the product obtained from the attempted template synthesis of $M1^{2-}$ using VO^{2+} as the templating ion.

The two spectra above have many common features, indicating that two unpredicted yet similar products have formed. Instead of finding a single weak -C≡N band at ~2236cm^{-1} as well as an anion band (as expected from guideline I), two bands are found in the -C≡N region at ~2227cm^{-1} and ~2202cm^{-1}; furthermore, no anion bands are observed (Yet, note a strong V=O stretch at 950cm^{-1} in Figure 3.3.9, indicating the presence of the complex cation). Since the IR spectra of these products did not fit any of the IR guidelines developed for the established copper(II) systems, C, H, N microanalytical data (as well as flame atomic absorption data for the products from the nickel(II) reactions) were acquired. Table 3.3.3 summarizes these data. It is immediately noted that for the nickel(II) reactions, the absolute percentages of C and N are too high and also that the Ni percentage is too low to conform to the analysis of a homobinuclear nickel(II) macrocyclic compound of $M1^{2-}$ or $M2^{2-}$. It may be deduced from the analytical C / N ratios in these products that the whole macrocyclic ligand ($M1^{2-}$ or $M2^{2-}$) has actually been formed in each case, but *mononuclear macrocyclic* products are proposed for these nickel(II) and vanadyl(II) reactions. This is in agreement with the experimental C, H, N results, and for the nickel(II) reactions, the nickel(II) content calculated for the mononuclear nickel(II) macrocyclic compounds of $M1^{2-}$ or $M2^{2-}$ is consistent with the value found by Ni flame atomic absorption analysis of the products.

It is not clear why copper(II) is able to template the formation of homobinuclear macrocyclic compounds of $M1^{2-}$ and $M2^{2-}$ while under analogous conditions all other ions employed would not. A point of consideration in attempting to explain this variation of

Table 3.3.3. Analytical Data for the Products Obtained from Attempts to Synthesize Binuclear Nickel(II) and Vanadyl(II) Compounds of $M1^{2-}$ and $M2^{2-}$.

Attempted Template Reaction	Found			
	C %	H %	N %	Ni %
$Ni(ClO_4)_2 \cdot 6H_2O$ + DFMP + DAMN	52.85	3.10	18.67	10.44
$Ni(NO_3)_2 \cdot 6H_2O$ + DFTBP + DAMN	61.32	4.76	17.10	8.98
$VO(SO_4) \cdot 2H_2O$ + DFMP + DAMN	56.00	3.14	20.07	-
$VO(SO_4) \cdot 2H_2O$ + DFTBP + DAMN	58.85	4.74	16.36	-

Attempted Template Reaction	Proposed Product	Calculated for Proposed Product				Yield (%)
		C %	H %	N %	Ni %	
$Ni(ClO_4)_2 \cdot 6H_2O$ + DFMP + DAMN	$[NiM1](H_2O)_{3.5}(C_2H_5OH)_{0.5}$	52.70	3.94	18.21	9.54	41
$Ni(NO_3)_2 \cdot 6H_2O$ + DFTBP + DAMN	$[NiM2](CH_3OH)$	61.42	4.69	17.36	9.09	29
$VO(SO_4) \cdot 2H_2O$ + DFMP + DAMN	$[(VO)M1](H_2O)$	56.21	2.91	20.17	-	32
$VO(SO_4) \cdot 2H_2O$ + DFTBP + DAMN	$[(VO)M2](H_2O)(CH_3OH)$	59.01	4.81	16.69	-	30

observed products is the variation in the ionic radii and preferred coordination environments of the metal ions. It is expected that the five-membered chelate ring generated by the DAM fragment leads to a small N_2O_2 coordination site which would perhaps be too small to effectively accommodate some metal ions. However, a survey of the effective ionic radii (Table 3.3.4, obtained from crystallographic data [63]) of the metal ions employed leads one to conclude that while ionic radius may be important, other factors such as preferred coordination number and the geometry of the metal ion also play significant roles in determining the nature of the product obtained from the DAM / diformylphenol template reaction for a given ion.

Table 3.3.4. Effective Ionic Radii of Metal Ions as Determined by X-ray Crystallography.

Metal ion	Cu(II)	Mg(II)	Mn(II)	Zn(II)	Pb(II)	Ni(II)	V(IV)
Ionic Radius, pm (Coordination Number)	71 (4)	71 (4)	80 (4)†	74 (4)	79 (4)	63 (4)	67 (5)

† Quoted for high spin Mn(II).

Magnesium(II) has the same effective ionic radius as copper(II), but the deficiencies of magnesium(II) as a templating ion are reasoned to be due to its poor Lewis acid character. Manganese(II), zinc(II) and lead(II), none of which produce the complete macrocyclic ligand framework, are all appreciably larger than copper(II), nickel(II) and vanadyl(II). Hence, while a large metal ionic radius may disfavour formation of the complete macrocyclic framework, a relatively small metal ionic radius does not ensure formation of a binuclear macrocyclic compound.

It is suggested that copper(II) forms binuclear compounds whereas nickel(II) and vanadyl(II) form mononuclear compounds because copper(II) readily undergoes distortions from square planar geometry. Distortion of the copper(II) square planar geometry places the metal ion out of the plane of the molecule; nickel(II) and vanadyl(II) are less prone to such distortions. It has been suggested [43] that Robson macrocycles with two-carbon spacer groups will always contain nickel(II) in square planar (as opposed to octahedral) geometry. Should nickel(II) and vanadyl(II) prefer to reside in the plane of the DAM-based macrocycles ($M1^{2-}$- $M3^{2-}$), this requirement may cause the ligands to flex and distort about the filled coordination cavity, thereby causing the second cavity to be unsuitable for metal ion coordination.

Further evidence from the literature which supports the argument that metal ion size and preferred coordination geometry are important factors in determining whether or not simple binuclear Robson macrocycles form is provided by Brychcy and coworkers [64]. These authors describe the reaction in Figure 3.3.10. Using 0.092mmol of <u>each</u> reagent dissolved in methanol, the expected product would be the heterobinuclear

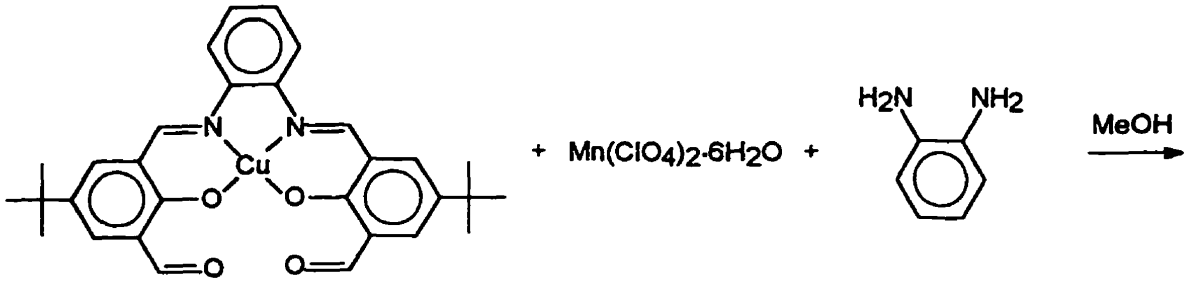

Figure 3.3.10. Attempted synthesis of Mn(II) / Cu(II) heterobinuclear Robson-type macrocycle, from reference [64].

copper(II) / manganese(II) macrocycle shown in Figure 3.3.11a. Yet, the product obtained was shown by x-ray crystallography to be that of the compound (shown schematically) in Figure 3.3.11b. The authors report the x-ray crystal structure of the product [64] as that of an eight coordinate manganese(II) ion sandwiched between the two unfilled (N_2O_2) sites of the two mononuclear copper(II) macrocyclic units. Such reactivity of manganese(II) in the presence of a completely formed macrocycle again suggests that metal ion radius versus hole size, combined with a consideration for preferred coordination number and geometry for a metal ion, are important factors in determining whether or not simple binuclear Robson macrocycles form.

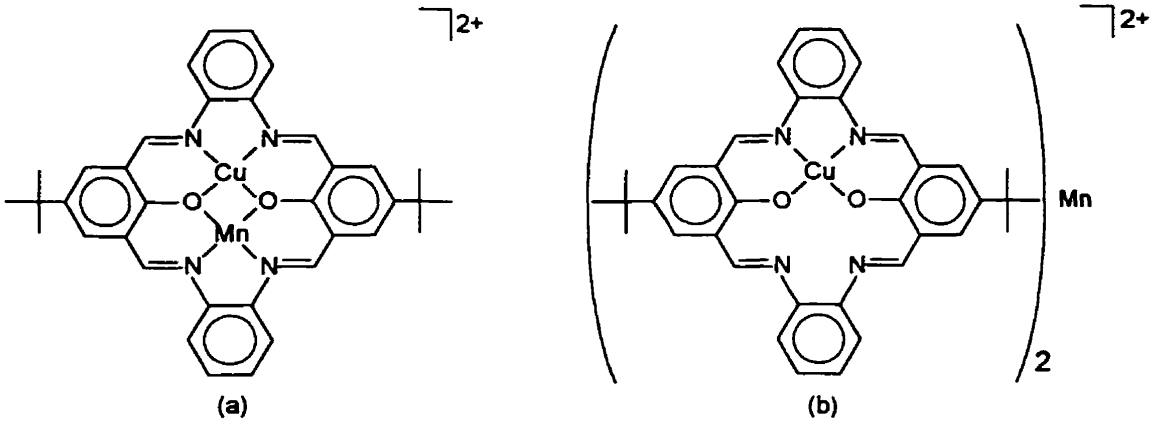

Figure 3.3.11. (a) Expected and (b) obtained product from the reaction shown in Figure 3.3.10 [64].

While copper(II) was successful in template formation of $[Cu_2L3]^+$ and $[Cu_4L4]^{2+}$, the same success was not found for template syntheses of $L3^{3-}$ or $L4^{6-}$ involving nickel(II). Attempts to synthesize $[Ni_2L3]^+$ and $[Ni_4L4]^{2+}$ by template syntheses analogous to those performed for copper(II) yielded in both cases the starting material HL5 after two days of

refluxing the reaction mixtures. No other template reactions aimed at synthesizing polynuclear coordination compounds of $L3^{3-}$ or $L4^{6-}$ were attempted.

The remainder of this thesis will focus on the copper(II) coordination compounds **(1)**, **(2)**, **(4)** - **(9)**, with emphasis placed on the coordination chemistry, spectroscopy, electrochemistry and magnetism of the polynuclear compounds.

3.4. UV-Visible Spectra of the Copper(II) Coordination Compounds

The copper(II) coordination compounds **(1)**, **(2)**, **(4)** - **(9)** have UV-visible spectra that are dominated by charge transfer transitions (Table 3.4.1). Intense orange-coloured solutions of the macrocyclic coordination compounds **(1)**, **(2)** and **(4)** in DMF have very similar electronic spectra, each having a band of maximum intensity peaking in the range of 427 - 429 nm that is sufficiently intense to mask any d-d transitions.

Figure 3.4.1 illustrates the UV-visible spectrum of **(1)** as a representative for the very similar spectra of **(1)**, **(2)** and **(4)**. Considering the extensive π conjugation throughout the ligand framework extending to the periphery of these macrocycles, the low energy charge transfer bands are expected to be a consequence of π–π^* transitions. DAM itself has a single intense absorption at 298nm (ε = 15 000 $L{\cdot}mol^{-1}{\cdot}cm^{-1}$, methanol solvent) [48], and a survey of the electronic spectra of Robson-type macrocycles with aliphatic spacer groups [65,30,31,38] reveals spectra that are devoid of an absorption band centred on 428nm. Absorption bands at 600nm (ε = 90 $L{\cdot}mol^{-1}{\cdot}cm^{-1}$, acetonitrile solvent) and

Table 3.4.1. Absorption Maxima and Extinction Coefficients for Copper(II) Compounds of Diaminomaleonitrile-Derived Ligands.

Chemical Formula and Number Designation	Solvent	λ_{max}, nm (ε; $x10^{-4}$ $L{\cdot}mol^{-1}{\cdot}cm^{-1}$)
$[Cu_2M1](ClO_4)_2{\cdot}(H_2O)_3(CH_3OH)$ **(1)**	DMF	322 (2.0), 380 (1.8), 427 (2.6)
$[Cu_2M2](ClO_4)_2$ **(2)**	DMF	322 (2.4), 376 (2.0), 429 (2.6)
$[Cu_2M3](ClO_4)_2(H_2O)_2$ **(4)**	DMF	321 (2.3), 374 (2.0), 429 (2.4)
$[Cu_2M4](CH_3COCH_3)$ **(5)**	DMF	263 (3.4), 338 (1.8), 440 (3.1), 482 (1.5)
[CuL1] **(6)**	$CHCl_3$	321 (2.4), 373 (3.0), 389 (3.2), 508 (1.7)
$[CuL2(CH_3SOCH_3)]$ **(7)**	DMSO	373 (1.6), 386 (1.7), 500-560 (1.0)
$[Cu_2L3](ClO_4)(C_2H_5OH)$ **(8)**	DMF	390 (4.1), 434 (4.8), 475 (4.4)
$[Cu_4L4](ClO_4)_2(C_2H_5OH)_2$ **(9)**	DMF	400 (9.7), 428 (9.6), 479 (7.1)

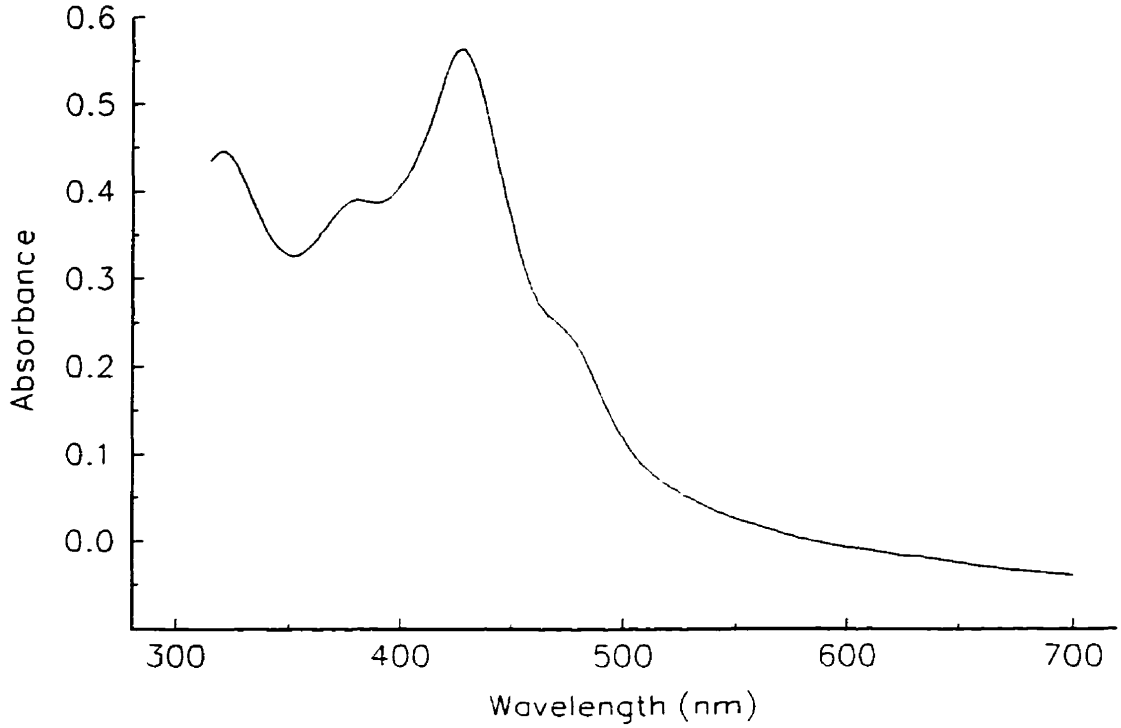

Figure 3.4.1. UV-visible spectrum of 2.2×10^{-5} mol·L^{-1} solution of **(1)** in DMF.

700nm (ε = 60 L·mol^{-1}·cm^{-1}) are found for the binuclear copper(II) compound of the original 1,3-diaminopropane based Robson macrocycle [65, 30] and are ascribed to d-d transitions [38], while a charge transfer band at 350nm (ε = 12 000 L·mol^{-1}·cm^{-1}) is the only other band in the spectrum. While this low energy band is comparable in intensity to the low energy bands found centred at 322nm and 376nm for **(1)**, **(2)** and **(4)**, it is approximately half as intense as the band found at 428nm for the binuclear copper(II) DAM-based macrocyclic compounds.

The UV-visible spectrum of the diacetonyl adduct **(5)** is shown in Figure 3.4.2 and has maxima at both lower (263nm) and higher (440nm, 482nm) wavelengths than its

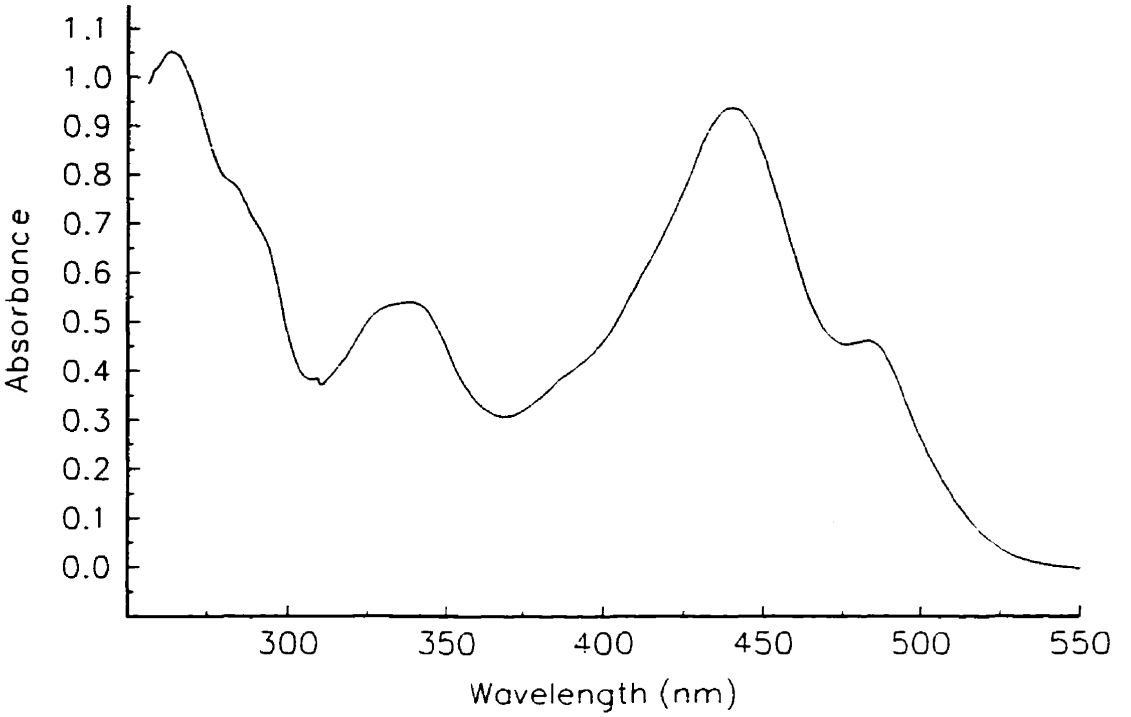

Figure 3.4.2. UV-visible spectrum of 3.1×10^{-5} mol·L^{-1} solution of **(5)** in DMF.

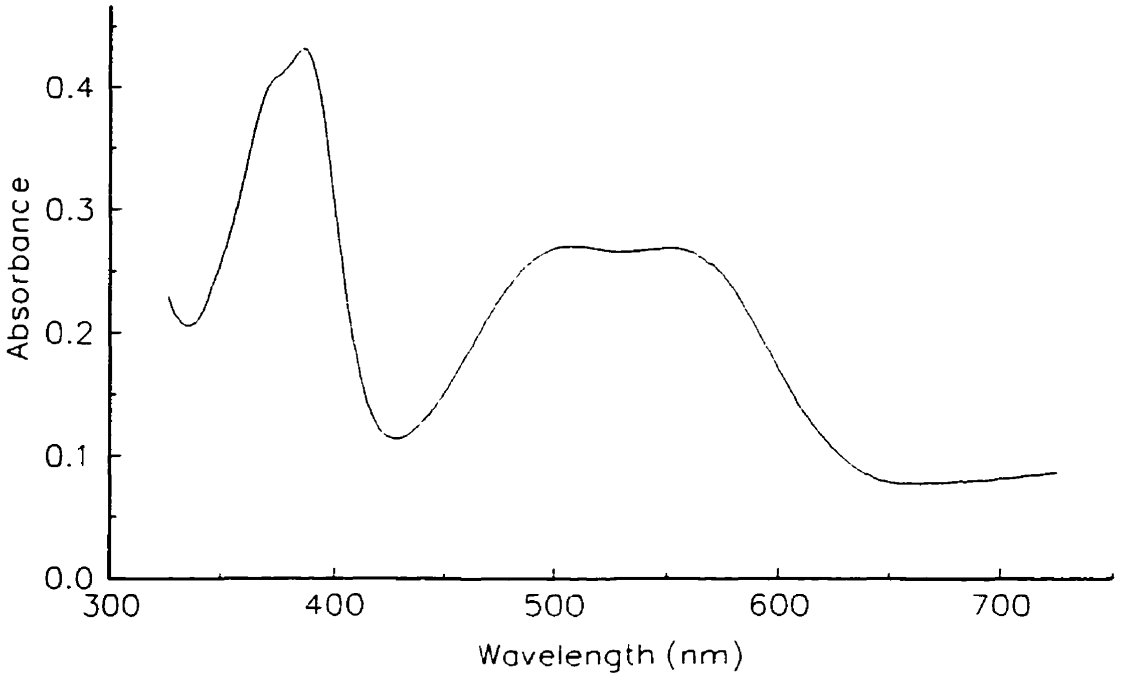

Figure 3.4.3. UV-visible spectrum of 2.6×10^{-5} mol·L^{-1} solution of **(7)** in DMSO.

parent compound **(1)**. Both visually and quantitatively, the electronic spectra of this compound provides further evidence that the electronic structure of **(5)** is quite different from that of its parent compound.

Comparison of the electronic spectrum of the mononuclear dialdehyde compound **(7)** (Figure 3.4.3) to that of the parent binuclear compound **(1)** at first glance may not reveal any similarities between the two. Yet, upon close inspection, it is noted that in the spectrum of **(7)** the two bands at 373nm (shoulder) and 386nm have intensities comparable to the band found at 380nm in the spectrum of **(1)**. Considering that the cyano functions of **(7)** and **(1)** should have similar local electronic environments, these low energy bands may be attributed to local n–π^* transitions within the cyano functions of the ligand. As for **(1)**, **(2)** and **(4)**, the spectrum of **(7)** has very intense broad bands (π–π^*, ε = 10 000 $L \cdot mol^{-1} \cdot cm^{-1}$) in the 450nm-650nm region, masking any d-d transition bands that may occur in this region.

Just as **(1)**, **(2)** and **(4)** were expected to have very similar electronic spectra, the expectation that **(8)** and **(9)** should have similar electronic spectra was experimentally confirmed. The UV-visible spectrum of **(8)** is illustrated in Figure 3.4.4. While the absorption bands of **(8)** and **(9)** occur at the same wavelengths, the extinction coefficients of **(9)** are essentially twice as large as those found for **(8)**. In the absence of x-ray crystal structures, these electronic spectra provide support for the proposed molecular structures of **(8)** and **(9)**, with the proposed molecular structure of **(9)** being essentially two units of **(8)** connected by a methylene ligand bridge. Bands at 370nm and 480nm for **(8)** and **(9)**,

respectively, resemble those found at 373-386nm for **(1)**, **(2)**, **(4)** and **(7)** and are attributed to cyano n–π^* transitions. While **(8)** and **(9)** are expected to have similar π frameworks, the extent of the π conjugation in these two compounds is less than that found for the macrocyclic compounds **(1)**, **(2)** and **(4)**. Accordingly, bands found at 428-434nm and 475-479nm for **(8)** and **(9)** are attributed to π–π^* transitions within their distinct π electron structures.

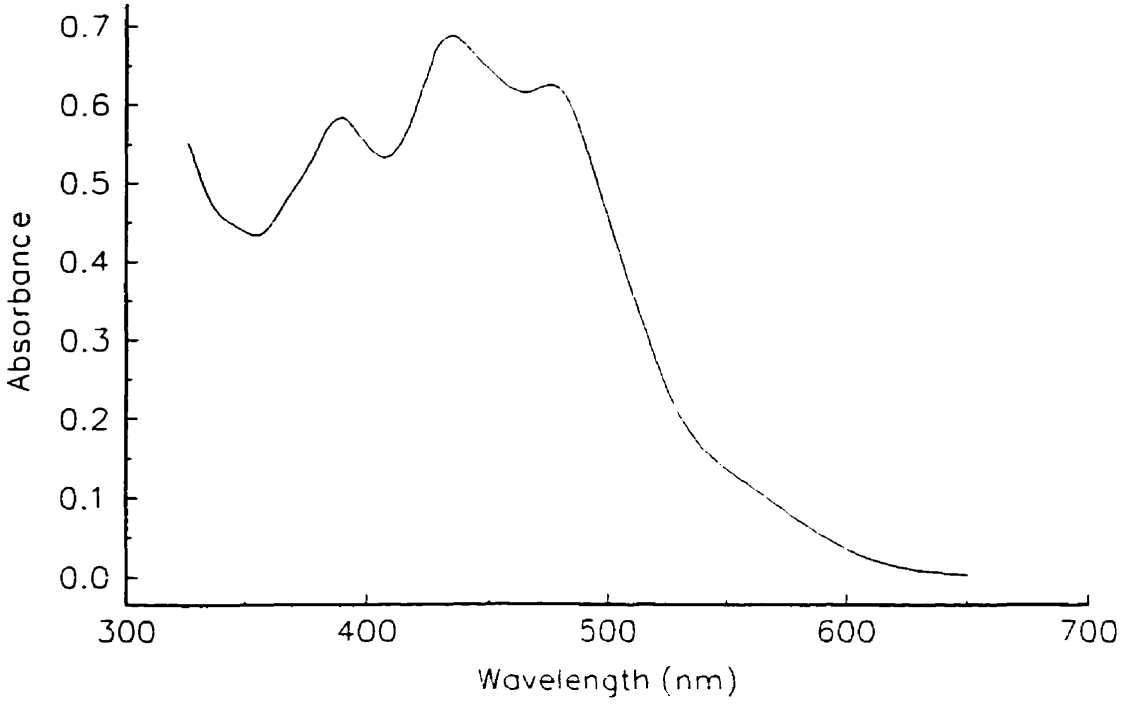

Figure 3.4.4. UV-visible spectrum of 1.4×10^{-5} mol·L^{-1} solution of **(8)** in DMF.

3.5. Electrochemical Studies

The cyclic voltammograms for all polynuclear compounds presented in this thesis have very poorly defined waves, with the exception of those of **(5)**.

Figure 3.5.1 depicts the cyclic voltammograms for **(1)** over the ranges ±1.50V and ±0.40V (voltammograms for **(2)** and **(4)** are very similar to those of **(1)**). Over the ±1.50V range a number of waves were observed, but only one at $E_{1/2}$= 0.010V could reasonably be associated with a copper based redox process. Recognizing the possibility that such a large voltage window could lead to secondary redox processes associated with initial redox products (e.g. a very strong anodic peak at E= 0.15V), the redox window was narrowed to ±0.40V. A series of waves ($E_{1/2}$= 0.010V) was obtained for **(1)** at

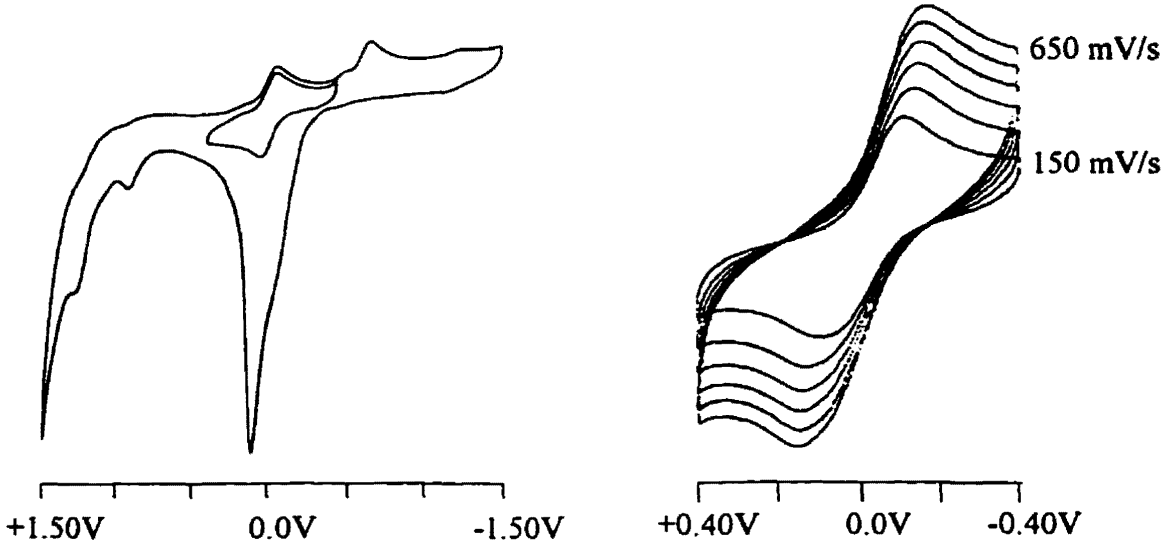

(a) **(1)**; GC/SCE/DMSO/TEAP; Scan Rate: 75mV/s.

(b) **(1)**; GC/SCE/DMSO/TEAP; Scan Rate: 150mV/s to 650mV/s at 100mV/s steps.

Figure 3.5.1. Cyclic voltammograms for **(1)** over the ranges of (a) outer ± 1.50V, inner ± 0.40V, and (b) ± 0.40V at variable scan rate.

variable scan rate (Figure 3.5.1b; ΔE_p= 220mV at 150mV/s) with large peak to peak separations, indicating an essentially non-reversible process (ΔE_p for Fc^+/Fc= 90mV (Fc = ferrocene) under the same conditions). While the $E_{1/2}$ value is higher than expected for a one electron reduction process at the binuclear copper(II) centre, this assignment is reasonable given the electronic influence of the ligand. As a comparison, the binuclear copper(II) Robson macrocycle derived from 2,6-diacetyl-4-methylphenol and ethylenediamine has two quasi-reversible waves found at -0.41V (ΔE_p= 120mV at 200mV/s) and -1.15V (ΔE_p= 100mV at 200mV/s) versus SCE [66]. It is reasoned that the $E_{1/2}$ values are much more positive for the DAM systems (Table 3.5.1) because the electron withdrawing cyano functions (electronically linked to the binuclear core via π conjugation) are able to produce enhanced electropositive character on the copper(II) core.

This electrochemical behaviour exhibited by **(1)** is expected to be a direct consequence of the rigid structure of the DAM-based Robson macrocycle. While a one electron reduction to Cu(II)-Cu(I) seems reasonable at 0.010V, a second cathodic peak is observed at -0.60V (Figure 3.5.1a). It is suggested that at -0.60V, the Cu(II)-Cu(I) species is unstable and the Cu(I) site is actually reduced to Cu(0), with Cu(0) being the cause of the intense anodic wave observed at 0.15V upon continuing the scan. Given the expected inability for the DAM-based Robson macrocycle to distort to satisfy the tetrahedral geometry preferred for Cu(I), it is most reasonable to assume that the Cu(I) generated at $E_{1/2}$= 0.010V is reduced to Cu(0); it is highly unlikely that the rigid, flat

ligand framework would be able to distort to accommodate a Cu(I)-Cu(I) species. For this reason, a single one electron non-reversible copper based process is found for the DAM-derived systems of **(1)**, **(2)** and **(4)** at $E_{1/2}$= ~ 0.01V, in contrast to the two quasi-reversible processes found for macrocycles with aliphatic spacer groups [66] such as the ethylenediamine-derived system noted above.

Table 3.5.1. $E_{1/2}$ Values (versus SCE) for the Non-Reversible Waves Found in the Cyclic Voltammograms of **(1)**, **(2)**, **(4)**, **(8)** and **(9)**.

Chemical Formula and Number Designation	$E_{1/2}$, (V)	$^{\dagger}\Delta E_p$, (mV)
$[Cu_2M1](ClO_4)_2(H_2O)_3(CH_3OH)$ **(1)**	0.010	220
$[Cu_2M2](ClO_4)_2$ **(2)**	0.0075	285
$[Cu_2M3](ClO_4)_2(H_2O)_2$ **(4)**	0.0065	297
$[Cu_2L3](ClO_4)(C_2H_5OH)$ **(8)**	0.038	155
$[Cu_4L4](ClO_4)_2(C_2H_5OH)_2$ **(9)**	0.068	145

†Scan rate for all quoted values of ΔE_p is 150mV/s. ΔE_p for Fc^+/Fc = 90mV.

Figure 3.5.2 reveals that the electrochemical behaviour of **(8)** is very similar to that of **(1)**, **(2)** and **(4)**, and the wave at $E_{1/2}$= 0.038V is attributed to a non-reversible reduction of Cu(II)-Cu(II) to Cu(II)-Cu(I) (ΔE_p= 155mV at 150mV/s). An interesting facet of the voltammogram of **(8)** over the ±1.25V range (Figure 3.5.2a) is the shoulder found on the cathodic peak at -0.85V. While the peak at -0.85V is attributed to the (newly generated)

Cu(II)-Cu(I) state being reduced to the Cu(II)-Cu(0) state (as for **(1)**), the shoulder at -0.75V is attributed to a small portion of Cu(II)-Cu(I) being reduced to Cu(I)-Cu(I). Accordingly, upon continuing the scan from -1.25V to the positive direction, an anodic shoulder is observed at -0.70V. Consistent with the structural differences between **(1)** and **(8)**, it appears that the non-macrocyclic framework of **(8)** may allow for distortions that may stabilize not only a small fraction of the Cu(II)-Cu(I) species, but also the Cu(I)-Cu(I) species. The voltammogram of **(9)** has the same features as that for **(8)**, in accordance with the structural similarities between the two compounds. The $E_{1/2}$ and ΔE_p values for **(8)** and **(9)** are also included in Table 3.5.1.

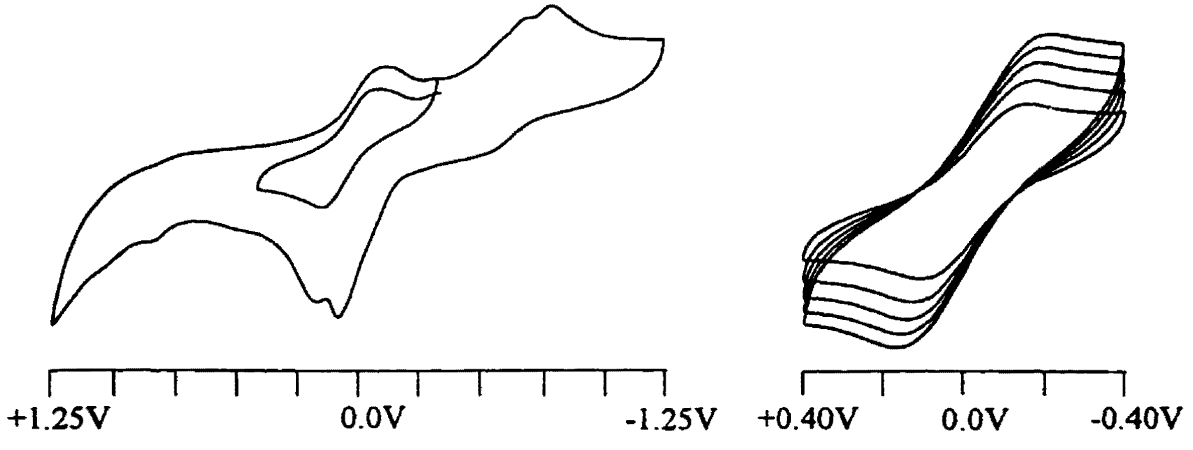

(a) **(8)**; GC/SCE/DMSO/TEAP; Scan Rate: 250mV/s

(b) **(8)**; GC/SCE/DMSO/TEAP; Scan Rate: 150mV/s to 550mV/s at 100mV/s steps.

Figure 3.5.2 Cyclic voltammograms for **(8)** over the ranges of (a) outer ℗1.25V, inner +0.40V to -0.30V, and (b) ℗0.40V at variable scan rate.

The acetonyl adduct, **(5)**, with comparatively more flexible chelate rings facilitated by tetrahedral C(8) and C(18) carbons (Figures 3.1.1, 3.1.2), has two well defined redox waves observed at $E_{1/2}$= -0.57V and -0.94V. The cyclic voltammograms for **(5)** obtained over the range of -0.20V to -1.35V in dried dimethylsulfoxide are displayed in Figure 3.5.3. Both waves are reversible, one-electron reductions, as confirmed by coulometric measurements performed at -0.82V, -0.20V and -1.25V. The wave at -0.57V (ΔE_p = 90mV at 150mV/s) is attributed to reduction of binuclear Cu(II)-Cu(II) to

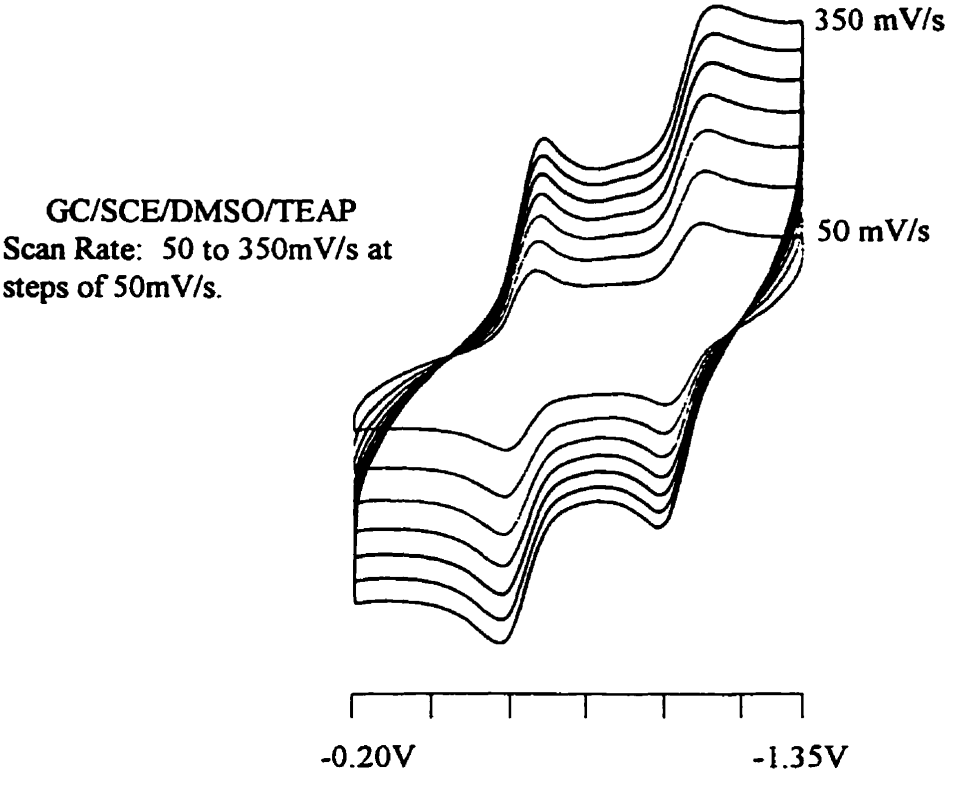

Figure 3.5.3. Variable scan-rate cyclic voltammograms of **(5)** in dry DMSO over the -0.20V to -1.35V range.

Cu(II)-Cu(I), as a result of coulometry performed at -0.82V which indicated the passage of one equivalent of electrons. When the same solution was then subjected to a controlled potential of -0.20V, the Cu(II)-Cu(I) system was readily oxidized back to Cu(II)-Cu(II), with passage again of one equivalent of electrons. The reversible wave at -0.94V (ΔE_p = 100mV at 150mV/s) is attributed to reduction of Cu(II)-Cu(I) to the binuclear copper(I) species, for upon applying a potential of -1.25V to a Cu(II)-Cu(II) solution of **(5)** and again performing coulometric measurements, the passage of two equivalents of electrons was observed. At no point during these coulometric studies were current fluctuations observed which would be indicative of radical processes.

The $E_{1/2}$ values for the stepwise reduction of **(5)** to first Cu(II)-Cu(I) and then Cu(I)-Cu(I) are very similar to those found for binuclear copper(II) Robson macrocycles with aliphatic spacer units [44]. This indicates that the cyano functions of **(5)** are essentially electronically disconnected from the binuclear core, and are not affecting the observed reduction potentials significantly. An interesting comparison exists between the electrochemistry of **(5)** and that of the compounds utilized by Mandal and coworkers [44] in a study of the variation in reduction potentials for binuclear copper(II) systems with the degree of saturation at the azomethine linkage of the Robson-type macrocycle (Figure 3.5.4). While all three macrocyclic coordination compounds [44] exhibit stepwise one-electron reduction from the binuclear copper(II) species through to the binuclear copper(I) species via an intermediate mixed valence species, the macrocyclic coordination compound with two reduced imine linkages (Figure 3.5.4b) has reduction potentials

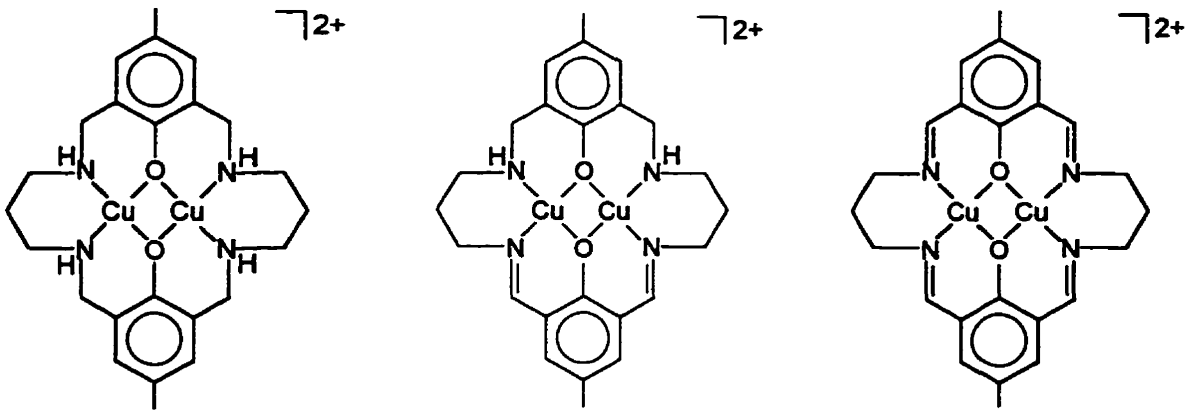

(a) (b) (c)

$E_{1/2}$ Cu(II)/Cu(I) = -0.76V | $E_{1/2}$ Cu(II)/Cu(I) = -0.58V | $E_{1/2}$ Cu(II)/Cu(I) = -0.43V

$E_{1/2}$ Cu(I)/Cu(I) = -0.90V | $E_{1/2}$ Cu(I)/Cu(I) = -0.90V | $E_{1/2}$ Cu(I)/Cu(I) = -0.90V

K_{con} = 2.3 x 10^2 | K_{con} = 2.6 x 10^5 | K_{con} = 9.0 x 10^7

Figure 3.5.4. Macrocyclic binuclear copper(II) compounds studied by Mandal and coworkers [44] to determine the variation in one-electron reduction potentials as a function of saturation at the azomethine linkage.

closest to that of **(5)**, with redox steps at $E_{1/2}$= -0.58V and -0.90V [44]. This adds further support for the assessment that two azomethine linkages of **(1)** have become single bonds upon addition of two acetonyl groups to form **(5)** (as discussed in Sections 3.1 and 3.2). The conproportionation constant, K_{con},

$$K_{con} = \frac{[\text{Cu(II)Cu(I)M}]^2}{[\text{Cu(II)Cu(II)M}][\text{Cu(I)Cu(I)M}]} = \exp(nF(\Delta E)/RT)$$

indicates the stability of the mixed valence species with respect to conproportionation (where ΔE = [($E_{1/2}$ Cu(II)/Cu(I)) - ($E_{1/2}$ Cu(I)/Cu(I))] and M = M^{2+}). For **(5)**, the above

expression yields K_{con}= 1.8x10^6, which is within the same order of magnitude as that of the compound in Figure 3.5.4b. As indicated by K_{con} and the large separation between the potentials of the redox couple, the mixed valence state generated from **(5)** may be considered to be very stable with respect to conproportionation.

3.6. Magnetochemistry

One of the main objectives of this study was to probe the magnetochemical behaviour of the copper(II) coordination compounds of the ligands derived from formylphenols and diaminomaleonitrile. Room temperature magnetic moments of the binuclear copper(II) macrocyclic compounds **(1)**, **(2)** and **(4)** (0.99μ_B, 1.05μ_B and 1.13μ_B, respectively) are considerably lower than the copper(II) spin-only value (1.73μ_B), indicating moderately strong antiferromagnetic exchange. For the non-macrocyclic polynuclear copper(II) compounds, the room temperature magnetic moments were found to be 1.38μ_B for **(8)** and 1.46μ_B for **(9)**, which are somewhat higher than expected when compared to the macrocycles **(1)**, **(2)** and **(4)**. The room temperature magnetic moment of **(5)** is 1.70μ_B, suggesting the possibility of a weakly antiferromagnetically coupled system. In the case of **(7)**, a moment of 1.75μ_B was recorded, consistent with the simple mononuclear nature of this copper(II) (d^9) coordination compound.

Variable temperature magnetic susceptibility data were obtained in the range 4-300K for the macrocyclic analogs **(1)**, **(2)** and **(4)**, and are plotted in Figures 3.6.1 to 3.6.3, respectively, along with the fitted curves generated from parameters obtained by

non-linear regression of the data using the Bleaney-Bowers equation (equation (1.3.7)). Table 3.6.1 reports the fitting parameters obtained from this treatment of the data, with the estimated standard deviation in the last digit (or last two digits) for $2J$ and g (from the non-linear regression) being reported in parentheses.

Table 3.6.1. Magnetic Data.

Compound	g	$2J$ (cm^{-1})	ρ	$N\alpha$ (10^6emu)	θ (K)	$10^2R^{\dagger}$
(1)	2.00(2)	-465(4)	0.012	45	-0.3	0.88
(2)	2.05(3)	-445(10)	0.03	74	-0.8	2.7
(4)	2.00(1)	-407(28)	0.0143	58	-1.5	4.7

$^{\dagger}R = [\Sigma(\chi_{obs} - \chi_{calc})^2/\Sigma\chi_{obs}^2]^{1/2}$

Though a poorer fit was obtained for **(4)** compared with **(1)** and **(2)**, the $2J$ value is consistent. As expected from the room temperature magnetic moments and the profiles of susceptibility versus temperature for **(1)**, **(2)**, and **(4)**, all exhibit moderate antiferromagnetic coupling with similar $2J$ values. The small negative θ values necessary for the magnetic analysis of **(1)**, **(2)** and **(4)** suggest the presence of very weak antiferromagnetic coupling between individual molecules [67]. Although no crystal structures were obtained, the flat nature of these coordination compounds should allow for close parallel stacking which might result in these weak intermolecular interactions.

To put the above $2J$ values in perspective, comparisons of the magnetic data of **(1)**, **(2)**, and **(4)** to those reported for compounds with similar geometric and/or electronic

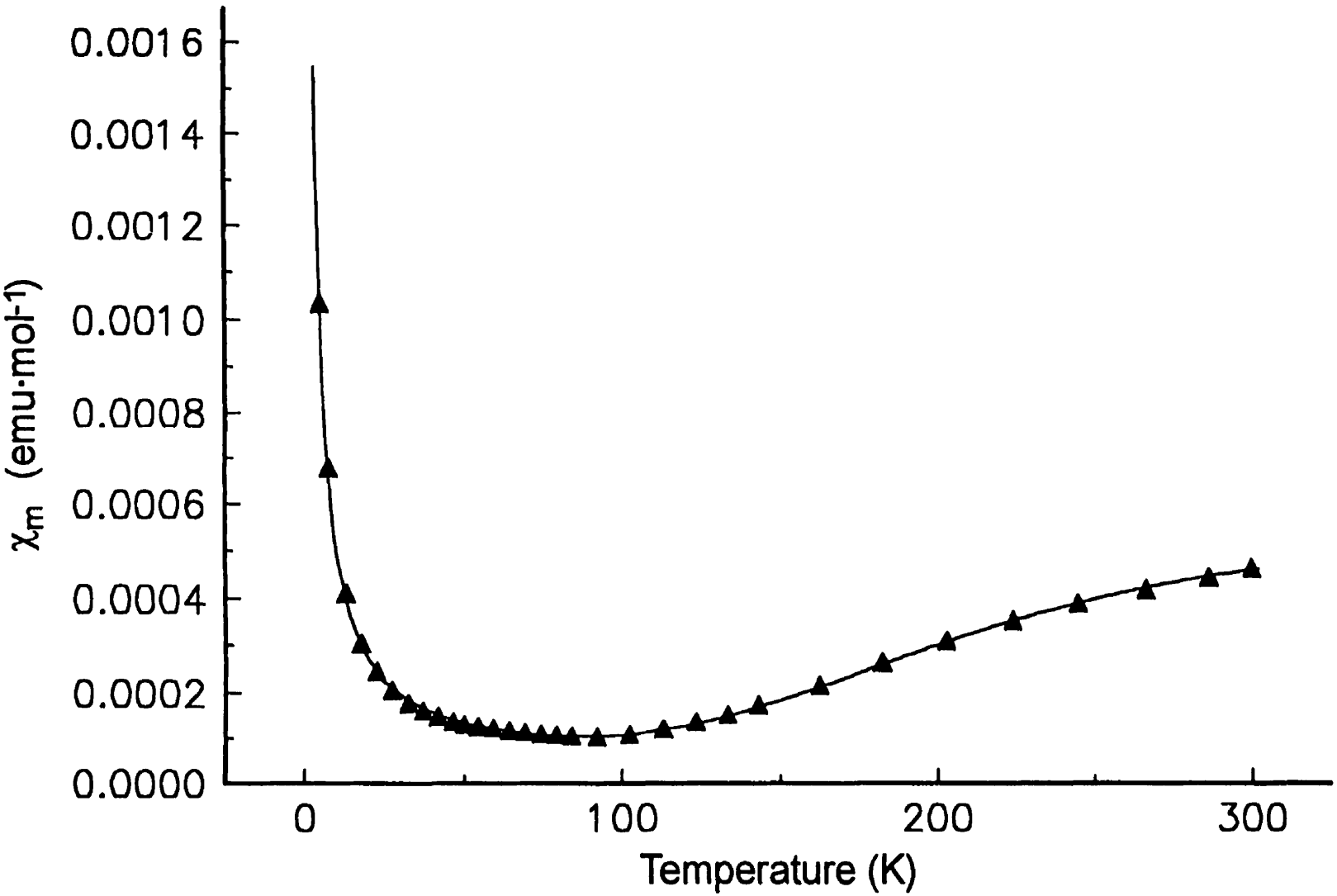

Figure 3.6.1. Variable temperature magnetic susceptibility data (▲) for $[Cu_2M1](ClO_4)_2(H_2O)_3(CH_3OH)$, **(1)** with least squares line (-). See Table 3.6.1 for the parameterization for the least squares line.

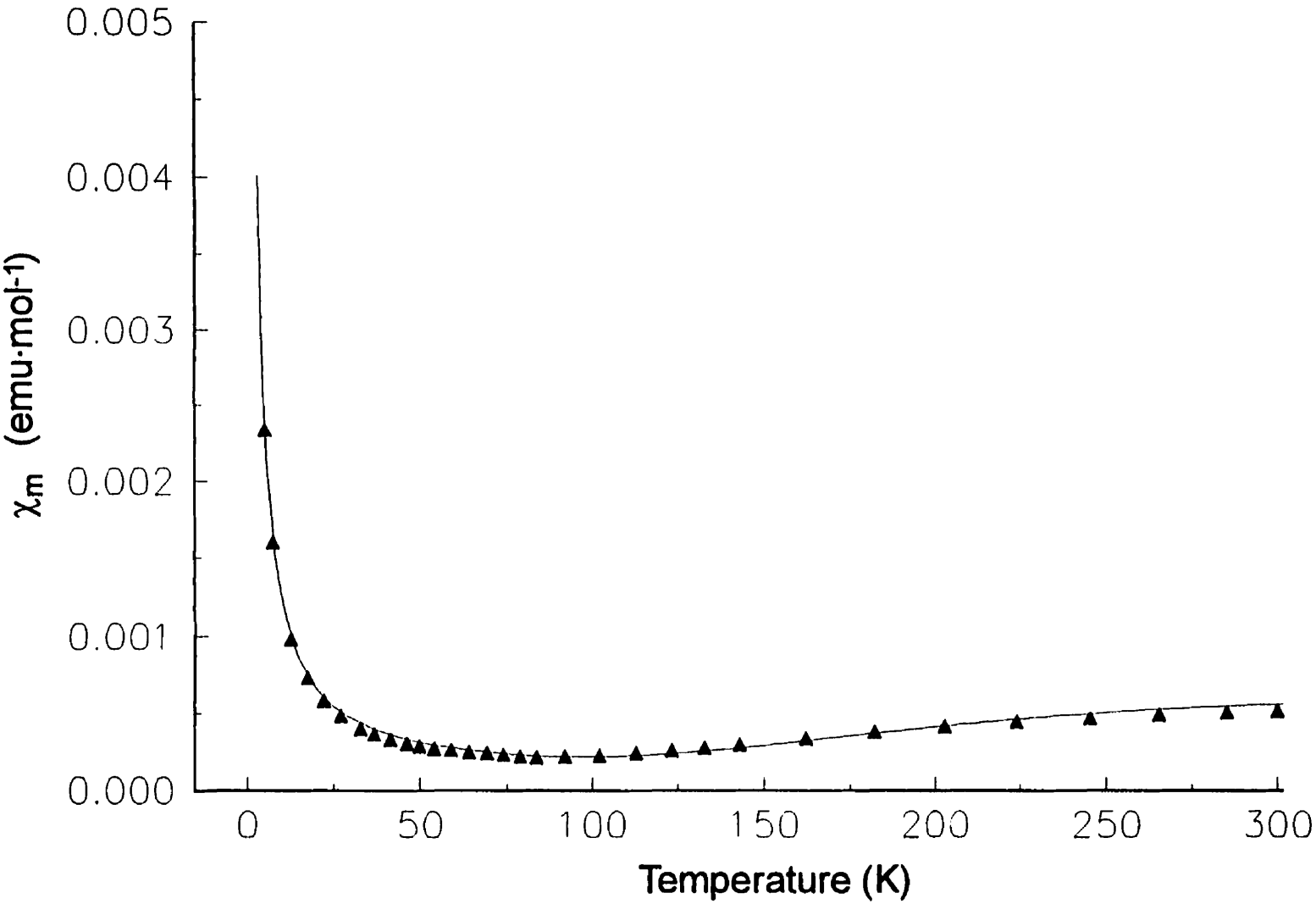

Figure 3.6.2. **Variable temperature magnetic susceptibility data (▲) for $[Cu_2M2](ClO_4)_2$, (2) with least squares line (-). See Table 3.6.1 for the parameterization for the least squares line.**

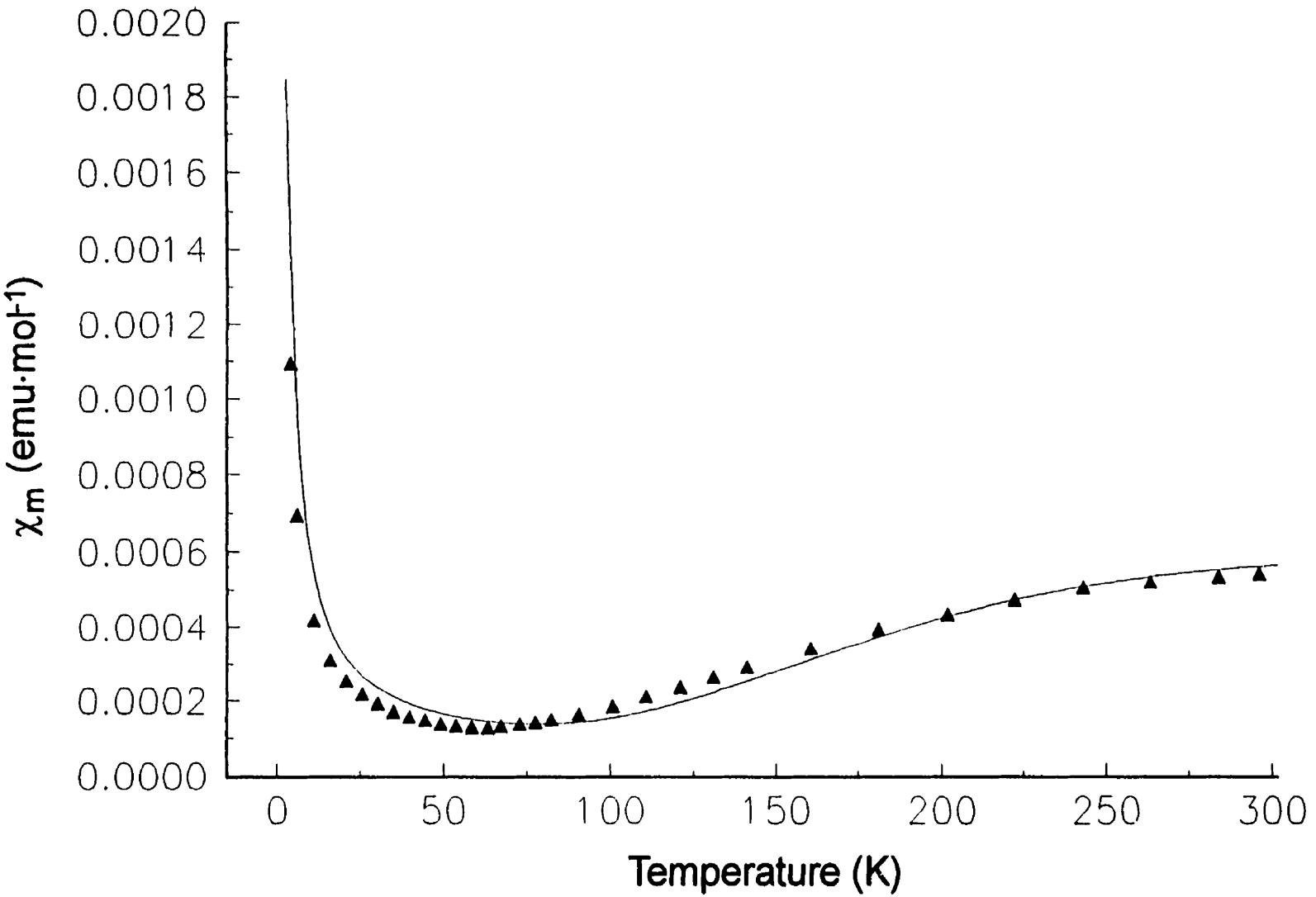

Figure 3.6.3. Variable temperature magnetic susceptibility data (▲) for $[Cu_2M3](ClO_4)_2(H_2O)_2$, **(4)** with least squares line (-). See the text for the parameterization for the least squares line.

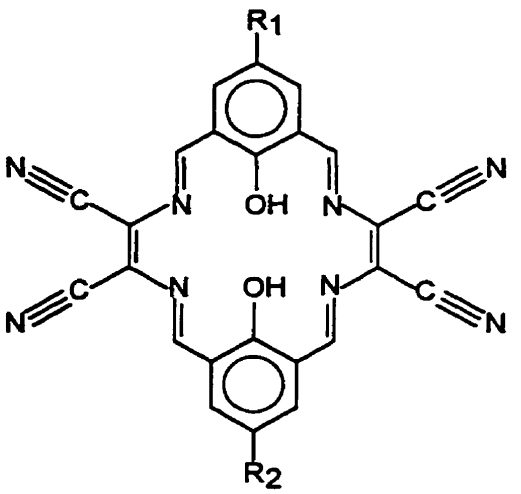

H_2M1: $R_1, R_2 = CH_3, CH_3$
H_2M2: R_1, R_2 = t-Bu, t-Bu
H_2M3: $R_1, R_2 = CH_3$, t-Bu

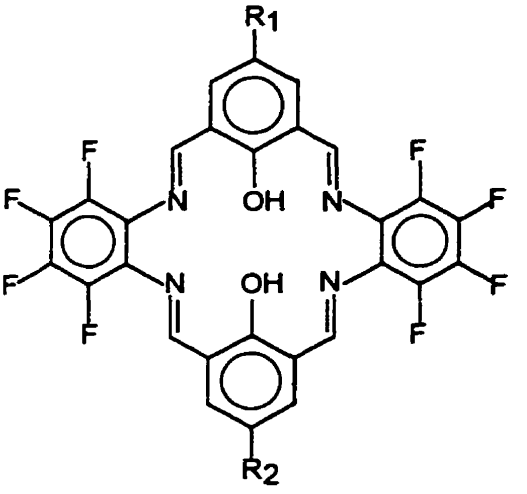

H_2M5: $R_1 = R_2 = C_3H_7$
H_2M6: $R_1 = R_2$ = t-Bu

Figure 3.6.4. Macrocyclic ligands with electronic or structural features similar to H_2M1-H_2M3.

structures follow. Figure 3.6.4 depicts the macrocyclic ligands in the compounds used in the comparisons. The x-ray crystal structures of the binuclear copper(II) coordination compounds of $M5^{2-}$ and $M6^{2-}$ have been reported by Brychcy and coworkers [61]. These macrocyclic compounds, with two electron withdrawing perfluoro *o*-phenylenediamine derived spacer units (π conjugated to the binuclear copper(II) core) are expected to be similar to **(1)**, **(2)**, and **(4)** in both geometric and electronic structure. For average Cu-OPh-Cu bridge angles of $\alpha = 100.8°$ ($[Cu_2M5]^{2+}$) and 99.2° ($[Cu_2M6]^{2+}$), respective $2J$ values of $-526cm^{-1}$ and $-581cm^{-1}$ were determined from the variable temperature magnetic susceptibility measurements. These values are much less negative than the values expected from the magnetostructural correlation (using equation (1.7.1), for $\alpha = 100.8°$,

$2J = -759cm^{-1}$; for $\alpha = 99.2°$, $2J = -707cm^{-1}$). Since these two macrocyclic compounds are essentially planar and have binuclear copper(II) centres with square planar $d_{x^2-y^2}$ magnetic ground states, the observed decrease from the expected antiferromagnetic exchange is attributed to the presence of four heavily electron-withdrawing fluorine atoms bound to each *o*-phenylenediamine spacer group. Considering the electronic similarities as well as the expected structural similarities between these perfluoro compounds and **(1)**, **(2)** and **(4)**, the following postulate may be made: *If a Robson-type binuclear macrocyclic coordination compound has electron withdrawing substituents within any part of the π framework that is linked to the binuclear core, the overall effect will be to lower the magnitude of the antiferromagnetic exchange from that which is expected according to the magnetostructural correlation* [8] *for phenoxide bridged binuclear copper(II) compounds.* The mechanism by which this occurs will be addressed in detail after considering the magnetochemistry of the acetonyl adduct, **(5)**.

The variable temperature magnetic data of **(5)** (Figure 3.6.5) are most unusual, with a sharp susceptibility maximum at ~ 30K indicating very weak antiferromagnetic exchange. Nonlinear regression of the data using the Bleaney-Bowers equation (equation (1.3.7) yielded a good least squares fit ($10^2R = 0.61$) for $g = 2.024(3)$, $2J = -25.2(3)cm^{-1}$, $N\alpha = 57 \times 10^{-6}$ emu, $\theta = -1.6K$ and $\rho = 0.034$ (The solid line in Figure 3.6.5 was calculated using these parameters). Again, the small negative θ value suggests a weak intermolecular antiferromagnetic interaction between neighbouring molecules [67]. However, apart from weak contacts between the free acetone oxygen O(5) and the

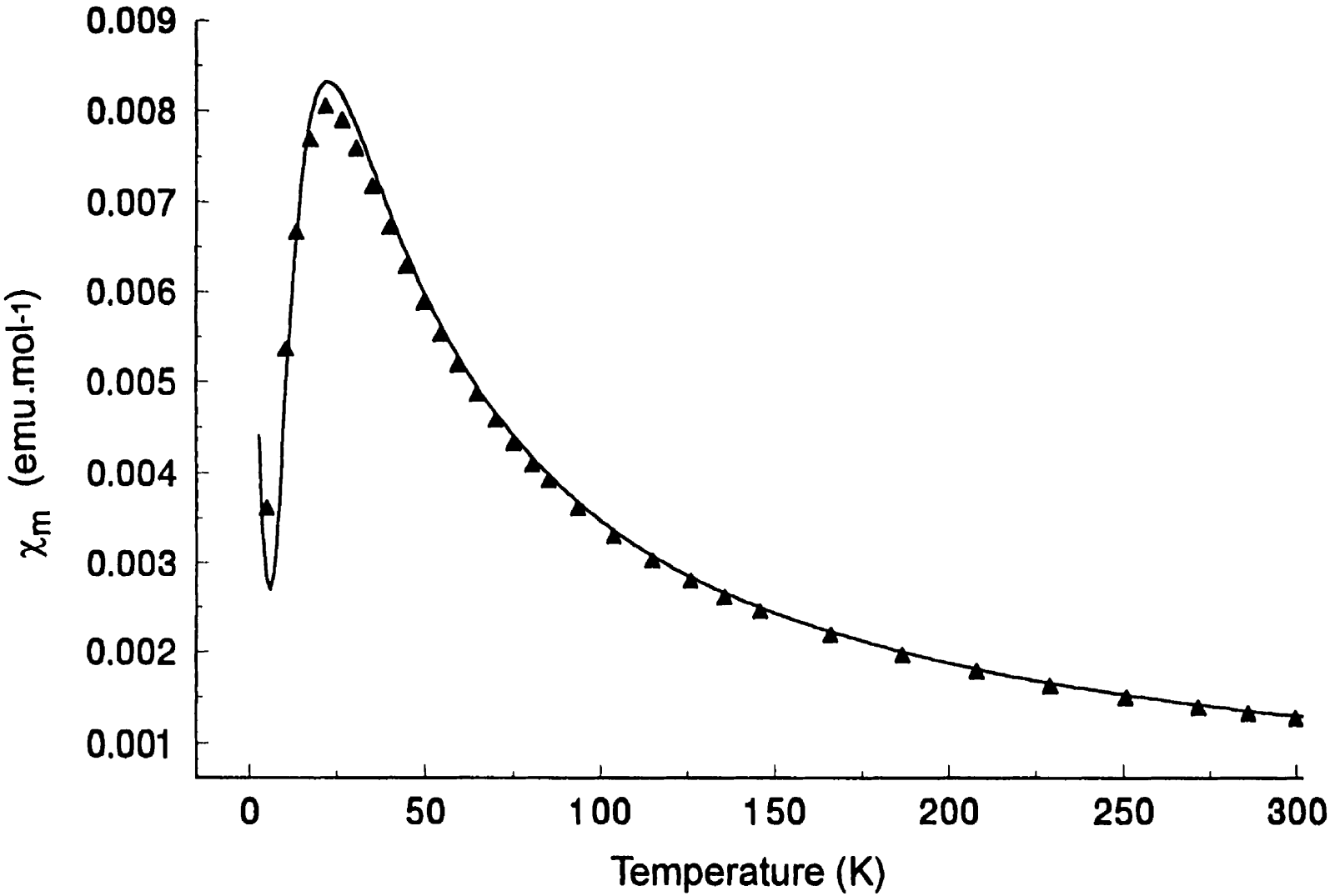

Figure 3.6.5. Variable temperature magnetic susceptibility data (▲) for $[Cu_2M4](CH_3COCH_3)$, **(5)** with least squares line(-). See the text for the parameterization for the least squares line.

copper(II) centres (Cu(1)-O(5) = 2.815 Å; Cu(2)-O(5) = 2.755 Å), no typical exchange pathways could be found. It should also be noted that although the Cu···Cu separation in **(5)** is only 2.788(2) Å, there are no anomalies in the susceptibility versus temperature profile for this compound which might indicate the presence of a direct metal-metal interaction.

It is quite remarkable that antiferromagnetic exchange prevails for the acetonyl adduct **(5)** in light of the following structural features. First of all, the binuclear Cu_2O_2 core is highly bent along the O(1)-O(2) axis, with an angle of 151.1° between the CuN_2O_2 least squares planes (Figure 3.1.2). Kahn has suggested [14] from his extended Hückel study of hydroxide bridged systems that such distortions from planarity would cause a drastic decrease in the extent of antiferromagnetic exchange (refer to Section 1.6 for a detailed discussion). Secondly, the acetonyl adduct also has an extremely low average Cu-OPh-Cu bridge angle (92.4°), well below the crossover angle (α_c) for planar hydroxide bridged systems (97.5°) [10] or planar alkoxide bridged systems (95.7°) [11]. Based on these two points alone, the persistence of antiferromagnetic behaviour is remarkable. It is quite important to state that the cyano functions at the periphery of the macrocyclic ligand of **(5)** are expected to have LITTLE EFFECT on the $2J$ value of this compound, since the cyclic voltammograms are very similar to binuclear copper(II) compounds with aliphatic spacer groups (Section 3.5). Since **(5)** is still antiferromagnetically coupled despite the structural features listed above, the acetonyl adduct in essence supports the proposition that binuclear copper(II) phenoxide bridged Robson macrocycles will exhibit

antiferromagnetic exchange at very low bridge angles [8].

Though experimentally untested to date, it has been proposed [8] that such phenoxide bridged systems derived from the Schiff base condensation of diformylphenols and diamines exhibit greater antiferromagnetic exchange than their hydroxide or alkoxide counterparts as a result of a secondary exchange mechanism propagated through the unsaturated azomethine linkages. Wieghardt and coworkers [68] have proposed a σ pathway exchange mechanism to explain intramolecular antiferromagnetic coupling ($2J = -62cm^{-1}$) between two copper(II) ions which are 15.6 Å apart, linked by a μ-dicarboxylato ligand (Figure 3.6.6). It is quite reasonable to suggest analogous imine exchange mechanisms for phenoxide bridged copper(II) compounds (Figure 3.6.7) over (a) eight bonds through both azomethine linkages via the aromatic ring carbons, or (b) only six bonds going to first the phenolate bridge and then to a single azomethine linkage again via the aromatic ring carbons. Note that there are multiples of these routes which are possible; only two are shown for each of (a) and (b) for clarity. Should such a

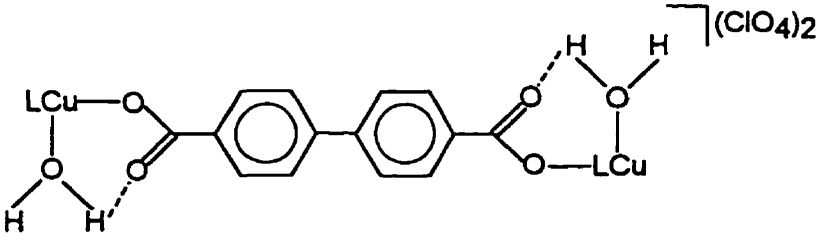

Figure 3.6.6. Binuclear copper(II) coordination compound shown by Wieghardt and coworkers [68] to exhibit intramolecular antiferromagnetic exchange. (L=1,4,7-trimethyl-1,4,7-triazacyclo-nonane)

(a)

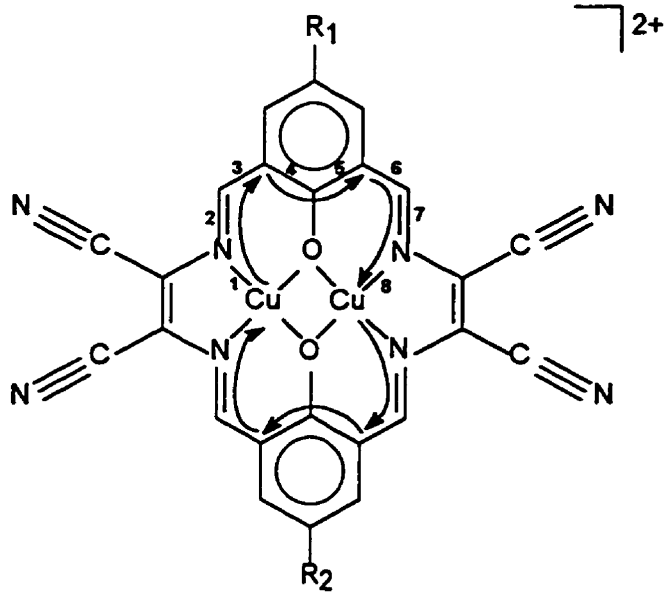

(b)

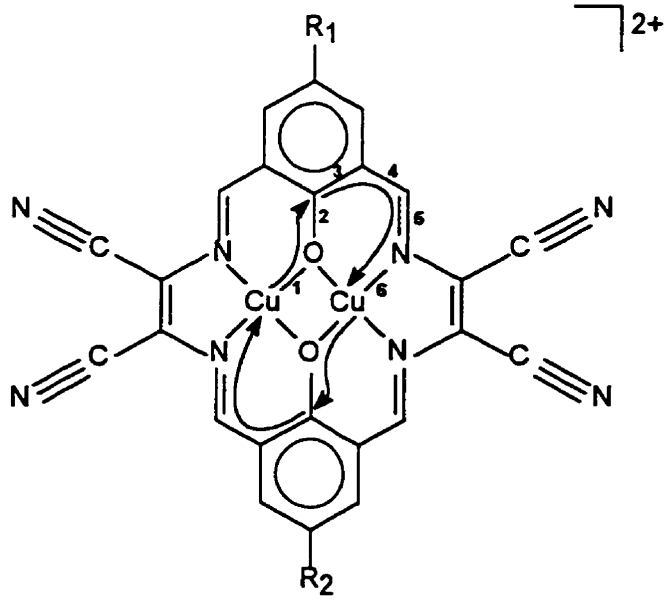

Figure 3.6.7. Proposed alternative antiferromagnetic exchange routes from the phenoxide bridge route which utilize the unsaturated azomethine linkages in binuclear Robson macrocylces.

mechanism entailing these exchange routes exist over the whole phenoxide bridge angle range, contributing a roughly constant value to the antiferromagnetic component of the observed exchange ($J_T = J_F + J_{AF}$, equation (1.6.3)), accidental orthogonality of the magnetic orbitals *at the phenoxide bridge* may in fact occur close to the more reasonably expected angle (~97°) although the $2J = 0$ angle may be actually projected to be much smaller. The acetonyl adduct **(5)**, with two remaining unsaturated imine linkages derived from its parent **(1)**, exhibits very weak antiferromagnetic behaviour, supporting this mechanism.

3.7. Extended Hückel Molecular Orbital Model Study

Robson-type copper(II) binuclear macrocycles having the same spacer groups about a Cu_2O_2 core are prime candidates for an extended Hückel molecular orbital study. A survey of the x-ray crystallographic structural details of the macrocycles [8,37,38,40, 44,45] used in the magnetostructural correlation for phenoxide bridged systems [8] reveals that while the $Cu\text{-}O_{phenoxide}$ and Cu-N bond distances show little variation, the Cu-OPh-Cu bridge angle varies in parallel with a variation in Cu···Cu separation. A similar situation was also observed by Kahn and coworkers [14] who carried out the molecular orbital analysis of hydroxide bridged systems described in Section 1.6. The study that follows will consider the relationship between phenoxide bridge angle, α, and the degree of antiferromagnetism, J_{AF}, as a function of the MO energies of the singly occupied molecular orbitals of a model system. The mathematical formulation used is that of Kahn [13,14] as

described in Section 1.6, utilizing both the extended Hückel program (EHC) and computer-aided composition of atomic orbitals (CACAO) program of Mealli and Proserpio [23]. The parameters for the optimized Slater type orbitals were provided by Dr. Francesc Lloret [69], and may be found in Appendix I along with the Z-matrix input file used with the EHC program.

The model compound is illustrated in Figure 3.7.1, with bond lengths and angles derived from averaging these parameters from the crystallographic data of the compounds used in the phenoxide bridge magnetostructural correlation [8]. The Cu-$O_{phenoxide}$ and Cu-N bond lengths were maintained constant at 1.975Å and 1.98Å, respectively. The N-Cu-N angle was also maintained constant at 99°, again derived from averaging the

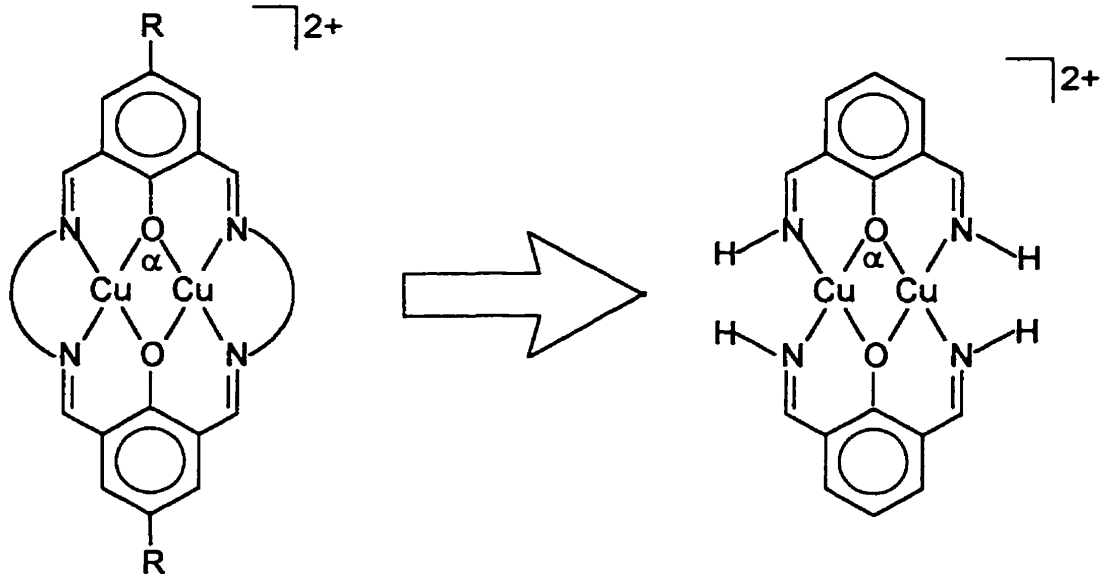

Figure 3.7.1. A schematic of the copper(II) phenoxide bridged compounds (left) from which the model compound (right) was derived. R = CH_3, t-Bu. The curved line denotes an aliphatic spacer group.

values quoted in the crystallographic data. As noted above, the Cu-OPh-Cu bridge angle α was varied as a function of Cu···Cu separation only, affording a direct correlation between the degree of antiferromagnetic coupling and α without any other variables complicating the analysis. It is important to note that independent variation of the Cu-O, Cu-N bond lengths and N-Cu-N angle, at constant Cu-OPh-Cu bridge angle, had very little effect on the difference between the energies of the singly occupied MOs. This difference, according to equation (1.6.8), is the preponderant factor in determining the magnitude of J_{AF} and indicates that it is the angle at the phenoxide bridge which emerges as the most important structural factor governing the magnitude of antiferromagnetic exchange.

Figure 3.7.2 (following page) yields illustrations of the triplet b_{3u} and b_{2g} molecular orbitals obtained by the extended Hückel calculations, while the crux of this study, the variation in the energies of these MOs as a function of bridge angle, is found in Figure 3.7.3. Recalling that $J_{AF} \propto \Delta^2$ (equation (1.6.8)), where Δ is the difference, in this case, in the energies of the triplet b_{3u} and b_{2g} MOs, it is seen that Δ decreases with decreasing phenoxide bridge angle α, the same trend as Kahn observed for the hydroxide bridged system [14]. The striking feature of Figure 3.7.3 is that *no angle of accidental orthogonaltity is found (at which $\Delta = 0$ and $J_T = J_F$) in the angle range studied.* Though the MO energies appear to converge upon decreasing α, at no bridge angle in the range of 88°-100° do they become equal; extending the lines to lower angles projects α_o ~75° as the angle of accidental orthogonality for this Schiff base derived phenoxide bridged model

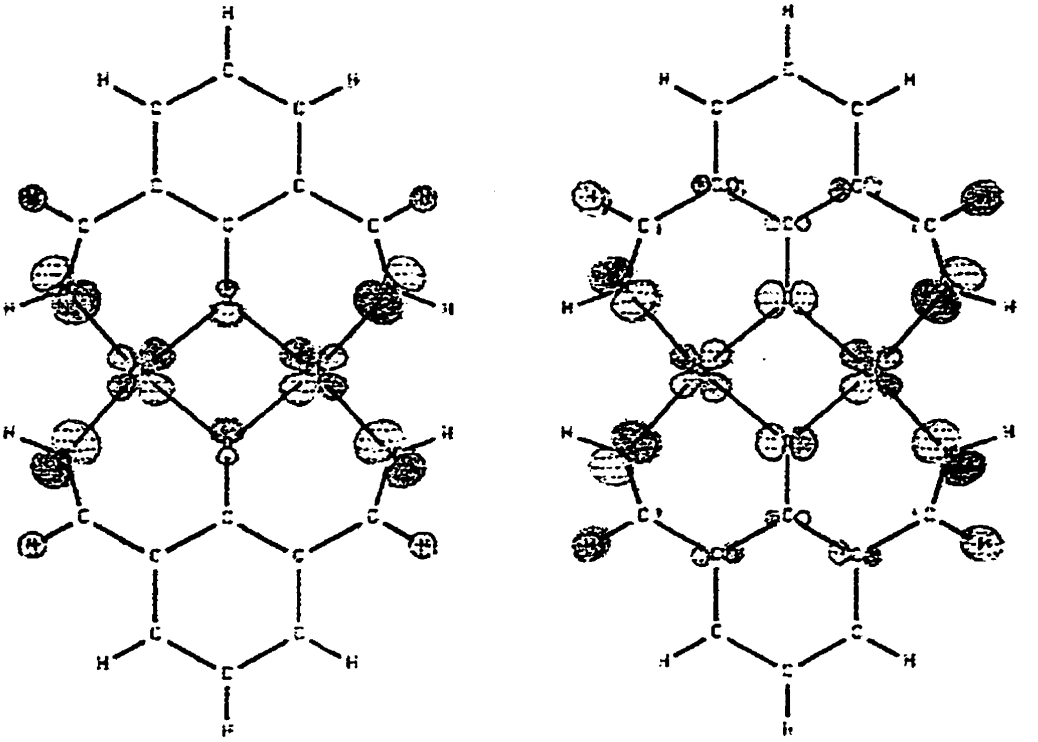

(a) (b)

Figure 3.7.2. Triplet molecular orbitals (contracted by the CACAO program by a factor of 1.5 for clarity) for the model system shown in Figure 3.7.1. (a) b_{3u}; (b) b_{2g}.

Following Page:

Figure 3.7.3. Variation in triplet MO energies (ε_{b3u}, ε_{b2g}) as a function of Cu-OPh-Cu bridge angle,α, of the model system shown in Figure 3.7.1.

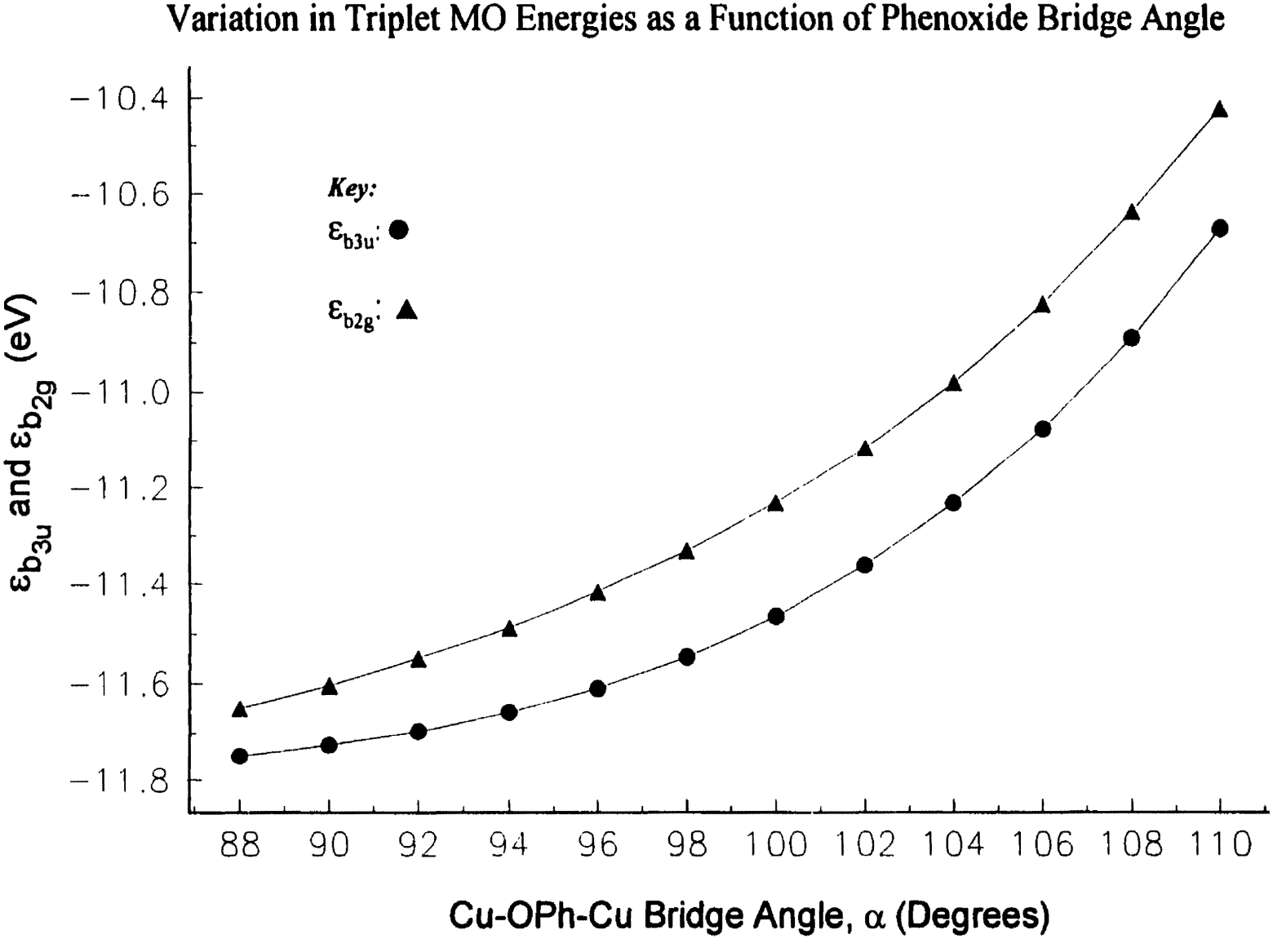
Variation in Triplet MO Energies as a Function of Phenoxide Bridge Angle
−10.4
−10.6
−10.8
−11.0
−11.2
−11.4
−11.6
−11.8
Key:
εb3u:
εb2g:
εb3u and εb2g (eV)
88
90
92
94
96
98
100
102
104
106
108
110
Cu-OPh-Cu Bridge Angle, α (Degrees)

system! This is quite remarkable, recalling that a crossover angle of $\alpha_c \sim 77°$ was predicted experimentally by the magnetostructural correlation [8] for phenoxide bridged binuclear copper(II) Robson-type macrocycles. The consistent experimental *and* computational results presented in this thesis add strong support to the earlier stated postulate: *It seems likely that all phenoxide bridged binuclear copper(II) macrocycles will exhibit overall antiferromagnetic behavior, even with very small bridge angles* α.

One last point to be addressed relates to the extended Hückel study above, the antiferromagnetic exchange mechanism proposed by Wieghardt and coworkers [68] discussed earlier and the possibility of a through ligand exchange contribution in the present systems. Over the angle range used in the extended Hückel study, the triplet state molecular orbitals displayed small atomic orbital contributions from the aromatic carbons, and virtually non-existent contributions from the azomethine carbons. With such a small atomic orbital contribution at the azomethine carbons, it is unclear whether or not this route yields a significant contribution, if any, to the exchange process. However, one weakness in the present model involves the rigid nature of the copper coordination plane with respect to the N-Cu-N angle. As the Cu···Cu separation and the Cu-O-Cu angle change, the angle at the azomethine carbon (C-C-N) clearly changes as well. Deviations from the ideal angle may be responsible for the apparent lack of involvement of this atom in the molecular orbital study, and future theoretical approaches to the exchange problem will address this situation in an attempt to resolve the question as to whether the ligand based, secondary exchange route is realistic.

4. Conclusions

The synthesis and characterization of the coordination compounds of ligands derived from template Schiff base condensation of formylphenols and diaminomaleonitrile has been presented, affording some very interesting final conclusions. First of all, it should be noted that in attempting to utilize diaminomaleonitrile as a diamine under established template conditions with metal salts and formylphenols, the expected straightforward reactivity does not always occur and consequently the 'normal' products are not always obtained. While general template methods yielded successful syntheses of binuclear copper(II) compounds for the [2+2] DAM / diformylphenol Schiff base derived macrocyclic ligands, the use of magnesium(II), nickel(II), vanadyl(II), manganese(II), lead(II) and zinc(II) was unsuccessful. Secondly, the binuclear copper(II) macrocycles of $M1^{2-}$-$M3^{2-}$ were expected to have a somewhat strained planar geometry due to the presence of very small chelate rings containing the two-carbon olefinic spacer groups. This appears to be the case, since $[Cu_2M1]^{2+}$ utilized the electronic influence of the peripheral cyano functions to facilitate the formation of the less strained acetonyl adduct **(5)** and the mononuclear dialdehyde compound **(7)**.

The magnetic properties of **(1)**, **(2)** and **(4)** were found to be anomalous with $2J$ values less than $-400cm^{-1}$. These values are much less negative than the lowest $2J$ value ($-689cm^{-1}$) of related phenoxide bridged Robson macrocycles with aliphatic spacer groups [8]. It is concluded that the electron withdrawing cyano functions, connected to the binuclear copper(II) core via π conjugation, are the cause of this observed decrease in the

magnitude of antiferromagnetic behaviour exhibited by the DAM systems.

A magnetostructural correlation for planar binuclear phenoxide bridged copper(II) macrocycles [8] suggested an extremely low antiferromagnetism / ferromagnetism crossover angle, α_c. Further evidence for a low α_c was provided by the experimentally observed antiferromagnetism of the acetonyl adduct (5) and the computational extended Hückel molecular orbital study. These results showed that antiferromagnetic behaviour may persist at very low bridge angles.

Considering future work, the possibile intramolecular azomethine mechanism of antiferromagnetic exchange in Robson macrocycles requires further experimental and computational study. As more Robson-type binuclear copper(II) compounds are synthesized, more data may be added to improve the phenoxide bridge correlation, which will hopefully provide answers to questions which lie at the heart of spin exchange phenomena in these coordination compounds.

References

1. Van Vleck, J.H. *The Theory of Electric and Magnetic Susceptibilities*; Oxford University Press: London, 1932.
2. Bleaney, B; Bowers, K.D. *Proc. R. Soc., London* **1952**, *A214*, 451.
3. Guha, B.C. *Proc. R. Soc., London* **1951**, *A206*, 353.
4. Brown, G.M.; Chidambaram, R. *Acta Crystallogr.* **1973**, *B29*, 2393.
5. de Meester, P.; Fletcher, S.R.; Skapski, A.C. *J. Chem. Soc., Dalton Trans.* **1973**, 2575.
6. Lippard, S.J.; Berg, J.M. *Principles of Bioinorganic Chemistry*; University Science Books: Mill Valley, CA, 1994.
7. Ochiai, E.-I. *Bioinorganic Chemistry - An Introduction*; Allyn and Bacon, Inc.: Toronto, 1977.
8. Thompson, L.K.; Mandal, S.K.; Tandon, S.S.; Bridson, J.N.; Park, M.K. *Inorg. Chem.* **1996**, *35*, 3117.
9. Earnshaw, A. *An Introduction to Magnetochemistry*; Academic Press Inc.: New York, NY, 1968.
10. Crawford, V.H.; Richardson, H.W.; Wasson, J.R.; Hodgson, D.J.; Hatfield, W.E. *Inorg. Chem.* **1976**, *15*, 2107.
11. Merz, L.; Haase, W. *J. Chem. Soc., Dalton Trans.* **1980**, 875.
12. Hay, P.J.; Thibeault, J.C.; Hoffmann, R. *J. Am. Chem. Soc.* **1975**, *97*, 4884.

13. a) Kahn, O. *Angew. Chem. Int. Ed. Engl.* **1985**, *24*, 834. b) Kahn, O. In *Magneto-Structural Correlations in Exchange Coupled Systems*; Willett, R.D.; Gatteschi, D.; Kahn, O., Eds.; D. Reidel Publishing Co.: Dordrecht, 1985. c) Kahn, O.; Briat, B. *J. Chem. Soc., Faraday Trans. II* **1976**, 268. d) Kahn, O.; Briat, B. *J. Chem. Soc., Faraday Trans. II* **1976**, 1441.

14. a) Charlot, M.F.; Jeannin, S.; Jeannin, Y.; Kahn, O.; Lucrece-Abaul, J.; Martin-Frere, J. *Inorg. Chem.* **1979**, *18*, 1675. b) Charlot, M.F.; Kahn, O.; Jeannin, S.; Jeannin, Y. *Inorg. Chem.* **1980**, *19*, 1410.

15. Kahn, O. *Inorg. Chim. Acta* **1982**, *62*, 3.

16. Kahn, O.; Mallah, T.; Gouteron, J.; Jeannin, S.; Jeannin, Y. *J. Chem. Soc., Dalton Trans.* **1989**, 1117.

17. de Loth, P.; Cassoux, P.; Daudey, J.P.; Malrieu, J.P. *J. Am. Chem. Soc.* **1981**, *103*, 4007.

18. Figgis, B.N.; Martin, R.L.; *J. Chem. Soc.* **1956**, 3837.

19. Astheimer, H; Haase, W. *J. Chem. Phys.* **1986**, *85*, 1427.

20. Handa, M.; Koga, N.; Kida, S. *Bull. Chem. Soc. Jpn.* **1988**, *61*, 3853.

21. Nishida, Y.; Kida, S. *Inorg. Chem.* **1988**, *27*, 447.

22. Nishida, Y.; Masumoto, M.; Mori, Y. *Z. Naturforsch., B: Chem. Sci.* **1989**, *44*, 307.

23. Mealli, C.; Proserpio, D.M. *J. Chem. Ed.* **1990**, *67*, 399.

24. Kahn, O. *Molecular Magnetism*; VCH Publishers: New York, NY, 1994.

25. Kahn, O.: personal communication

26. Girerd, J.J.; Journeaux, Y.; Kahn, O. *Chem. Phys. Lett.* **1981**, *82*, 534.

27. Heitler, W.; London, F. *Z. Phys.* **1927**, *44*, 455.

28. Kahn, O.; Briat, B.; Galy, J; *J. Chem. Soc., Dalton Trans.* **1977**, 1453.

29. Iitaka, Y.; Shimizu, K.; Kwan, T. *Acta Crystallogr.* **1966**, *20*, 803.

30. Pilkington, N.H.; Robson, R. *Aust. J. Chem.* **1970**, *23*, 2225.

31. Ōkawa, H.; Kida, S. *Bull. Chem. Soc. Jpn.* **1972**, *45*, 1759.

32. Addison, A.W.; *Inorg. Nucl. Chem. Lett.* **1976**, *12*, 899.

33. Gagné, R.R.; Spiro, C.L.; Smith, T.J.; Hamann, C.A.; Thies, W.R.; Shiemke, A.K. *J. Am. Chem. Soc.* **1981**, *103*, 4073.

34. Long, R.C.; Hendrickson, D.N., *J. Am. Chem. Soc.* **1983**, *105*, 1513.

35. Mandal, S.K.; Adhikary, B.; Nag, K. *J. Chem. Soc., Dalton Trans.* **1986**, 1175.

36. Carslisle, W.D.; Fenton, D.E.; Roberts, P.B.; Casellato, U.; Vigato, P.A.; Graziani, R. *Trans. Met. Chem. (London)* **1986**, *11*, 292.

37. Mandal, S.K.; Thompson, L.K.; Newlands, M.J.; Biswas, A.K.; Adhikary, B.; Nag, K.; Gabe, E.J.; Lee, F.L. *Can. J. Chem.* **1989**, *67*, 662.

38. Tandon, S.S.; Thompson, L.K.; Bridson, J.N.; McKee, V.; Downward, A.J. *Inorg. Chem.* **1992**, *31*, 4635.

39. Ōkawa, H.; Nishio, J.; Ohba, M.; Tadokoro, M; Matsumoto, N.; Koikawa, M.; Kida, S.; Fenton, D.E. *Inorg. Chem.* **1993**, *32*, 2949.

40. Tandon, S.S.; Thompson, L.K.; Bridson, J.N. *Inorg. Chem.* **1993**, *32*, 32.

41. Brychcy, K.; Dräger, K.; Jens, K.-J.; Tilset, M.; Behrens, U.; *Chem. Ber.* **1994**, *127*, 1817.

42. Kumar, D.S.; Alexander, V. *Inorg. Chim. Acta* **1995**, *238*, 63.

43. Atkins, A.J.; Black, D.; Blake, A.J.; Marin-Becerra, A.; Parsons, S.; Ruiz-Ramirez, L.; Schröder, M. *J. Chem. Soc., Chem. Commun.* **1996**, 457.

44. Mandal, S.K.; Thompson, L.K.; Nag, K.; Charland, J.-P. *Inorg. Chem.* **1987**, *26*, 1391.

45. Lacroix, P.; Kahn, O.; Theobold, F.; Leroy, J.; Wakselman, C. *Inorg. Chim. Acta* **1988**, *142*, 129.

46. Gryszkiewics-Trochimowski, E.; *Roczniki Chem.* **1928**, *8*, 165.

47. Penfold, B.R.; Lipscomb, W.N. *Acta Crystallogr.* **1961**, *14*, 589.

48. Roberstson, P.S.; Vaughan, J.; *J. Am. Chem. Soc.* **1958**, *80*, 2691.

49. Iwamoto, T.; Suzuki, H. *Chem. Lett.*, **1976**, 343.

50. Begland, R.W.; Neumer, J.F. *U.S. Patent* **1975**; 3,912,274; 3,914,726.

51. Miles, M.G.; Hursthouse, M.B.; Robinson, A.G. *J. Inorg. Nucl. Chem.* **1971**, *33*, 2105.

52. Lauher, J.W.; Ibers, J.A. *Inorg. Chem.* **1975**, *14*, 640.

53. Wöhrle, D.; Buttner, P. *Polymer Bull.* **1985**, *13*, 57.

54. Lacroix, P.G.; Di Bella, S.; Ledoux, I. *Chem. Mater.* **1996**, *8*, 541.

55. Tandon, S.S.; Thompson, L.K. unpublished results.

56. Drago, R.S.; Desmond, M.J.; Corden, B.B.; Miller, K.A. *J. Am. Chem. Soc.* **1983**, *105*, 2287.

57. Marvel, C.S.; Tarköy, N. *J. Am. Chem. Soc.* **1957**, *79*, 6000.

58. Dickson, I.E.; Robson, R. *Inorg. Chem.* **1974**, *13*, 1301.

59. Mandal, S.K.; Nag, K. *J. Chem. Soc., Dalton Trans.* **1984**, 2141.

60. MacLachlan, M.J.; Park, M.K.; Thompson, L.K. *Inorg. Chem.* **1996**, *35*, 5492.

61. Brychcy, K.; Dräger, K.; Jens, K.-J.; Tilset, M.; Behrens, U. *Chem. Ber.* **1994**, *127*, 465.

62. Handa, M; Thompson, L.K. unpublished results.

63. Huheey, J.E.; Keiter, E.A.; Keiter, R.L. *Inorganic Chemistry: Principles of Structure and Reactivity, 4th Edition*; HarperCollins Publishers: New York, NY, 1993.

64. Brychcy, K.; Jens, K.-J.; Tilset, M.; Behrens, U. *Chem. Ber.* **1994**, *127*, 991.

65. Mandal, S.K.; Nag, K. *J. Chem. Soc., Dalton Trans.* **1983**, 2429.

66. Mandal, S.K.; Thompson, L.K.; Newlands, M.J.; Gabe, E.J. *Inorg. Chem.* **1989**, *28*, 3707.

67. (a) M^{c}Gregor, K.T.; Barnes, J.A.; Hatfield, W.E. *J. Am. Chem. Soc.* **1973**, *95*, 7993. (b) Sikorav, S.; Bkouche-Waksman, I.; Kahn, O. *Inorg. Chem.* **1984**, *23*, 490.

68. Bürger, K.-S.; Chaudhuri, P.; Wieghardt, K.; Nuber, B. *Chem. Eur. J.* **1995**, *1*, 583.

69. Lloret, F.: personal communication.

Appendix I

Input File and Parameters Used in the Extended Hückel MO Model Study.

Input File for the 98° phenoxide bridge angle:*

```
# 98 Cu-O-Cu angle
 38  2DIST
0.,0.,0.,DU
-1,1,CU 1.490551,0.,0.
-1,2,CU 1.490551,180.,0.
-1,3, O 1.295717,90,0.
-1,4, O 1.295717,-90,0.
 3,5, C 1.36, 180,0.
 5,-2,DU 1.38,180,0.
-2,6, C 1.38,-60,0.
-2,7, C 1.38,60,0.
 4,8, C 1.36,180,0.
 8,-3,DU 1.38,180,0.
-3,9, C 1.38,60,0.
-3,10, C 1.38,-60,0.
-2,11, C 1.38,-120,0.
-2,12, C 1.38,120,0.
-3,13, C 1.38,120,0.
-3,14, C 1.38,-120,0.
-2,15, C 1.38,180,0.
-3,16, C 1.38,180,0.
-2,17, C 2.83,60,0.
-2,18, C 2.83,-60,0.
-3,19, C 2.83,60,0.
-3,20, C 2.83,-60,0.
-2,21, H 2.44,-120,0.
-2,22, H 2.44,120,0.
-3,23, H 2.44,120,0.
-3,24, H 2.44,-120,0.
-2,25, H 2.44,180,0.
-3,26, H 2.44,180,0.
17,27, H 1.06,-120,0.
18,28, H 1.06,120,0.
19,29, H 1.06,-120,0.
20,30, H 1.06,120,0.
 1,31,AM 1.98,-130.5,180.
 1,33,AM 1.98,-130.5,0.
 2,35,AM 1.98,-130.5,0.
 2,37,AM 1.98,-130.5,180.
FMO
 2  2 36  4 -2
```

*Bond distanes and angles were averaged from the x-ray crystal structures of the planar binuclear copper(II) macrocyclic coordination compounds found in reference [8].

Parameters (exponents and atomic orbital energies) used in the MO calculations:

Atom	ζs	Hss (eV)	ζp	Hpp (eV)	ζd	ζd'	Hdd (eV)
H	1.300	-13.60					
C	1.625	-21.40	1.625	-11.40			
N	1.950	-26.00	1.950	-13.40			
O	2.275	-32.30	2.275	-14.80			
Cu	2.800	-9.40	2.800	-5.06	9.150	3.000	-12.60
					0.5933†	0.5744†	

†Contraction coefficients for d orbitals.

Appendix II

Crystallographic Data

Crystal data for $[Cu_2M4](CH_3COCH_3)$, (5).

Parameter	Value
Empirical formula	$C_{35}H_{30}N_8O_5Cu_2$
Formula weight	769.76
Crystal colour	orange
Crystal dimensions (mm)	0.400 x 0.050 x 0.400
Crystal system	monoclinic
Space group	C2/c (#15)
a (Å)	38.33 (2)[a]
b (Å)	8.059 (4)
c (Å)	22.67 (2)
β (°)	105.09 (6)
d_{calcd} ($g cm^{-3}$)	1.512
Z	8
Abs. coeff., μ(cm^{-1})	13.13
Radiation, λ (Å)	0.71069
T (°C)	26
F_{000}	3152
Scan rate ($°\cdot min^{-1}$)	4.0
$2\theta_{max}$ (deg)	50.1
Data collected	6551
No. of unique data ($I>2.00\sigma(I)$)	3311
No. of variables	452
Goodness of fit[b]	2.57
R[c]	0.064
R_w[d]	0.054

[a] Throughout this work, esd's are in parentheses and refer to the last digit printed.

[b] Goodness of fit = $[\Sigma w(|Fo| - |Fc|)^2 / (\text{number of reflections - number of parameters})]^{1/2}$.

[c] $R = \Sigma(|Fo| - |Fc|) / \Sigma|Fo|$.

[d] $R_w = [(\Sigma\omega(|Fo| - |Fc|)^2 / \Sigma\omega (|Fo|)^2]^{1/2}$.

Crystal data for [CuL2(CH_3SOCH_3)], (7).

Parameter	Value
Empirical formula	$C_{24}H_{20}N_4O_5SCu$
Formula weight	540.05
Crystal colour	red
Crystal dimensions (mm)	0.350 x .030 x 0.350
Crystal system	triclinic
Space group	$P\bar{1}$ (#2)
a (Å)	10.236 (4)[a]
b (Å)	13.514 (4)
c (Å)	9.655 (4)
β (°)	113.6 (3)
d_{calcd} ($g \cdot cm^{-3}$)	1.515
Z	2
Abs. coeff., μ(cm^{-1})	10.50
Radiation, λ (Å)	0.71069
T (°C)	26
F_{000}	554
Scan rate ($° \cdot min^{-1}$)	4.0
$2\theta_{max}$ (°)	50.1
Data collected	4453
No. of unique data (I>2.00σ(I))	2491
No. of variables	317
Goodness of fit[b]	1.64
R[c]	0.043
R_w[d]	0.036

[a] Throughout this work, esd's are in parentheses and refer to the last digit printed.

[b] Goodness of fit = $[\Sigma w(|Fo| - |Fc|)^2 / (\text{number of reflections} - \text{number of parameters})]^{1/2}$.

[c] $R = \Sigma(|Fo| - |Fc|) / \Sigma|Fo|$.

[d] $R_w = [(\Sigma\omega(|Fo| - |Fc|)^2 / \Sigma\omega (|Fo|)^2]^{1/2}$.

Appendix III

Magnetic Data

Magnetic data for $[Cu_2M1](ClO_4)_2(H_2O)_3(CH_3OH)$, **(1)**.

T(K)	χ_m (emu·mol^{-1})
4.80	1.037E-003
7.46	6.787E-004
12.76	4.115E-004
17.49	3.065E-004
22.26	2.469E-004
27.17	2.069E-004
32.15	1.796E-004
36.83	1.617E-004
41.55	1.492E-004
46.23	1.381E-004
49.76	1.325E-004
54.08	1.270E-004
58.90	1.225E-004
64.08	1.182E-004
69.16	1.141E-004
73.99	1.114E-004
78.97	1.080E-004
83.77	1.049E-004
92.00	1.038E-004
102.05	1.098E-004
112.78	1.210E-004
122.99	1.369E-004
133.10	1.544E-004
142.94	1.747E-004
162.40	2.179E-004
182.27	2.662E-004
202.93	3.117E-004
223.87	3.543E-004
244.54	3.916E-004
266.33	4.204E-004
286.22	4.459E-004
299.91	4.648E-004

Magnetic data for $[Cu_2M2](ClO_4)_2$, **(2)**.

T(K)	χ_m (emu·mol^{-1})
5.13	2.336E-003
7.57	1.600E-003
12.71	9.850E-004
17.39	7.315E-004
22.20	5.804E-004
27.12	4.826E-004
32.78	3.986E-004
36.81	3.649E-004
41.52	3.289E-004
46.23	3.009E-004
49.80	2.875E-004
54.08	2.752E-004
58.90	2.625E-004
64.08	2.502E-004
69.16	2.410E-004
73.99	2.306E-004
78.97	2.216E-004
83.65	2.175E-004
92.00	2.185E-004
102.05	2.265E-004
112.78	2.406E-004
123.24	2.585E-004
132.82	2.771E-004
142.94	2.964E-004
162.40	3.363E-004
182.27	3.784E-004
202.93	4.146E-004
223.87	4.471E-004
245.32	4.713E-004
265.45	4.916E-004
285.24	5.070E-004
299.91	5.150E-004

Magnetic data for $[Cu_2M4](ClO_4)_2(H_2O)_2$, **(4)**.

T(K)	χ_m (emu·mol^{-1})
4.02	1.094E-003
5.84	6.957E-004
10.83	4.197E-004
15.86	3.122E-004
20.74	2.547E-004
25.60	2.194E-004
30.27	1.961E-004
34.99	1.793E-004
39.78	1.725E-004
44.48	1.662E-004
49.14	1.623E-004
53.86	1.592E-004
58.59	1.568E-004
63.33	1.556E-004
67.25	1.548E-004
72.71	1.539E-004
77.52	1.543E-004
82.29	1.565E-004
90.59	1.675E-004
100.71	1.862E-004
110.81	2.110E-004
120.93	2.376E-004
131.06	2.649E-004
141.20	2.919E-004
160.42	3.433E-004
180.99	3.946E-004
201.62	4.351E-004
222.14	4.732E-004
242.83	5.061E-004
263.22	5.212E-004
283.85	5.358E-004
296.00	5.483E-004

Magnetic data for $[Cu_2M4](CH_3COCH_3)$, (5).

T(K)	χ_m (emu·mol^{-1})
5.04	3.607E-003
10.49	5.365E-003
13.43	6.669E-003
17.31	7.689E-003
21.88	8.049E-003
26.65	7.896E-003
30.71	7.586E-003
35.26	7.171E-003
40.02	6.726E-003
44.89	6.292E-003
49.88	5.879E-003
54.57	5.531E-003
59.55	5.190E-003
64.93	4.866E-003
70.23	4.580E-003
75.32	4.324E-003
80.60	4.097E-003
85.24	3.911E-003
93.76	3.613E-003
104.02	3.301E-003
115.15	3.028E-003
126.04	2.802E-003
135.73	2.611E-003
145.92	2.449E-003
166.11	2.186E-003
186.80	1.960E-003
208.33	1.777E-003
229.43	1.624E-003
250.90	1.497E-003
271.72	1.389E-003
286.22	1.326E-003
299.91	1.270E-003

IMAGE EVALUATION
TEST TARGET (QA-3)

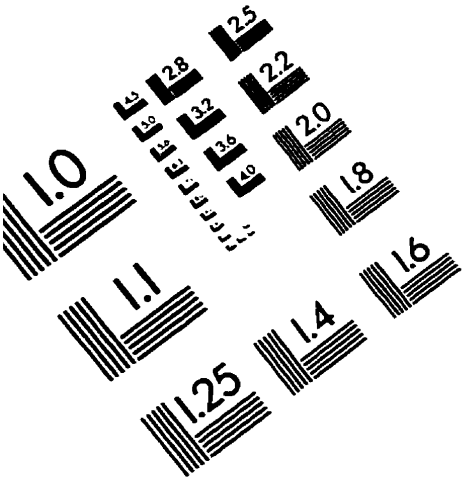

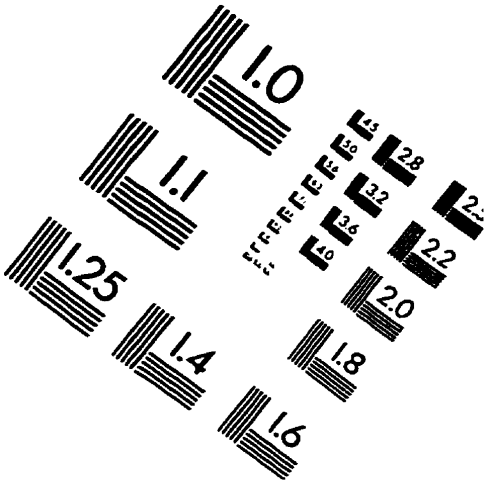

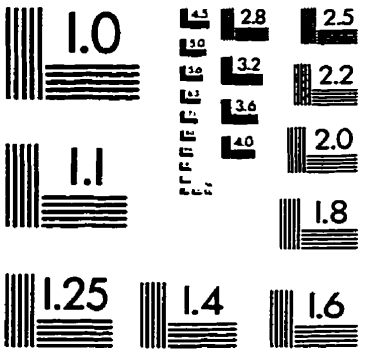

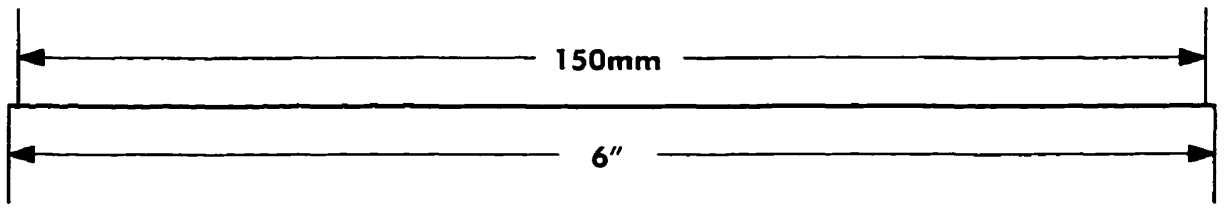

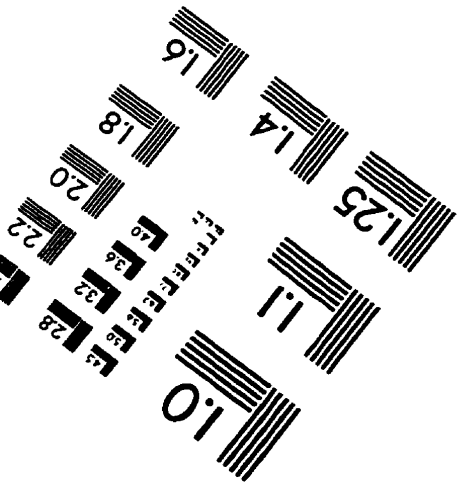

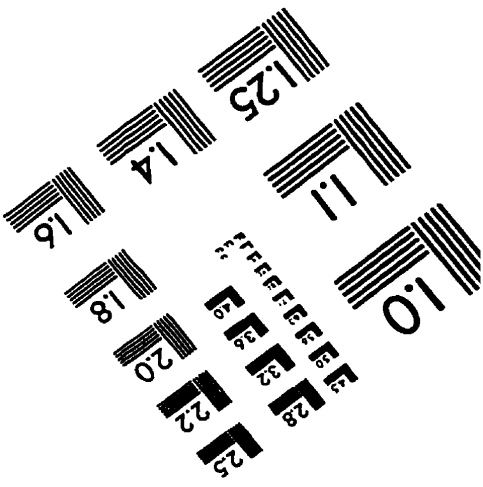

APPLIED IMAGE, Inc
1653 East Main Street
Rochester, NY 14609 USA
Phone: 716/482-0300
Fax: 716/288-5989